FIXED-TRIM RE-ENTRY GUIDANCE ANALYSIS

by

Christopher Gracey

Dissertation submitted to the Graduate Faculty of the

Virginia Polytechnic Institute and State University

in partial fulfillment of the requirements for the degree of

DOCTOR OF PHILOSOPHY

in

Aerospace and Ocean Engineering

APPROVED:

H. J. Kelley, Chairman

E. M. Cliff

J. A. Burns

F. H. Lutze

H. F. VanLandingham

April, 1981

Blacksburg, Virginia

TABLE OF CONTENTS

ACKNOWLEDGEMENTS

The author expresses his gratitude to Professor H. J. Kelley who guided this research effort to a successful conclusion, to Professor E. M. Cliff for pointing out the solution to the time-optimal control problem, and to Professor F. H. Lutze for his assistance in the implementation of the steering algorithm in the fifth-order, roll system.

The author is also indebted to the staff of the Naval Surface Weapons Center who sponsored this effort, and

.

Further appreciation is expressed to and of the Naval Surface Weapons Center, of Virginia Polytechnic Institute and State University, and of Sperry Systems Division for their valuable comments, suggestions, and programming assistance.

Finally, a special thanks is made to members of the staff of NASA Langley Research Center: for his assistance in the completion of this effort, and for generously devoting her time to typing the manuscript.

LIST OF TABLES AND FIGURES

Tables

Figures

LIST OF SYMBOLS

A	magnitude of the acceleration of the vehicle
C_D	drag coefficient of the vehicle
C_{L_α}	lift curve slope for the vehicle
D	drag force on the vehicle
$\hat{e}_y$	unit vector in the y-axis direction
$\hat{e}_D$	unit vector along a dive-line, passing through the aimpoint
F	generic force
g	acceleration due to gravity
H	Hamiltonian
h	Heaviside unit step function
I_x	roll moment of inertia
J	performance index
$k, k_1, k_2, k_\alpha, k_\phi$	guidance law constants
$\hat{k}$	time-varying guidance gain
k_ρ	time-varying guidance gain
L	lift force on the vehicle
L_{δ_ϕ}	roll moment due to actuator deflection
m	mass of the vehicle
P_c	commanded roll-rate
P_L	roll-rate limit of the vehicle
q	dynamic pressure
q_v	angular velocity of the non-rolling velocity frame about its y-axis

r	magnitude of the position of the vehicle with respect to the target
r_v	angular velocity of the non-rolling velocity frame about its z-axis
S	reference area of the vehicle
t	elapsed time-of-flight
t_f	final time-of-flight
T	generic coordinate transformation matrix
u	generic control
V	airspeed of the vehicle
$(x,y,z)^T$	position coordinates of the vehicle with respect to a target centered, inertial coordinate system
$\underline{y}$	vehicle navigation system output vector
α_T	total, trim angle of attack of the vehicle
γ,χ	flight-path and heading angles, respectively, of the vehicle with respect to an inertial frame
δ	polar orientation of the projection of the sight-line to the aimpoint with respect to the non-rolling velocity frame
δ_i	Dirac delta or impulse function
δ_ϕ	actuator deflection
δ_{ϕ_c}	commanded value of δ_ϕ
ε	angle between the velocity and sight-line vectors
ε_1 (ε_2)	angle between the horizontal-plane projections (respectively, vertical-plane projections) of the velocity and sight-line vectors
ζ	roll-orientation of the vehicle relative to a rolling, velocity frame

ζ_a actuator damping ratio

ζ_c commanded value of ζ

$\underline{n}_c$ commanded acceleration vector

$\lambda_o, \lambda_z, \lambda_\gamma$ Lagrange multipliers

$\mu_L = L/mV_o$

$\mu_o = \varepsilon_o/(1/m)t_f$

ρ air density

$\left(\rho_{v_x}, \rho_{v_y}, \rho_{v_z}\right)^T$ line-of-sight vector

$\rho_{v_p} = \left(\rho_{v_y}^2 + \rho_{v_z}^2\right)^{1/2}$

τ_φ roll autopilot/airframe time constant, (sec)

φ_v roll orientation of the lift vector in a non-rolling velocity frame

φ_c commanded value of φ_v

$\Delta\varphi_c = \varphi_c - \varphi_v = \zeta_c - \zeta$

$\Delta\dot{\varphi}_c = \dot{\varphi}_c - \dot{\varphi}_v$

ω_n actuator natural frequency

Subscripts:

o constant, reference, or initial value

x,y,z components in the inertial x, y, or z directions, respectively

x_v, y_v, z_v components in the non-rolling, x, y, or z directions, respectively

() indicates a vector quantity

Superscripts:

$(\dot{}) = d/dt()$

$(\ddot{}) = d^2/dt^2()$

$()'$ indicates the rolling, velocity frame

I. INTRODUCTION

Maneuvering re-entry of strategic missiles is attractive for the evasion capability it furnishes against target defenses. Three bank-to-turn vehicle designs may be considered for this mission: variable-trim, discrete-trim, or fixed-trim. The simplest of these configurations is fixed-trim, wherein the maneuver-level capability is not controlled but fixed by body geometry. The vehicle is steered in a bank-to-turn mode, adequate for most purposes, but potentially troublesome in the terminal phase for lack of precision, especially with a severe combination of roll-rate-limit and roll-control system lag. The technical material presented herein deals entirely with the fixed-trim, terminal-steering case.

In Chapter II a simplified model for the re-entry-body control system and motion is described for use in analyzing the fixed-trim guidance problem on a digital computer. This model also serves as a departure point for analytical investigations of the steering problem.

With a model established for the reentry system, a brief survey of existing, fixed-trim, re-entry guidance laws[1,2,4,11] is presented in Chapter III. The guidance laws surveyed are of the explicit-guidance type and do not reuqire nominal trajectory storage for implementation. Non-explicit guidance laws cause targeting problems and tend to be more sensitive to off-nominal parameters than do explicit guidance laws.[4] In addition, it should be noted that attempts by researchers to solve the fixed-trim, re-entry guidance problem in other than explicit terms have had questionable success.[1] Therefore, only explicit guidance laws

have been included in the survey. The analysis reveals that all of the guidance laws linearize to one of two similar results. The survey also reveals that existing fixed-trim steering laws have been developed from successful variable-trim laws by using roll-angle commands while ignoring maneuver-level commands. This approach is questionable since it forces inconsistencies to occur in the implementation of the feedback control and subsequent analysis of the motion. Under these circumstances, it is not surprising that numerical studies show that precision, fixed-trim, terminal-steering is not characteristic of existing algorithms. The alternative approach, taken herein, is to concentrate attention on the fixed-trim case.

The fixed-trim, terminal-guidance problem is thus formulated with the objective of synthesizing a closed-loop steering law that compensates for roll-lags while maintaining moderate roll-rates. En route to satisfying these objectives, an intermediate result is obtained (Chapter IV) that has both practical and frame-of-reference value. It is shown that the time-optimal-linear-regulator results[3,9] can be applied, in certain settings to the fixed-trim steering problem. However, in scenarios of primary interest the extension of these results encounter difficulty due to the high-order and nonlinear features of the model describing the fixed-trim vehicle motion.

To circumvent these difficulties in treating the guidance problem analytically, a systematic order-reduction of the original system of equations is performed (Chapter V) that simplifies a determination of the control law effective in meeting the objectives of this study. The

foundation for a reduction in the order of the state system is prepared by performing a transformation of variables that results in the introduction of the vehicle's lift-force orientation into the kinematic description of the motion. A subsequent, linearization of the motion, with the sight-line to the aimpoint as a reference, shows that the state variables used in the dynamical description of the motion, that involve the lift-force orientation, are "ignorable" in the sense that they are no longer essential to describe the motion of the vehicle in the transformed coordinate system. Further order-reductions are obtained by assuming constant flight speed and a small autopilot time constant. The final reduced-order system is essentially a polar-coordinate description of the motion of the sight-line about the velocity vector of the vehicle. While the reduced-order system is both nonlinear and time-varying, it is simple enough to lend itself to synthesis of a class of feedback control laws, in terms of the state variables of the reduced-order system, that will accurately steer the vehicle to the aimpoint. Analysis indicates, however, that the feedback control will only be effective in producing precision terminal-steering if the roll-control-system lag be reduced or compensated.

If one presumes that the missile, autopilot, and actuator contributions to the roll-system-lag are unalterable elements of the system, then any reduction in lag must be accomplished through guidance compensation. This assumption, together with the physical interpretation of the coordinate transformation--that the vehicle must be capable of rolling while maintaining small roll-angle errors, $\varphi_c - \varphi_v$,--suggest

that feedforward compensation,[6,10] a device borrowed from classical control theory, will successfully compensate roll-system lags. In Chapter VI the compensation network is easily synthesized for a first-order roll-system model by differentiating the feedback control and commanding the vehicle to roll at this rate. The rate command is approximated in terms of the reduced-order states and hence requires no numerical scheme for performing the differentiation. Thus, two of the objectives of this study, development of a feedback control and a compensation network to reduce roll-system lags, are satisfied. It remains to show that the steering law can be implemented without exceeding the physical limitations of the control system; notably, moderate roll-rates must be maintained.

The proposed steering law is evaluated computationally in Chapter VIII using the numerical model described in Chapter II. Preliminary results, useful in evaluating the adequacy of the reduced-order approximation of Chapter V, are presented first, using a first-order roll-system model. Based upon time-histories of trajectories that originate at different flight-path-angles a guidance gain is selected that will cause the feedback control law to accurately steer the vehicle at moderate roll-rates. The ability of the feedforward technique to compensate for roll-system lags is then demonstrated by varying roll time-constant, initial flight-path-angle, trim angle-of-attack, roll-rate limit, and initial roll-angle.

Following the examination of the guidance algorithm with the simple, first-order roll-system model, the steering law is next

implemented with a realistic, non-linear, fifth-order roll-system that models the airframe, actuator, and autopilot. The robustness of the proposed steering law with respect to initial conditions and maneuver level is examined.

Finally, in Chapters IX and X conclusions and recommendations are made and a summary given.

II. SIMPLIFIED EQUATIONS OF MOTION FOR A FIXED-TIME RE-ENTRY BODY

A block diagram for an inertially guided re-entry body is sketched in Figure 1, illustrating the flow of information between the major subsystems. Estimates of the vehicle's true acceleration, velocity, and position are provided by the navigation subsystem and are indicated by hats over the variables in the diagram. These estimates are used to implement a steering law in a digital, on-board computer. The steering algorithm commands the autopilot to orient the vehicle's lift vector in a desired direction, ϕ_c. This command is translated into an actuator command, δ_{ϕ_c}, to produce the desired actuator response, δ_ϕ, which will cause the vehicle to roll in the proper direction, ϕ_v. As the vehicle rolls to a new orientation, the specific forces (gravity-free) on the body are estimated by accelerometers mounted on an inertial platform. The new estimates of acceleration can then be integrated numerically to obtain new velocity and position estimates, thus completing the closed-loop operation of the system.

To approximate the actual operation of a fixed-trim re-entry body during terminal guidance, the following simplifying assumptions are made:

1. The earth's rotation and curvature are neglected, and the acceleration due to gravity is considered constant.
2. Pitch and yaw plane dynamics are not modelled, and the total angle of attack is assumed to be small and constant.

3. The vehicle roll-dynamics/roll-autopilot is modelled as a first-order system.
4. The navigation measurement system, guidance computer, and errors associated with these systems are not modelled.

Under these assumptions, the equations of motion of a fixed-trim, maneuvering re-entry body may be written in the inertial-coordinate system of Figure 2 as

$$\ddot{x} = (D_x + L_x)/m \tag{1.1}$$

$$\ddot{y} = (D_y + L_y)/m \tag{1.2}$$

$$\ddot{z} = (D_z + L_z)/m + g \tag{1.3}$$

$$\tau_\phi \dot{\phi}_v = \phi_c - \phi_v; \; |\dot{\phi}| \leq p_L \tag{1.4}$$

where,

$$D = qSC_D$$

$$L = qSC_{L_\alpha}\alpha$$

$$q = 1/2\rho V^2$$

$$V = (\dot{x}^2 + \dot{y}^2 + \dot{z}^2)^{1/2}$$

$$D_x = -D \cos\gamma \cos\chi$$

$$D_y = -D \cos\gamma \sin\chi$$

$$D_z = D \sin\gamma$$

$$L_{y_v} = -L \sin \phi_v$$

$$L_{z_v} = L \cos \phi_v$$

$$L_x = -L_{y_v} \sin \chi + L_{z_v} \sin \gamma \cos \chi$$

$$L_y = L_{y_v} \cos \chi + L_{z_v} \sin \gamma \sin \chi$$

$$L_z = L_{z_v} \cos \gamma$$

$$\gamma = \sin^{-1}(-\dot{z}/V)$$

$$\chi = \tan^{-1}(\dot{y}/\dot{x})$$

$$\rho = .2377 \times 10^{-2}\, e^{z/21000.}, \quad |z| \leq 30800.$$

C_D, $C_{L\alpha}$ are tabular functions of Mach number

By assumption (4), the output of the navigation system is idealized to be the same as the acceleration, velocity and position of the re-entry body relative to the target obtained by integrating equations (1.1) through (1.4). In addition, roll-angle and roll-rate sensors are assumed to be on the vehicle, so that the output vector available for guidance implementation is taken to be

$$\underline{y} = (\underline{r}, \underline{V}, \underline{A}, \phi_v, \dot{\phi}_v)^T. \tag{2}$$

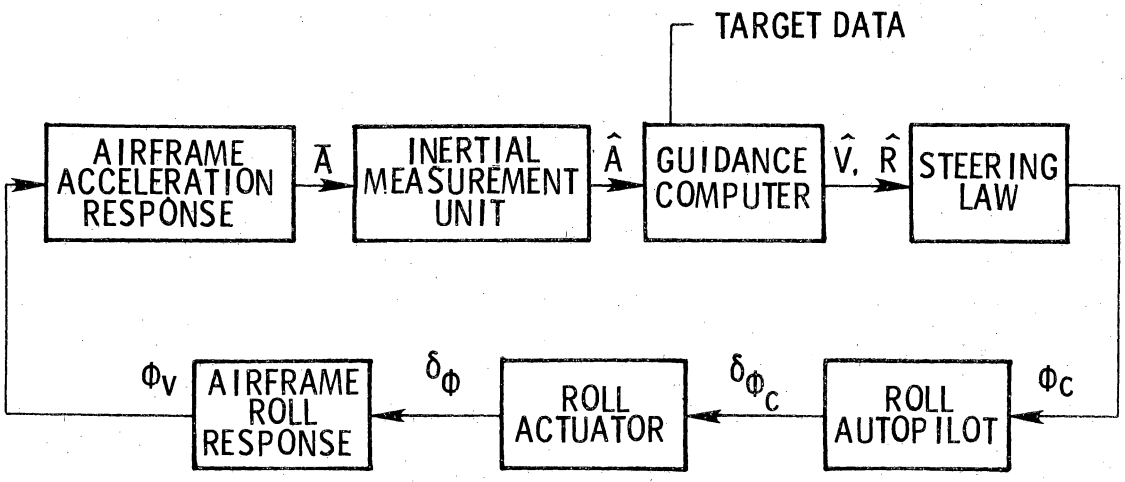

Figure 1.- Subsystem block diagram for a guided re-entry body.

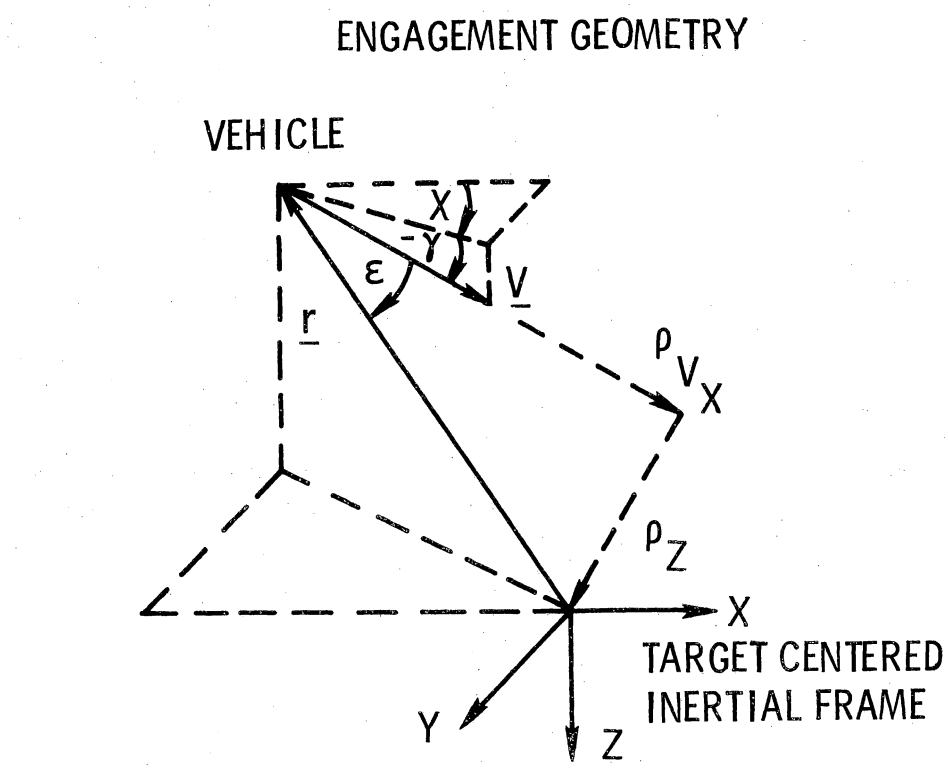

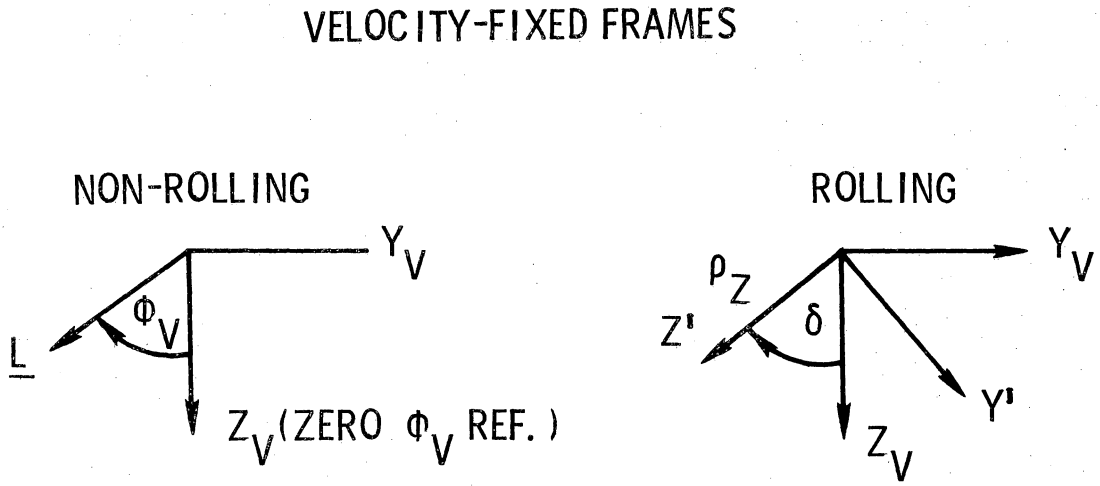

Figure 2.- Engagement geometry and coordinate system descriptions.

III. SUMMARY OF OTHER EXPLICIT GUIDANCE LAWS

Several explicit guidance laws appear in the literature, and these may be categorized[11] as (1) cross-product steering; (2) proportional navigation; and (3) polynomial curve-fit guidance. All of these laws apply strictly only to vehicles with variable trim geometry. However, by using only the bank angle component of the variable-trim command (while ignoring the maneuver level command), the variable-trim laws have been "restricted" to apply to vehicles with only fixed-trim capability. The fixed-trim version of these guidance laws will be stated and then linearized during the terminal guidance phase of flight in order to compare and interpret them.

A. Cross-Product Steering

Numerous versions of cross-product steering[2,4,11] are cited in the literature, two of which are examined herein.

The first version of cross-product steering[11] attempts to null the error angle between the velocity vector and the line-of-sight vector. The error angles in the y and z planes are calculated using vector cross and dot products as follows:

z-plane error angle, ε_1:

$$\underline{V} \times (-\underline{r}) = -|\underline{V}||\underline{r}| \sin \varepsilon_1 \, \hat{e}_y \tag{3}$$

$$\underline{V} \cdot (-\underline{r}) = |\underline{V}||\underline{r}| \cos \varepsilon_1 . \tag{4}$$

Therefore, from (3),

$$|\underline{V}||\underline{r}| \sin \varepsilon_1 = -\dot{x}y + x\dot{z}, \tag{5}$$

and from (4),

$$|\underline{V}||\underline{r}| \cos \varepsilon_1 = -x\dot{x} - z\dot{z}. \tag{6}$$

Dividing (5) by (6), gives

$$\varepsilon_1 \simeq \tan \varepsilon_1 = (-\dot{x}z + x\dot{z})/(-x\dot{x} - z\dot{z}), \text{ for } \varepsilon_1 << 1. \tag{7}$$

y-plane error angle, ε_2:

Similarly, the y-plane error angle is given by

$$\varepsilon_2 \simeq (-\dot{x}y + x\dot{y})/(-x\dot{x} - y\dot{y}), \text{ for } \varepsilon_2 << 1. \tag{8}$$

The bank angle is commanded to orient the vehicle's lift vector opposite the error vector, i.e.,

$$\phi_c = \tan^{-1}(-k_2\varepsilon_2/k_1\varepsilon_1), \tag{9}$$

where, k_1 and k_2 are guidance constants. Note that the error angles in (7) and (8) may be rewritten as

$$\varepsilon_1 \simeq [-z + (x/\dot{x})\dot{z}]/[-x - (\dot{z}/\dot{x})z] \simeq [-z - (t_f - t)\dot{z}]/(-x) \tag{10}$$

$$\varepsilon_2 \simeq [-y + (x/\dot{x})\dot{y}]/[-x - (\dot{y}/\dot{x})y] \simeq [-y - (t_f - t)\dot{y}]/(-x), \tag{11}$$

where, the x-axis is taken to be colinear with the final flight path direction, and the second approximations in (10) and (11) hold during

the terminal phase of flight. Under these stipulations, (9) may be approximated as

$$\phi_c \simeq \tan^{-1}\{k_2[y + (t_f - t)\dot{y}]/(-k_1)[z + (t_f - t)\dot{z}]\}. \quad (12)$$

Note that the bracketed terms in (12) represent the predicted miss distance components, which the guidance law attempts to null. When these quantities become small, the control command given by (12) would be expected to be a sequence of large bank angle excursions, resulting in a modulated roll-rate history. It will be shown in Chapter IV, that in the case of unlimited roll rate capability, (9) represents the time optimal solution to maneuver to null the error angles, ε_1 and ε_2.

A second form of cross-product steering[4] can be developed from a variable-trim, bank-to-turn law that commands an acceleration vector, $\underline{n}_c$, given by

$$\underline{n}_c = -k_\alpha \underline{V} \times\{[\underline{r} + k_\phi(t_f - t)\underline{V}]\times\hat{e}_D\} \quad (13)$$

where,

k_α, k_ϕ are guidance constants

$\hat{e}_D$ is a unit dive line vector.

If the inertial coordinate system x-axis is taken to be colinear with $\hat{e}_D$, then (13) reduces to

$$n_{c_y} = -k_\alpha \dot{x}[y + k_\phi(t_f - t)\dot{y}] \quad (14)$$

$$n_{c_z} = -k_\alpha \dot{x}[z + k_\phi(t_f - t)\dot{z}] \tag{15}$$

so that

$$\phi_c = \tan^{-1}(-n_{c_y}/n_{c_z}) \quad \text{or}$$

$$\phi_c = \tan^{-1}\{[y + k_\phi(t_f - t)y]/[-z - k_\phi(t_f - t)\dot{z}]\} \tag{16}$$

Note that (16) reduces to (12) when the guidance constants are equal to unity.

B. Proportional Navigation

The fixed-trim version of proportional navigation[11] commands a bank angle to orient the lift vector in a direction proportional to the direction which will null the line-of-sight-rate vector. This condition may be expressed mathematically as

$$\phi_c = \tan^{-1}(-k_2\dot{\psi}/k_1\dot{\theta}). \tag{17}$$

where

$$\psi = \sin^{-1}(-y/r \cos \theta) \tag{18}$$

$$\theta = \sin^{-1}(z/r). \tag{19}$$

Differentiating (18) and (19) with respect to time, gives

$$\dot{\theta} = -\dot{r}[z + (r/\dot{r})\dot{z}]/r(x^2 + y^2)^{1/2} \tag{20}$$

and

$$\dot{\psi} = -\dot{x}(x^2 + y^2)^{1/2}[y + (x/\dot{x})\dot{y}]/x^3. \qquad (21)$$

If (20) and (21) are linearized during the terminal phase of flight and substituted into (17), the fixed-trim bank angle command for proportional navigation may be approximated as

$$\phi_c \simeq \tan^{-1}\{k_2[y + (t_f - t)\dot{y}]/(-k_1)[z + (t_f - t)\dot{z}]\}. \qquad (22)$$

A comparison of (12) with (22) indicates that the first version of cross-product steering and proportional navigation linearize to the same fixed-trim guidance law during terminal guidance.

C. Polynomial Curve-Fit Guidance

Polynomial curve-fit guidance[1,4] is derived as follows:

1. The independent variable in the governing equations of motion is changed from time to some measurable variable, such as the ground-track range-to-go.
2. A polynomial form for the trajectory state variables, in terms of the new independent variable, is assumed.
3. The coefficients in the polynomial are determined by imposing desired trajectory constraints.
4. The control commands are then determined from the governing equations of motion in terms of known navigation information and desired trajectory constraints.

Cameron[4] derives a general class of such guidance laws, which may be linearized to the following form:

$$\phi_c = \tan^{-1}\{[k_1 y/(t_f - t)^2 + k_2/(t_f - t)\dot{y}]/$$

$$[-k_1 z/(t_f - t)^2 - k_2\dot{z}/(t_f - t)]\} \qquad (23)$$

By rearrangement, (23) may be rewritten as

$$\phi_c = \tan^{-1}\{[y + (k_2/k_1)(t_f - t)\dot{y}]/[-z - (k_2/k_1)(t_f - t)\dot{z}]\} \qquad (24)$$

A comparison of (24) with (16) indicates that when $k_\phi = k_2/k_1$, the linearized expressions for the second form of cross product steering and polynominal curve-fit guidance are identical.

The results of the linearized analysis of the guidance laws discussed in this section indicate that they fall into only two, similar categories; those described by

$$\phi_c = \tan^{-1}\{k_2[y + (t_f - t)\dot{y}]/(-k_1)[z + (t_f - t)\dot{z}]\}; \qquad (25)$$

and those described by

$$\phi_c = \tan^{-1}\{[y + k_\phi(t_f - t)\dot{y}]/[-z - k_\phi(t_f - t)\dot{z}]\}. \qquad (26)$$

Improvements in bank-to-turn steering results using these guidance laws, have been obtained by employing multiple aimpoints and final aimpoint shifting.[4]

IV. APPLICATION OF THE TIME-OPTIMAL, LINEAR REGULATOR TO FIXED-TRIM STEERING

As a first approach to the fixed-trim steering problem, one may neglect gravity and dynamic pressure variations and seek the open-loop, time-optimal control that will result in aligning the velocity vector of the body with its line-of-sight to the target. With this accomplished the missile would momentarily be on a ballistic (zero-lift) trajectory passing through the aimpoint, and the optimal control problem would be over. Subsequent control will be taken up after a presentation of the optimal control solution.

As a preliminary for the optimal control problem, the inertial states of system (1) are transformed to variables more suited for analytical work. The equations of motion may be rewritten in a wind-axis system as

$$m(\dot{\underline{V}}+\underline{\omega}_V x \underline{V}) = \underline{F}, \tag{27}$$

with scalar components:

$$\dot{V} = -D/m \tag{28.1}$$

$$r_V V = -L \sin \phi_V/m \tag{28.2}$$

$$-q_V V = L \cos \phi_V/m, \tag{28.3}$$

where, for constant angle-of-attack,

$$q_V = \dot{\gamma} \tag{29.1}$$

$$r_v = \dot{\chi} \cos \gamma. \tag{29.2}$$

Substituting (29) into (30) and including the roll-rate equation from (1), one obtains the following seventh-order system in the transformed variables:

$$\dot{V} = -D/m \tag{30.1}$$

$$\dot{\chi} = - L \sin \phi_v/mV \cos \gamma \tag{30.2}$$

$$\dot{\gamma} = - L \cos \phi_v/mV \tag{30.3}$$

$$\dot{x} = V \cos \gamma \cos \chi \tag{30.4}$$

$$\dot{y} = V \cos \gamma \sin \chi \tag{30.5}$$

$$\dot{z} = -V \sin \gamma \tag{30.6}$$

$$\tau_\phi \dot{\phi}_v = \phi_c - \phi_v; \quad |\dot{\phi}_v| \leq p_L. \tag{30.7}$$

A number of simplifying assumptions are now made so that the problem can be restated in a more convenient form:

1. The magnitude of the lift force is permitted to vary between zero and its maximum value. This specializes the problem to variable-trim vehicles and is introduced, temporarily, to convexize the hodograph figure.[8] A relaxation of control, in this manner avoids the occurrence of "chattering" or instantaneous switches in maneuver level commands of variable-trim vehicles.

2. Only motion in the vertical plane is considered, and the inertial-coordinate system is chosen so that its x-axis aligns with the initial line-of-sight vector. This permits a linearization of the trajectory path about the initial sight-line.
3. The roll-rate restriction is removed and the time-constant allowed to approach zero. This results in a reduction in the number of state variables in (30), coupled with a loss in the roll-angle boundary condition.
4. Finally, only constant-speed trajectories are assumed.

Under these assumptions, system (30) reduces to the following set of equations:

$$\dot{V} = \dot{\chi} = \dot{y} = 0 \tag{31.1}$$

$$x = x_o + V_o t \tag{31.2}$$

$$\dot{\gamma} = -\mu_L u; \quad \gamma(0) = \gamma_o \tag{31.3}$$

$$\dot{z} = -V_o \gamma; \; z(0) = 0 \tag{31.4}$$

where,

$$\mu_L = L/mV_o.$$

$$-1 \leq u \leq 1.$$

The optimal control problem may be restated as

$$\min_{u}(J=t_f)$$

subject to (31.3) and (31.4) with end conditions $\gamma(t_f) = z(t_f) = 0$. The problem is now in the form of the classical, one-dimensional, time-optimal regulator.[3,9] The Hamiltonian for this problem is

$$H = \lambda_o t_f - \lambda_z V_o \gamma - \lambda_\gamma \mu_L u, \tag{32}$$

and the adjoint equations are given by

$$\dot{\lambda}_z = -\partial H/\partial z = 0 \tag{33.1}$$

$$\dot{\lambda}_\gamma = -\partial H/\partial \gamma = \lambda_z V_o. \tag{33.2}$$

From (33.1)

$$\lambda_z = \lambda_z(t_f) = \lambda_{z_f}$$

and thus from (33.2)

$$\lambda_\gamma = \lambda_{\gamma_f} - \lambda_{z_f} V_o (t_f - t). \tag{34}$$

Since the Hamiltonian is linear in the control, extremal control is given by $u = \pm 1$. For the re-entry problem, the relaxation of controls, thus, does not preclude applicability to the present study since the optimal control will be at the maneuverability limit (i.e., fixed-trim), with roll-angle chattering required to switch the sign on u. Thus the lift is instantaneously directed either toward or away from the

line-of-sight. The sign of the "switching function," λ_γ, given by (34) determines the sign on u that produces the smaller value for H, that is

$$u = \begin{cases} -1; & \lambda_\gamma < 0 \\ +1 & \lambda_\gamma > 0. \end{cases} \tag{35}$$

To investigate the trajectories in state-space, one may integrate (31.3) and (31.4) to obtain

$$\int_{\gamma_o}^{\gamma} \gamma \, d\gamma = \frac{\mu_L \, u}{V_o} \int_o^z dz$$

or

$$\gamma^2 = \gamma_o{}^2 + \mu_L \, z \, u/V_o. \tag{41}$$

The resulting paths are thus parabolas in z-γ space. The initial control, u, is chosen so that the trajectories will tend toward the "switching curve,"* For the re-entry problem, this choice of initial control corresponds to pointing the lift vector toward the line-of-sight.

In applying the time-optimal linear regulator to the present steering problem, one may think of re-solving the optimal control problem at each guidance update. If this is done, a feedback control

*See Figure 3.9.1, p. 113 of Reference 3.

law is obtained that simply requires that the lift vector point toward the instantaneous line-of-sight. Thus, the time-optimal, linear regulator is seen to be identical to the version of cross-product steering given by equation (9).

The time-optimal linear regulator has practical value for engagements that are marginal in the sense of the sight-line being contained within the reachable set. In these cases the sight-line should be approached as quickly as possible. In engagements for which the sight-line may be reached, however, a more satisfactory control is sought so that once the sight-line has been attained, no wild roll gyrations are required to stay on it.

V. APPROXIMATE, REDUCED-ORDER MODEL FOR FIXED-TRIM RE-ENTRY

The combined difficulties of nonlinearity and high system order, presented by (30), inhibit analytical and/or intuitive approaches to solution of the fixed-trim steering problem. However, the engagement geometry of Figure 2 does suggest that a necessary condition for obtaining small aimpoint dispersion is that ε, the "error angle" between the vehicle's velocity vector and the line-of-sight to the aimpoint, be kept small. An alternate description of the motion of the vehicle, which involves the error angle, may be obtained by re-writing the governing equations in a velocity-fixed reference frame that rolls with the plane containing ε. The development is carried out in detail in Appendix I and results in the following system of equations:

$$\dot{V} = -D/m \tag{42.1}$$

$$\dot{\gamma} = -(L/mV)\cos\phi_V \tag{42.2}$$

$$\dot{\chi} = -(L/mV\cos\gamma)\sin\phi_V \tag{42.3}$$

$$\dot{\rho} = -V\cos\varepsilon \tag{42.4}$$

$$\dot{\varepsilon} = (V/\rho)\sin\varepsilon - (L/mV)\cos(\phi_V-\delta) \tag{42.5}$$

$$\dot{\delta} = -(L/mV)[\cos\varepsilon\sin(\phi_V-\delta) + \tan\gamma\sin\phi_V] \tag{42.6}$$

$$\tau_\phi\dot{\phi}_V = \phi_C - \phi_V;\ |\dot{\phi}_V| \leq p_L. \tag{42.7}$$

where, in terms of the output vector, $\underline{y} = (\underline{r}, \underline{V}, \underline{A}, \varphi_V, \dot{\varphi}_V)$

$$\rho = \sqrt{x^2 + y^2 + z^2}$$

$$\varepsilon = \tan^{-1}\left(\rho_{V_p}/\rho_{V_x}\right)$$

$$\delta = \tan^{-1}\left(-\rho_{V_y}/\rho_{V_z}\right)$$

$$\begin{bmatrix} \rho_{V_x} \\ \rho_{V_y} \\ \rho_{V_z} \end{bmatrix} = T(\gamma,\chi) \begin{bmatrix} -x \\ -y \\ -z \end{bmatrix}$$

$$\rho_{V_p} = \sqrt{\rho_{V_y}^2 + \rho_{V_z}^2}.$$

The transformed system, (42), may be approximated for small ε and γ as follows:

$$\dot{V} = -D/m \tag{43.1}$$

$$\dot{\gamma} = -(L/mV)\cos\phi_V \tag{43.2}$$

$$\dot{\chi} = -(L/mV)\sin\phi_V \tag{43.3}$$

$$\dot{\rho} = -V \tag{43.4}$$

$$\dot{\varepsilon} = (V/\rho)\varepsilon - (L/mV)\cos(\phi_V - \delta) \tag{43.5}$$

$$\varepsilon\dot{\delta} = -(L/mV)\sin(\phi_V - \delta) \tag{43.6}$$

$$\tau_\phi \dot{\phi}_V = (\phi_C - \phi_V);\ |\dot{\phi}_V| \leq p_L. \tag{43.7}$$

In system (43) the path angles, γ and χ, do not appear on the right hand sides of any of the state equations and are thus "ignorable" in the sense that they are not essential to describe the approximate motion of the vehicle. Thus, system (43) is reduced to the following fifth-order system:

$$\dot{V} = -D/m \tag{44.1}$$

$$\dot{\rho} = -V \tag{44.2}$$

$$\dot{\varepsilon} = (V/\rho)\varepsilon - (L/mV)\cos(\phi_V - \delta) \tag{44.3}$$

$$\varepsilon\dot{\delta} = -(L/mV)\sin(\phi_V - \delta) \tag{44.4}$$

$$\tau_\phi \dot{\phi}_V = \phi_C - \phi_V;\ |\dot{\phi}| \leq p_L. \tag{44.5}$$

Over several guidance-update intervals the speed of the vehicle may be approximated as a constant, V_o. This eliminates equation (44.1) from system (44) and allows equation (44.2) to be integrated to yield

$$\rho/V_o = t_f - t, \tag{45}$$

where, t_f is the final time and ρ/V_o the "time-to-go." When (45) is substituted into (44), the order is again reduced by two to obtain the following system of equations:

$$(t_f-t)\dot{\varepsilon} = \varepsilon - L(t_f-t)/mV_o \cos(\phi_v-\delta) \tag{46.1}$$

$$\varepsilon\dot{\delta} = -(L/mV_o) \sin(\phi_v-\delta) \tag{46.2}$$

$$\tau_\phi\dot{\phi}_v = \phi_c - \phi_v;\ |\dot{\phi}_v| \leq p_L. \tag{46.3}$$

A final order-reduction, which is in the singular-perturbation category, may be made by removing the roll-rate restriction and permitting the roll-system time-constant to tend toward zero. The roll-response is thus instantaneous so that

$$\phi_v = \phi_c,$$

and when this result is substituted into (46), the behavior of the vehicle's motion, which was originally described by a seventh-order system, has been approximated by the following system, described by only two first-order differential equations:

$$(t_f-t)\dot{\varepsilon} = \varepsilon - [L(t_f-t)/mV_o] \cos(\phi_c-\delta) \tag{47.1}$$

$$\varepsilon\dot{\delta} = -(L/mV_o) \sin(\phi_c-\delta). \tag{47.2}$$

While system (47) is both non-linear and time-varying, it is now of low order. In addition, the roll orientation of the lift vector, ϕ_v, and the polar orientation, δ, of the component of the line-of-sight vector, ρ_{v_p}, perpendicular to the velocity vector are related as arguments of the trigonometric terms. This relationship suggests the following physical interpretation of the fixed-trim guidance problem: the component of control acceleration, $(L/m)\cos(\phi_c-\delta)$ parallel to ρ_{v_p} controls the error angle, ε, and hence the position error itself, ρ_{v_p}, while the component of control acceleration $(L/m)\sin(\phi_c-\delta)$, controls the rate-of-rotation, $\dot{\delta}$, of ρ_{v_p} about the velocity vector.

The low order and simplicity of equation (47) may now be exploited in synthesizing a guidance law which will control the magnitude of the position error, ρ_{v_p}, while maintaining moderate rates of rotation of the error about the velocity vector.

VI. GUIDANCE SYNTHESIS

A. Feedback Control

As mentioned previously, one method to insure small aimpoint dispersion is to control ε so that its value is small near the aimpoint. From (47.1), one can attempt to control $\dot{\varepsilon}$ so that it is non-positive by requiring that

$$\cos(\phi_c-\delta) = k\varepsilon/(L/mV_o)(t_f-t), \tag{48}$$

where, k is a suitably chosen guidance parameter or gain. To determine acceptable values for the guidance parameter equation (48) is substituted into (47.1) to obtain

$$\dot{\varepsilon}/\varepsilon = (1-k)(t_f-t), \tag{49}$$

which has the solution

$$\varepsilon = \varepsilon_o(1-t/t_f)^{k-1}. \tag{50}$$

Thus, for $k \geq 1$, ε is either constant or monotone decreasing, and moreover, when k is strictly greater than one,

$$\lim_{t\to t_f} \varepsilon = 0,$$

insuring negligible aimpoint dispersion.

One notes that the control law can only be implemented under the mathematical restriction that the right hand side of equation (48) be less than or equal to unity. Because of the physical limitations of

the fixed-trim vehicle, the maneuver level, L/m, cannot be adjusted to satisfy the mathematical constraint. Hence, this restriction leads to the requirement that

$$\cos(\phi_c-\delta) = 1 \quad \text{for} \quad \varepsilon \geq (L/mV_o k)(t_f-t). \tag{51}$$

Combining equations (48) and (51) and solving for the roll-control command, one obtains the feedback control as a non-linear combination of the reduced system states with time varying coefficients:

$$\phi_c = \begin{cases} \delta + \cos^{-1}(\hat{k}\varepsilon); & \varepsilon < 1/\hat{k} \\ \delta; & \varepsilon \geq 1/k, \end{cases} \tag{52}$$

where,

$$\hat{k} = k/(L/mV_o)(t_f-t). \tag{53}$$

With given initial conditions and vehicle maneuver capability the non-dimensional gain, $\hat{k}$, determines whether or not the error can be nulled. When the initial error is sufficiently small, $\varepsilon_o < 1/\hat{k}_o$, the feedback control given by (52) will adjust the component of the lift vector in the plane containing the error so that the error is reduced to zero as the aimpoint is approached. When the initial error is larger than $1/\hat{k}_o$, the "contingency" control, i.e., $\varphi_c = \delta$ given by (52) reduces the error as quickly as possible by directing the total available lift appropriately.

In summarizing these results, one can see that the feedback control given by equation (52) reduces aimpoint dispersion as much as possible for given initial conditions and vehicle maneuver capability. Within the restrictions set forth by equation (50) there are many values of the guidance parameter that will result in a stable error angle response. Therefore, (52) actually represents a class of fixed-trim steering laws. The choice of the guidance parameter will ultimately depend on roll-rate restrictions imposed upon a given vehicle's control system. As a caveat to the results presented in this section, the reader must be reminded that an instantaneous control system has been assumed, which implies both zero roll-response lag and infinite roll-rate capability.

B. Feedforward Compensation

As noted, when the lateral-control-system response is not instantaneous, equation (46.3) must be included in the system of state equations, and the error angle response given by (50) is no longer valid. If, however, the roll-angle lag were small, equation (50) could be expected to approximate the error angle response. To examine the effect of small roll-angle lags on the roll-system response, one observes that, under the assumed first-order autopilot model, (46.3), small actuator errors,

$$\phi_e = \phi_c - \phi_v, \tag{54}$$

result in near zero roll-rates. However, this is contrary to the mathematical and physical analysis that led to the feedback control law. Indeed, the reduced-order system resulted from a description of the motion in a coordinate system that rolled with a rate equal to the polar rate of rotation of the line-of-sight error, ρ_{V_p}, about the velocity vector. The feedback control was derived relative to the rolling coordinate system. By defining

$$\zeta_c = \phi_c - \delta \tag{55}$$

and

$$\zeta = \phi_v - \delta, \tag{56}$$

one observes that the actuation error (54), may be expressed in terms of the actuation error relative to the rolling coordinate system, namely

$$\phi_e = \zeta_c - \zeta. \tag{57}$$

When the actuation error is represented by (57), one observes that, at least conceptually, the error signal can be nulled while the re-entry body is still rolling. To implement this concept in the first-order autopilot, one must add a commanded roll-rate, p_c, to the right-hand side of (46.3), that is,

$$\tau_\phi \dot{\phi}_v = \phi_c - \phi_v + p_c. \tag{58}$$

With this autopilot model it is apparent that the actuation error can be nulled (thus insuring that the line-of-sight error may be approximated by (50)) while the re-entry body is rolling.

To determine the proper roll-rate command to implement (58), one may temporarily isolate the control system from the remainder of the system dynamics, described by (46), by opening the feedback control loop. Thus (58) represents a simple linear system which can be analyzed by applying classical control technqiues. In the frequency domain, the autopilot lag is represented by a stable pole in the complex plane. By cancelling this pole with a zero, the autopilot lag can be eliminated and the system response-time considerably increased. Figure 4 is a block diagram illustrating how the pole/zero cancellation is implemented in the control system. The dashed lines in the diagram indicate the compensation network for a first-order system. Because the flow of information in the diagram is from left to right, the compensation technique is referred to as feedforward control, as opposed to the more familiar concept of feedback control.

Mathematically, the feedforward compensation technique translates into a roll-rate command, so that (58) may be rewritten as

$$\dot{\phi}_V = (\phi_C - \phi_V)/\tau_\phi + \dot{\phi}_C, \tag{59}$$

where,

$$\dot{\phi}_C = d/dt(\phi_C).$$

To illustrate the increase in response time produced by the feedforward compensation technique, one may compute the unit step responses from equations (46.3) and (59) and compare the results. From (46.3), the uncompensated response for a unit step in p_c is given by

$$\phi_V = 1 - (1-\phi_{V_o})e^{-t/\tau_\phi} \tag{60}$$

while the response for the compensated system is, from (59), given by

$$\phi_V = 1 - (1-\phi_{V_o})e^{-t/\tau_\phi} + e^{-t/\tau_\phi} h(t), \tag{61}$$

where, $h(t)$ is the Heaviside unit step function. Notice that the exponentially decaying error in the response for the uncompensated system is completely compensated by the addition of the feedforward term, resulting in a roll-angle response that duplicates the command. As demonstrated for the simple, linear system with a first-order lag, the feedforward compensation technique is a good candidate for reducing the lateral-control-system lag in the nonlinear reduced-order system given by (46).

To apply the feedforward concept to the fixed-trim, control problem, one must differentiate the roll-angle command. As an alternative to differentiating the roll-angle command numerically, one may approximate the derivative in terms of the reduced-order states by differentiating (52). To do this correctly, (48) is first rewritten as

$$\cos(\phi_c-\delta) = \begin{cases} \hat{k}\varepsilon; & \varepsilon \leq 1/\hat{k} \\ h(t); & \varepsilon \geq 1/\hat{k} \end{cases} \tag{62}$$

and then differentiated to obtain

$$\dot{\phi}_c = \begin{cases} \dot{\delta} - \hat{k}\varepsilon(2-k)/(t_f-t) \sin \zeta_c; & \varepsilon < 1/\hat{k} \\ \dot{\delta} + \delta_i(t); & \varepsilon \geq 1/\hat{k}, \end{cases} \tag{63}$$

where, $\delta_i(t)$ is the Dirac delta or impulse function applied at commencement of the terminal maneuver, $t = 0$. The algebraic details leading to equation (63) are provided in Appendix B.

Since the system, (46), is time-varying and non-linear, the feed-forward compensation given by (59) represents a generalization of the linear-autonomous-system-theory concept of pole/zero cancellation. For implementation purposes, equation (63) requires an approximation to the delta function.

In summary, equations (52), (59), and (63) represent the guidance scheme synthesized to reduce the error angle between the velocity vector and the line-of-sight vector according to the time-to-go schedule given by equation (50).

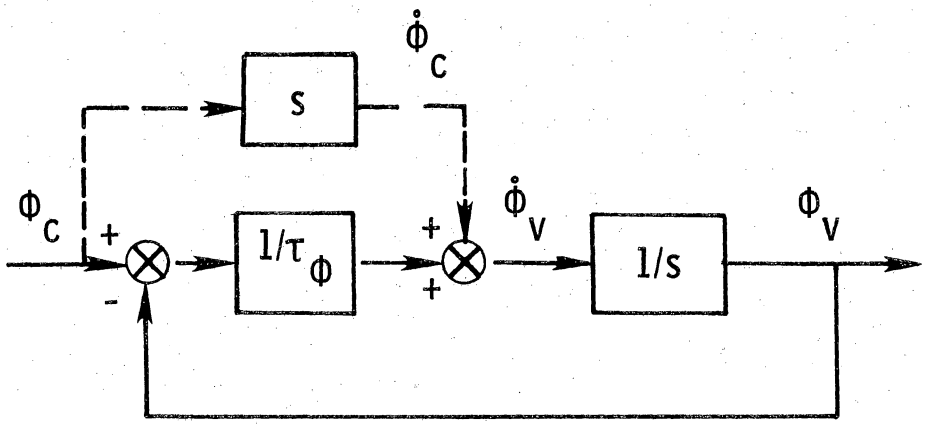

Figure 3.- Block diagram of a first-order roll-system illustrating the feedforward compensation network.

VII. GUIDANCE IMPLEMENTATION

A. First-Order Roll System Model

The following formulas permit implementation of the guidance equations, (52), (59), and (63), in terms of the navigation system output vector, $\underline{y} = (\underline{r}, \underline{V}, \underline{A}, \varphi_V, \dot{\varphi}_V)$.

Transformation of variables.- Let T_{I2V} be the transformation from the inertial-navigation frame to the non-rolling velocity frame. Then the projection of the line-of-sight vector onto the velocity frame may be written as

$$\begin{bmatrix} \rho_{V_x} \\ \rho_{V_y} \\ \rho_{V_z} \end{bmatrix} = -T_{I2V} \begin{bmatrix} x \\ y \\ z \end{bmatrix}. \tag{64}$$

Then, by definition, from (42)

$$\rho_{V_p} = \sqrt{\rho_{V_y}^2 + \rho_{V_z}^2} \tag{65}$$

$$\varepsilon = \tan^{-1}\left(\rho_{V_p}/\rho_{V_x}\right) \tag{66}$$

$$\delta = \tan^{-1}\left(-\rho_{V_y}/\rho_{V_z}\right). \tag{67}$$

Time-to-go calculation.- The time-to-go is estimated based upon observations made in the velocity frame, namely

$$t_f - t = \rho_{V_x}/V. \tag{68}$$

Bank-angle-command computations.- Let

$$\zeta_c = \phi_c - \delta \tag{69}$$

and

$$\zeta = \phi_v - \delta. \tag{70}$$

Then from equation (52),

$$\cos \zeta_c = \begin{cases} \hat{k}\varepsilon; & \varepsilon < 1/\hat{k} \\ 1; & \varepsilon \geq 1/\hat{k}. \end{cases} \tag{71}$$

Making use of the small-angle approximation for ε, one obtains from (66)

$$\varepsilon \approx \rho_{v_p}/\rho_{v_x}. \tag{72}$$

Substituting (72) and (53) into (71), one may rewrite the bank-angle command, relative to the plane containing the velocity and line-of-sight vectors, in terms of the magnitude of the line-of-sight error:

$$\cos \zeta_c = \begin{cases} k_\rho \rho_{v_p}; & \rho_{v_p} < 1/k \\ 1; & \rho_{v_p} \geq 1/k_\rho, \end{cases} \tag{73}$$

where the line-of-sight feedback gain is

$$k_\rho = k/(L/m)(t_f-t)^2. \tag{74}$$

To determine ζ, one first writes, by definition,

$$\zeta = \tan^{-1}(\sin \phi_v \cos \delta - \cos \phi_v \sin \delta)/(\cos \phi_v \cos \delta + \sin \phi_v \sin \delta), \tag{75}$$

where

$$\sin \delta = -\rho_{v_y}/\rho_{v_p} \tag{76}$$

$$\cos \delta = \rho_{v_z}/\rho_{v_p}. \tag{77}$$

Substituting (76) and (77) into (75), one obtains

$$\zeta = \tan^{-1}(\rho_{v_z} \sin \phi_v + \rho_{v_y} \cos \phi_v)/(\rho_{v_z} \cos \phi_v - \rho_{v_y} \sin \phi_v). \tag{78}$$

Thus,

$$\sin \zeta_c = \text{sgn}(\zeta) \sqrt{1-\cos^2 \zeta_c}. \tag{79}$$

Since

$$\phi_c-\phi_v = \zeta_c - \zeta = \tan^{-1}[\sin(\zeta_c-\zeta)/\cos(\zeta_c-\zeta)], \tag{80}$$

then

$$\phi_c-\phi_v = \tan^{-1}(\sin \zeta_c \cos \zeta - \cos \zeta_c \sin \zeta)/(\cos \zeta_c \cos \zeta + \sin \zeta_c \sin \zeta), \tag{81}$$

and the formula used to compute the control is given by

$$\phi_c = \phi_v + \tan^{-1}(\sin \zeta_c \cos \zeta - \cos \zeta_c \sin \zeta)/(\cos \zeta_c \cos \zeta + \sin \zeta_c \sin \zeta), \tag{82}$$

where, $\cos \zeta_c$, ζ, and $\sin \zeta_c$ are given by equations (73), (78), and (79), respectively. Formulas (73), (74), (78), (79) and (82) in conjunction with an arc tangent routine generating values lying between plus π and minus π insure that $|\phi_c-\phi_v| \leq \pi$, so that the roll-angle-error signal, $\phi_c - \phi_v$, generates a roll-rate in the direction of the shorter of the two angular arcs through which the body could roll to null the error.

Roll-rate command computation.- Since the trajectories of primary interest for this study are those for which the sight-line may be reached, an approximation to the impulse function, required by equation (63), is not implemented. Therefore, the roll-rate command is from equation (73)

$$\dot{\phi}_c = \begin{cases} \dot{\delta} - (2-k)\cos\zeta_c/(t_f-t); & \rho_{V_p} < 1/k_\rho \\ \dot{\delta}; & \rho_{V_p} \geq 1/k_\rho \\ p_L \operatorname{sgn}(\dot{\phi}_c); & |\dot{\phi}_c| \geq p_L. \end{cases} \tag{83}$$

where, from equation (46.2),

$$\dot{\delta} = -(L/m)(t_f-t)\sin\zeta/\rho_{V_p}. \tag{84}$$

In summary, only the eight equations, (64), (68), (73), (78), (79), (82), (83) and (84), are required to implement the feedback control law and feedforward compensation technique, developed from the reduced-order model, into the computational model described by equations (1) and (2).

B. Fifth-Order Roll-System Model

To study the performance of the present guidance algorithm in a more realistic setting, one may assume second-order airframe and actuator dynamics and an integral-plus-proportional autopilot to arrive at the following fifth-order roll system:

Airframe: $$\ddot{\phi}_V = L_{\delta_\varphi}\,\delta_\varphi/I_x \tag{85.1}$$

Actuator: $$\ddot{\delta}_\phi + 2\zeta_a\omega_n\dot{\delta}_\phi + \omega_n^2\delta_\phi = \omega_n^2(\dot{\delta}_{\phi_c} + \delta_{\phi_c}) \tag{85.2}$$

$$\text{Autopilot:} \qquad \dot{\delta}_{\phi_C} = K_\delta \left[\frac{1}{\tau_\varphi} (\varphi_C - \varphi_V) - \dot{\varphi}_V \right] . \tag{85.3}$$

One notes that as in the first-order roll-system, the autopilot (85.3) cannot follow both a roll-angle and roll-rate command, as required by the present guidance algorithm. By feeding forward the commanded roll-rate the autopilot equation may be rewritten as

$$\dot{\delta}_{\phi_C} = K_\delta \left[\frac{1}{\tau_\varphi} \Delta\varphi_C + \Delta\dot{\varphi}_C \right] \tag{86}$$

where,

$$\Delta\phi_C = \phi_C - \phi_V . \tag{87}$$

The compensated autopilot, given by (86), now permits the vehicle to have a sustained roll-rate, while maintaining small errors in roll angle. The compensation network for the fifth-order roll-system is illustrated by the dashed lines in Figure 4.

The feedforward algorithm outlined in section A of this chapter is thus easily extended to a fifth-order, roll system which models the airframe, actuator, and autopilot. Numerical studies will be presented for this non-linear roll model, which incorporates limits on various signals in the control path, to examine the performance of the guidance algorithm.

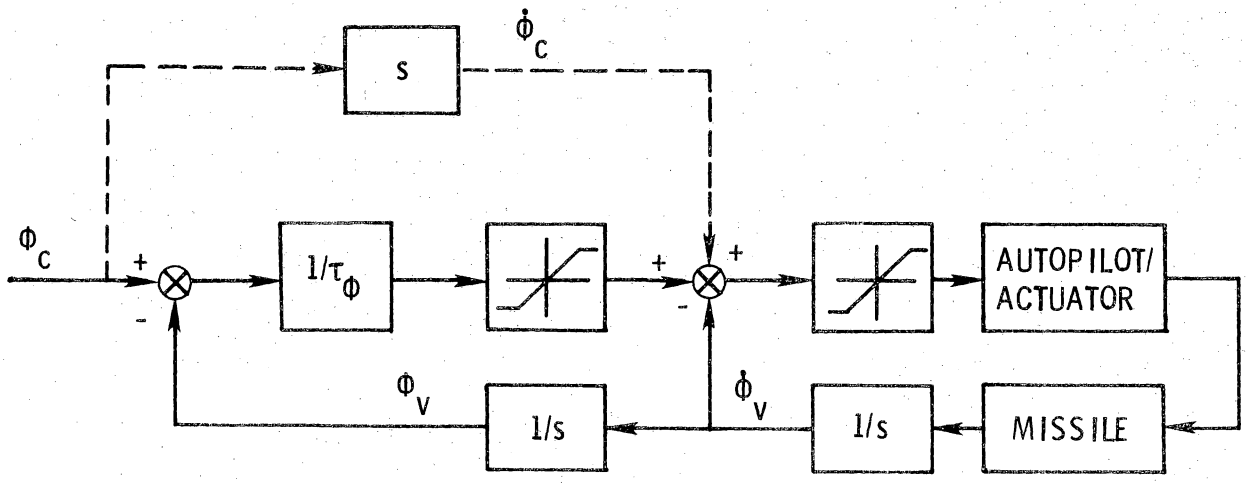

Figure 4.- Block diagram of a fifth-order roll-system, illustrating the feedforward compensation network.

VIII. RESULTS AND DISCUSSION

The simplified equations of motion for a fixed-trim re-entry vehicle, presented in Chapter II, the guidance algorithm presented in Chapter VII, and the two versions of cross-product steering given by equations (9) and (16) of Chapter III were programmed on a digital computer. Numerical studies were conducted to determine the validity of the reduced-order analytical model, on which the present guidance law is based, and to compare the performance of the present law with a representative sample of existing guidance laws.

Table 1 lists the nominal parameters for the simulation results presented herein. The nominal initial conditions are for a high-supersonic terminal-maneuver which produces a ballistic (i.e., zero-lift) trajectory passing through the aimpoint.

The series of trajectories, presented in Figures 5 and 6, were computed to compare the error-angle time histories predicted with the approximate reduced-order model of Chapter V with numerical results obtained with the full modelling of Chapter II. The effect of guidance gain, k, on the ε-time history is examined for a small initial error-angle in Figure 5 and for a large initial error angle in Figure 6. The first observation that one makes from an examination of Figures 5 and 6 is that the error angle is never driven to zero, regardless of the value of guidance gain, contrary to the result obtained for the reduced-order model, which predicted that ε would tend to zero with time-to-go for $k > 1.0$. The fact that the angle between the velocity vector and

line-of-sight must increase rapidly for non-zero aimpoint misses, no matter how small, is merely a consequence of the engagement geometry for small time-to-go and, thus, should not have a large effect on the final miss distance.

The second observation that one makes is that the analytical prediction, that the error angle be constant for $k = 1.0$, is not true in the numerical model. In Figure 5.1 the error angle increases, while in Figure 6.1 it decreases, prior to the rapid buildup in ε near the origin.

Based upon the ε-time histories obtained with the numerical model, one may modify the results obtained for the analytical model and state that the error angle will be constant or monotonically decreasing with time-to-go for $k > 1.0$, except in a small region near the origin. One further notes that the rapid rise in ε near the origin implies that the control always reverts to "contingency" control near the origin, regardless of the guidance gain.

To select a guidance gain (or gains) that will produce small aimpoint misses, one may examine the time-histories of the line-of-sight errors, i.e., line-of-sight components perpendicular to the velocity vector, for $k > 1.0$. These results are presented in Figure 7 for a small initial error angle and in Figure 8 for a large initial error angle. To obtain small miss-distances one notes from Figure 7 that the guidance gain must be at least 1.5, while from Figure 8 the gain must be at least 2.0. The gain that produces small misses for both large and small initial error angles is $k = 2.0$.

Having narrowed the choices for guidance gain, based on miss distance, one may examine the effect of k on roll rate. In Figure 9 roll-angle and roll-rate time-histories are presented for a small initial error angle and several values of k, while in Figure 10 roll time-histories are presented for a large initial error angle. The first observation one makes is that the feedforward compensation technique works extremely well in maintaining small roll errors, $\phi_c - \phi_v$, when ε is small. Secondly, peak roll-rates occur near the aimpoint independent of the value of guidance gain. Finally, an average roll-rate increase is observed as the gain increases. Thus, by selecting the smallest gain that will not compromise miss-distance performance, moderate roll-rates can be maintained over most of the trajectory. Based on these results, the gain may be bracketed as follows:

$$1.0 \leq k \leq 2.0.$$

To compute k for different initial values of the non-dimensional parameter,

$$\mu_o = \frac{\varepsilon_o}{(L/V_o m)t_f} \tag{88}$$

the following empirical formula is used:

$$k = \begin{cases} 1. + 5\mu_o; & \mu_o < .2 \\ 2.; & \mu_o \geq .2 \end{cases} \tag{89}$$

Formula (89) is an estimate of the gain that produces small miss-distances at moderate roll-rates. A more refined analysis may lead to a better empirical formula, but (89) seems adequate for the present study.

Having selected a guidance gain, one may examine the effect of parameter changes on vehicle performance using the present steering law. In Figures 11 and 12 the roll time-constant is varied from .5 to 1.0 second for both small and large initial error angles. The feedforward compensation technique appears to be adequate in reducing roll-errors, $\phi_c - \phi_v$, for time-constants up to 1.0 second, although a deterioration of its effectiveness can be observed by comparing the roll-angle time-histories of Figure 11.2 with Figure 12.2 and Figure 11.4 with Figure 12.4. Moreover, from a comparison of Figures 11.1 and 12.1, the increased time-lag noticeably effects the line-of-sight error response. Ultimately, for time-constants larger than 1.0 second serious degradations in miss-distance performance can be expected.

In Figure 13 the line-of-sight error and roll time-histories are plotted for 6.0 units trim angle-of-attack. The change to a lower angle of attack increases the value of μ_0, and hence from formula (89) the value of gain is increased from 1.5 to 1.9. The increase in gain is adequate in reducing the line-of-sight error, while maintaining moderate roll-rates.

In Figures 14 and 15 the effect of roll-rate limit on the present steering law performance is examined. In Figure 14 a roll-rate limit

of 1.0 unit/second is applied to the control system and time-histories are displayed for both large and small initial error angles. From the roll time-histories of Figures 14.2 and 14.4, only the roll-rate peaks near the aimpoint are affected by the limit, and this occurrence does not seriously degrade terminal accuracy. In Figure 15 a roll-rate-command limit of .5 units/second is applied and is effective in modifying the control commands during the last time-unit of flight. Even with this rate-limiting, however, the feedforward compensation technique works sufficiently well in reducing roll-errors, $\varphi_C - \varphi_V$, as can be observed in Figures 15.2 and 15.4. A deterioration in accuracy is observed with the .5 unit/second rate-limit.

In Figure 16, the effect of initial roll-angle on steering-law performance is exhibited for a small initial error angle. In Figure 16.2 the feedforward compensation technique is not effective in quickly reducing the large initial roll-angle-error, $\varphi_C - \varphi_V$, the reduction requiring nearly one-quarter time-unit to accomplish. In this particular engagement no degradation in steering accuracy results; however, in engagements that are marginal with respect to being able to reach the sight-line, a one-quarter time-unit lag in roll-angle response may lead to a significant loss in accuracy. For such engagements the roll-rate command should be given by a delta function, which was neglected in these studies. By using an approximation to the delta function a high roll-rate-command would cause the vehicle to rapidly orient its lift vector in the proper direction. The previously noted

one-quarter time-unit lag in roll-response would thus be reduced, allowing enough time for the vehicle to reach the sight-line.

Having utilized a first-order roll system to establish guidance gains that achieve desired accuracy at moderate roll-rates and having verified that the performance of the steering algorithm is robust with respect to parameter and initial conditions variations, one may now, with some confidence, apply the steering algorithm to the non-linear, fifth-order, roll system described in Chapter VII.B. The autopilot incorporates realistic limits on both $\Delta\phi_c$ and $\Delta\dot{\phi}_c$ as well as on signals in the actuation system.

In Figure 17 time-histories are presented for both small and large initial error angles with α_T = 10 units. No performance degradation is noted using the realistic control system and the present steering algorithm. In Figures 18 and 19 the effect of initial roll-angle and initial error-angle on the maneuver is displayed for α_T = 6 units.

In summary, the feedback control law and feedforward compensation technique work effectively in steering the vehicle when a realistic model for the roll system is used. The robustness of the present guidance law with respect to initial conditions and maneuver level has been amply demonstrated. The guidance gain computed from formula (89) has proven to be adequate in steering the vehicle accurately while maintaining roll-control-commands that are compatible with realistic autopilot and actuator limits.

Having verified the robustness of the current steering algorithm in a realistic model of the roll system, one may compare its accuracy with that obtained using the existing steering laws from equations (9) and (16). In Table 2 normalized steering errors are tabulated for the three steering laws using a trim angle of attack of 10 units, while in Table 3 steering errors are tabulated for α_T = 6 units. To obtain a range of initial error angles, the initial flight-path-angle is varied from 0. to -50 degrees holding initial position constant. From Table 2 (α_T = 10 units) one observes that the time-optimal steering law, equation (9), exhibits somewhat better accuracy than the dive-line steering law, equation (16). More dramatic, however, is the order-of-magnitude improvement in accuracy of the present steering law as compared to the existing laws. These same comments apply to results presented in Table 3 (α_T = 6 units) for those trajectories for which the sight-line is reachable. A slight improvement in accuracy is noted for these trajectories with, however, a large penalty being paid for reducing the maneuverability of the vehicle (by reducing α_T to 6 units) and, therefore, precluding trajectories originating at γ_0 = 0. and γ_0 = -50.° from reaching the sight-line.

Table 1

Nominal Trajectory Parameters

Velocity	High supersonic
Bank angle	0. deg.
Autopilot time-constant	.3 sec.
Trim angle-of-attack	10. units
Dive line	Oriented along nominal path
Cross-product gain (k_{φ} in eq. (42))	2/3
Cross-product gains (k_1 and k_2 in eq. (38))	1.0

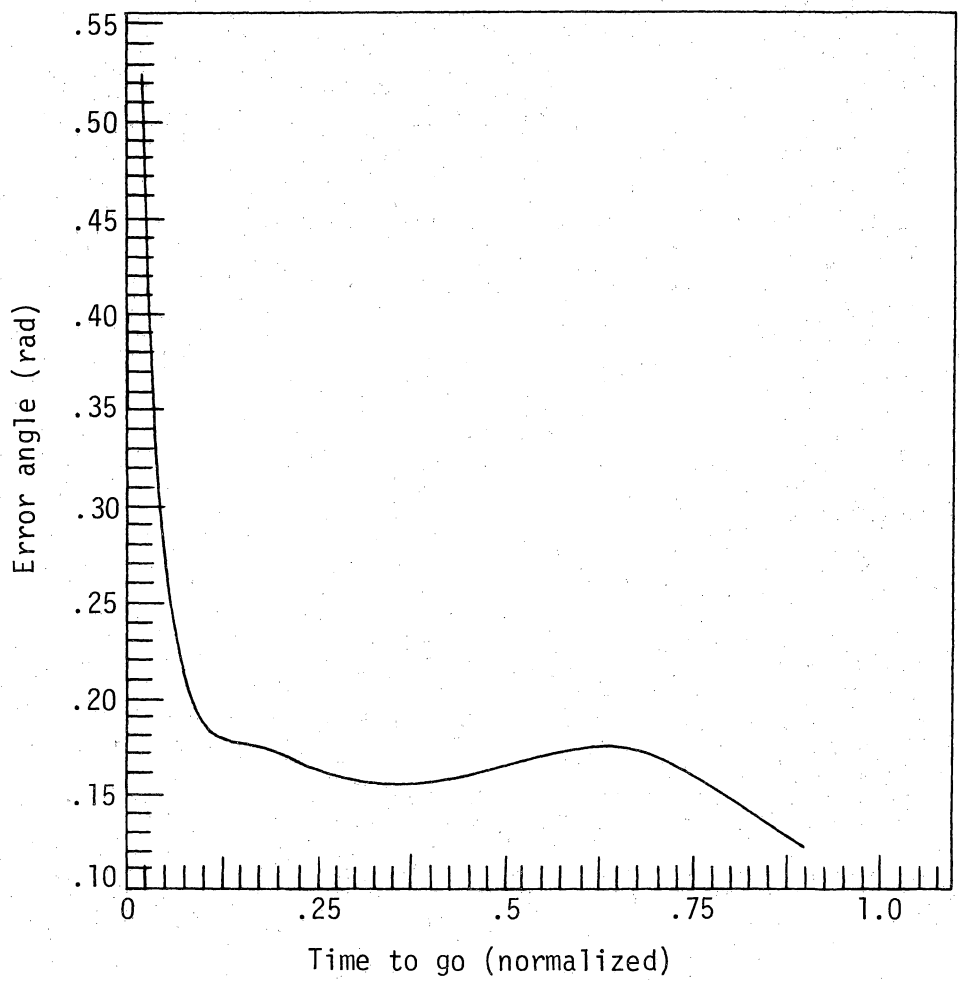

Parameters and initial conditions		
$k = 1.0$	$\phi_o = 0.0^o$	$\alpha_T = 10.0$ units
$\tau_\phi = .3$ sec	$\gamma_o = -35.0^o$	$p_L = 2.0$

Figure 5.1.- Error angle time-histories for variations in guidance gain and initial error angle.

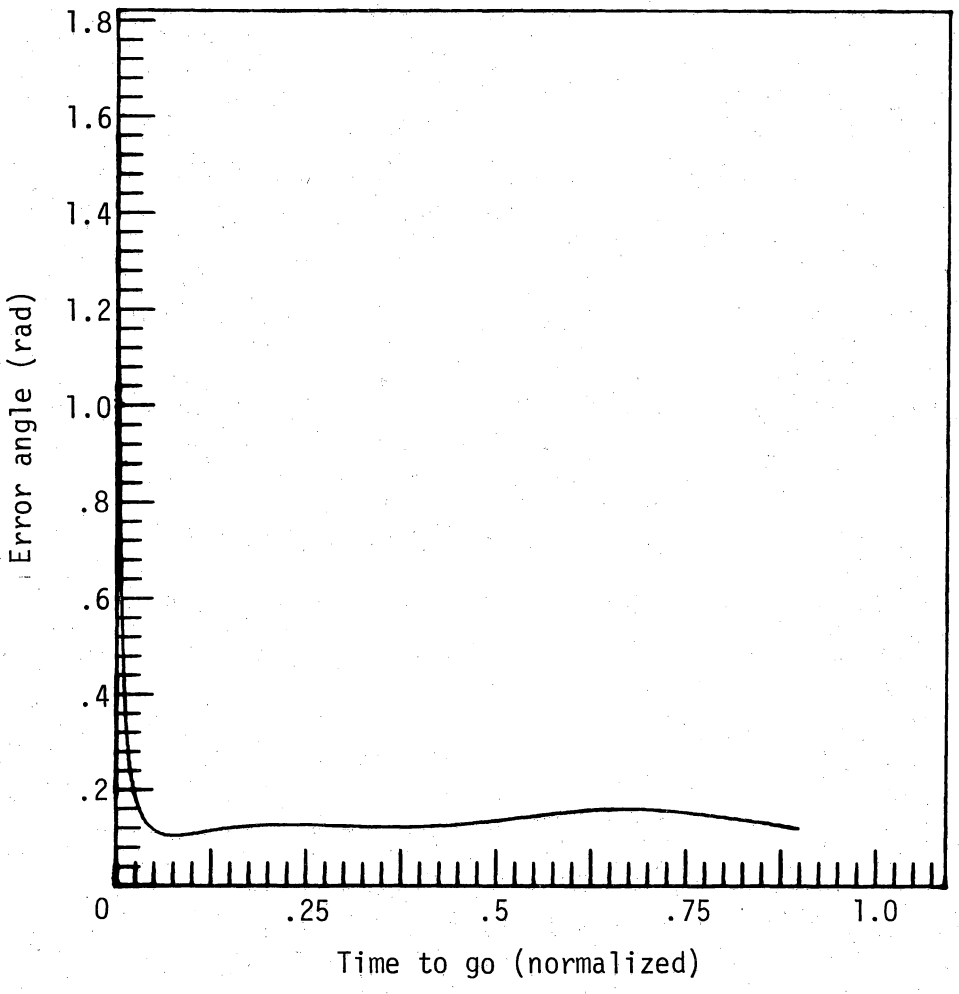

Parameters and initial conditions		
$k = 1.3$	$\phi_o = 0.0^o$	$\alpha_T = 10.0$ units
$\tau_\phi = .3$ sec	$\gamma_o = -35.0^o$	$p_L = 2.0$

Figure 5.2.- Error angle time-histories for variations in guidance gain and initial error angle.

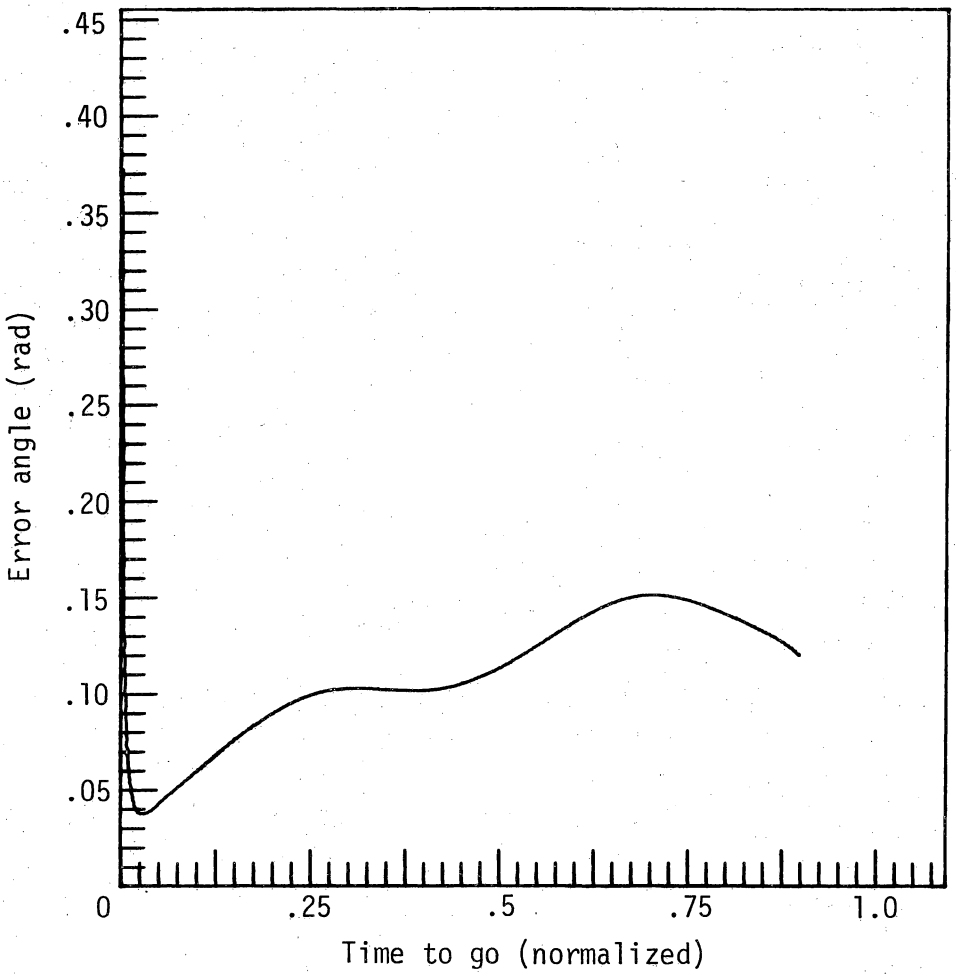

Parameters and initial conditions		
$k = 1.5$	$\phi_o = 0.0^o$	$\alpha_T = 10.0$ units
$\tau_\phi = .3$ sec	$\gamma_o = -35.0^o$	$p_L = 2.0$

Figure 5.3.- Error angle time-histories for variations in guidance gain and initial error angle.

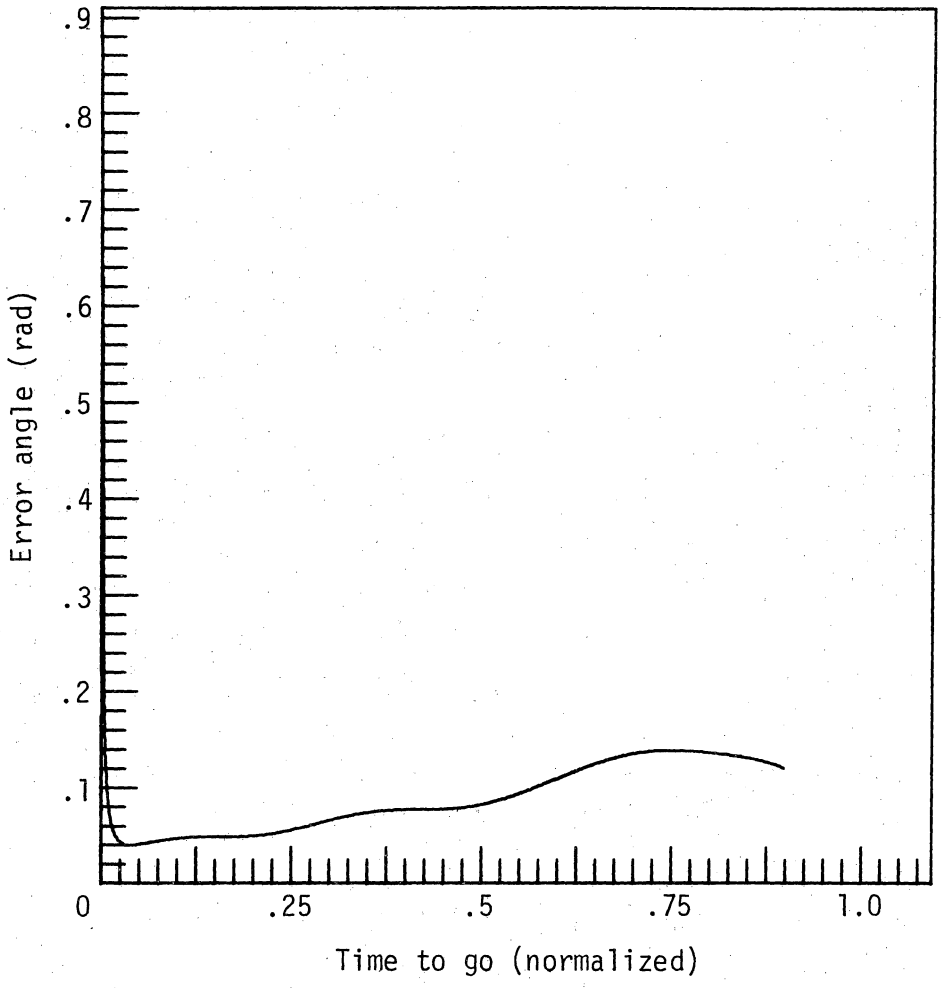

Parameters and initial conditions		
$k = 2.0$	$\phi_o = 0.0^o$	$\alpha_T = 10.0$ units
$\tau_\phi = .3$ sec	$\gamma_o = -35.0^o$	$p_L = 2.0$

Figure 5.4.- Error angle time-histories for variations in guidance gain and initial error angle.

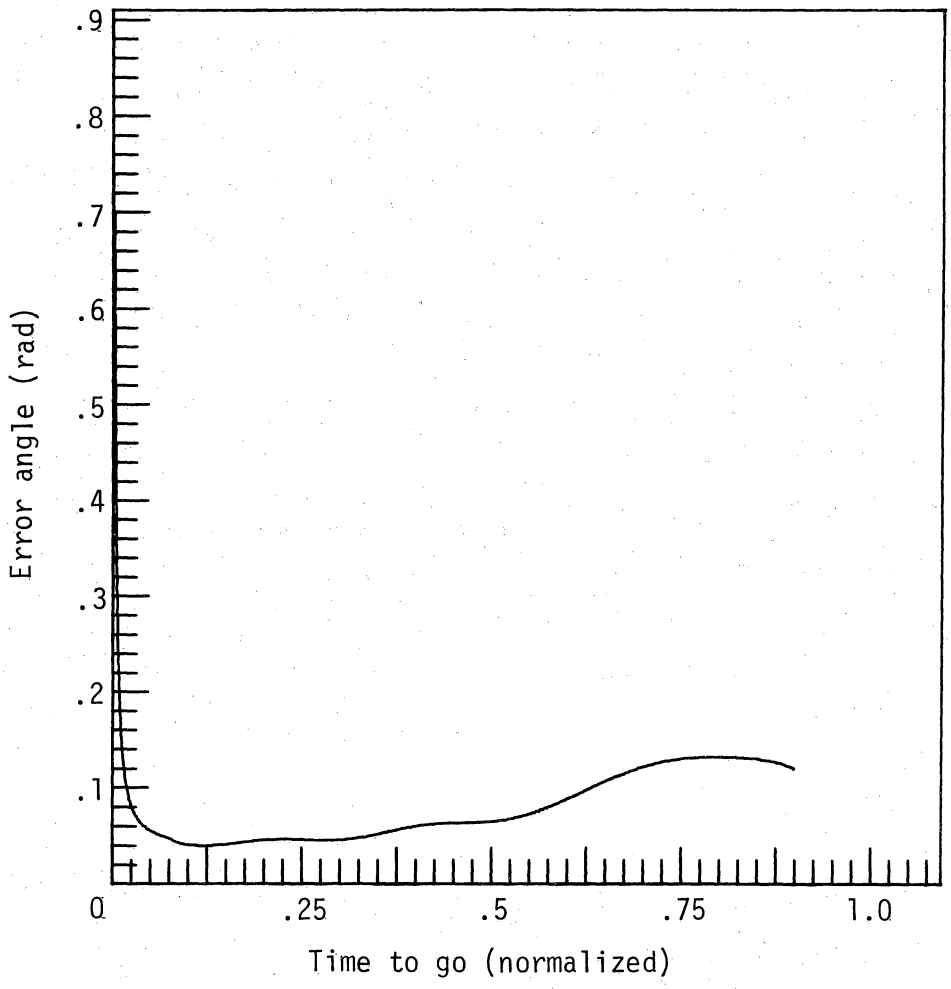

Parameters and initial conditions		
$k = 2.5$	$\phi_o = 0.0^o$	$\alpha_T = 10.0$ units
$\tau_\phi = .3$ sec	$\gamma_o = -35.0^o$	$p_L = 2.0$

Figure 5.5.- Error angle time-histories for variations in guidance gain and initial error angle.

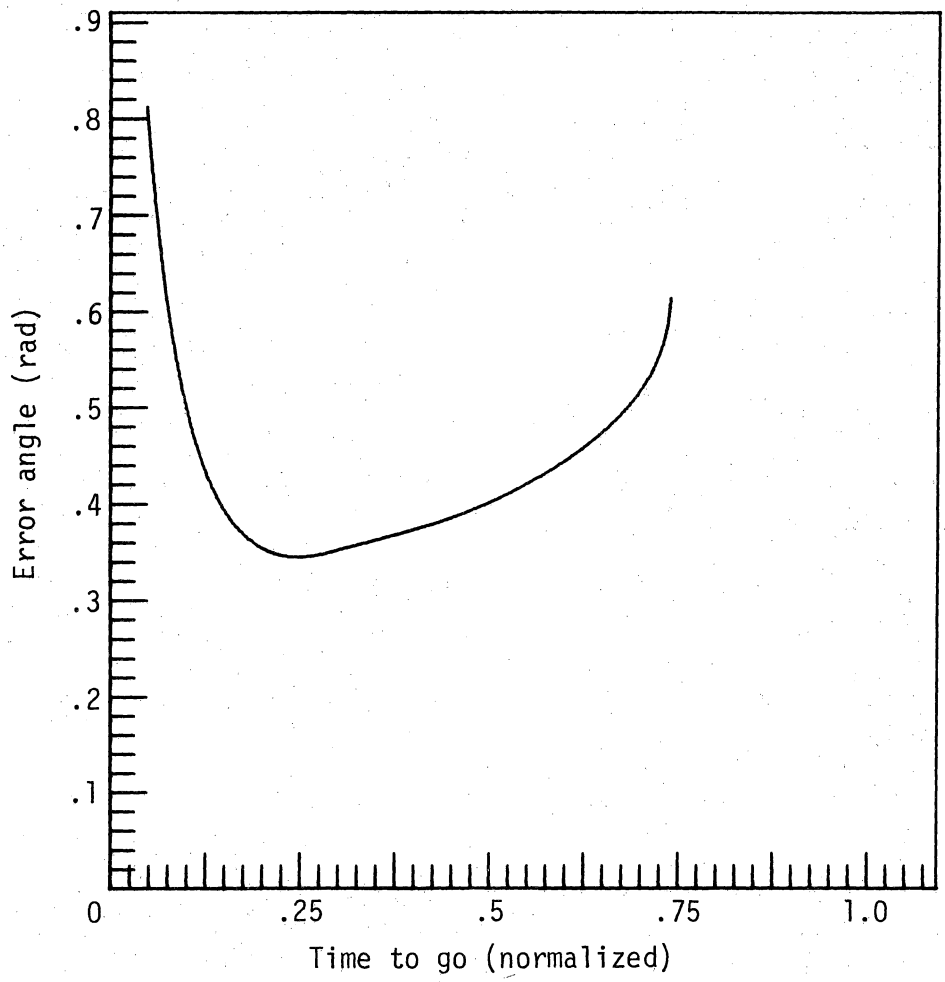

Parameters and initial conditions		
$k = 1.0$	$\phi_o = 0.0^o$	$\alpha_T = 10.0$ units
$\tau_\phi = .3$ sec	$\gamma_o = 0.0^o$	$p_L = 2.0$

Figure 6.1.- Error angle time-histories for variations in guidance gain and initial error angle.

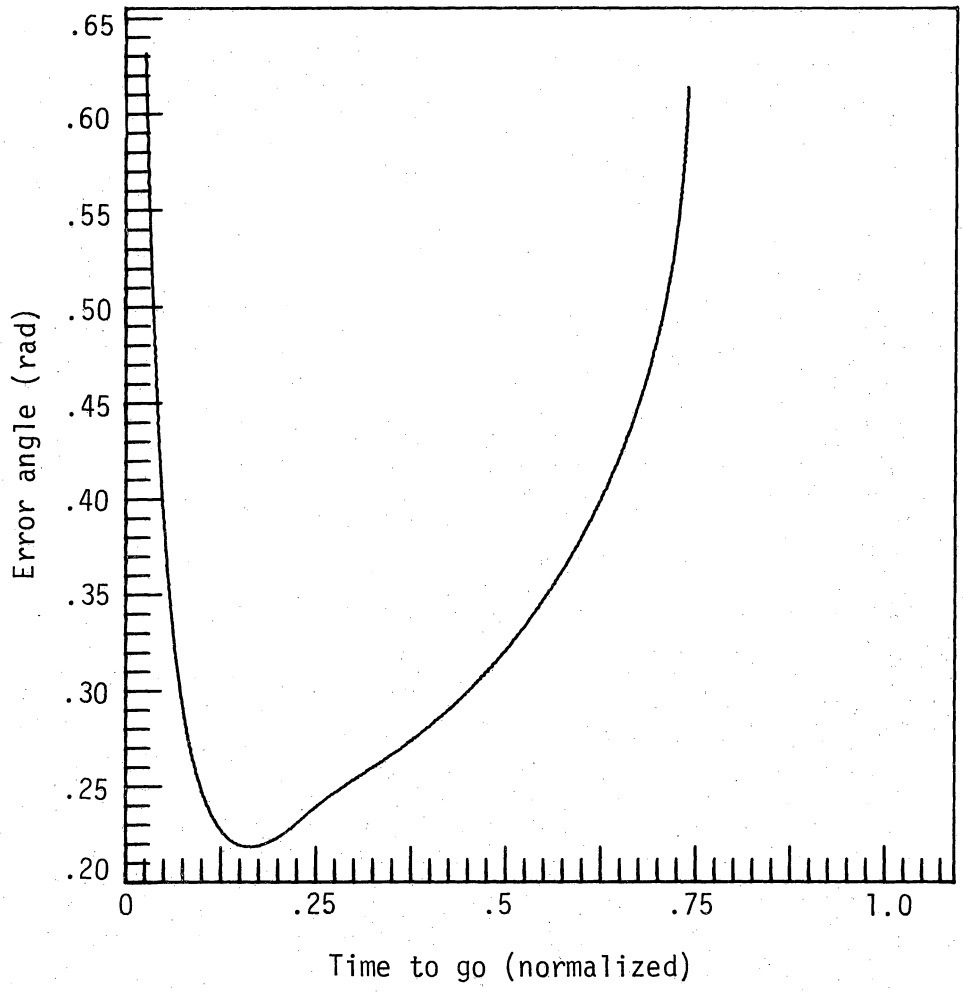

Parameters and initial conditions		
$k = 1.3$	$\phi_o = 0.0^o$	$\alpha_T = 10.0$ units
$\tau_\phi = .3$ sec	$\gamma_o = 0.0^o$	$p_L = 2.0$

Figure 6.2.- Error angle time-histories for variations in guidance gain and initial error angle.

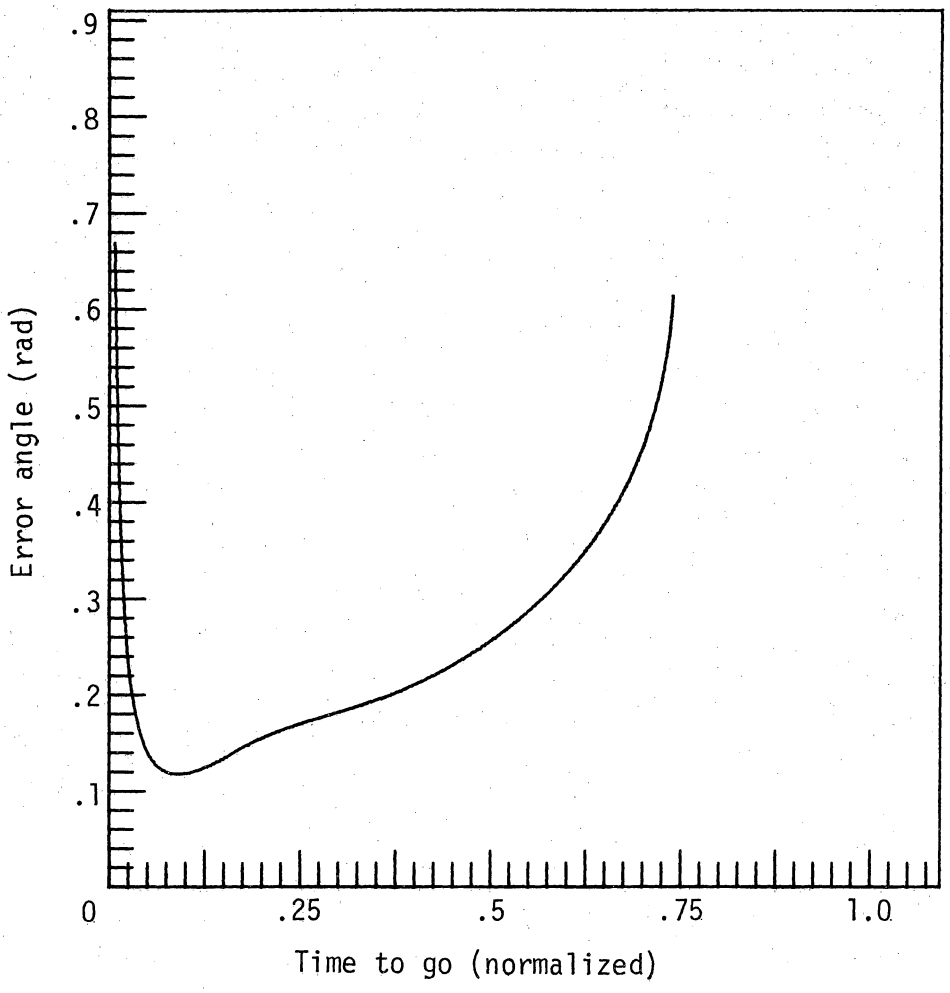

Parameters and initial conditions		
$k = 1.5$	$\phi_o = 0.0^o$	$\alpha_T = 10.0$ units
$\tau_\phi = .3$ sec	$\gamma_o = 0.0^o$	$p_L = 2.0$

Figure 6.3.- Error angle time-histories for variations in guidance gain and initial error angle.

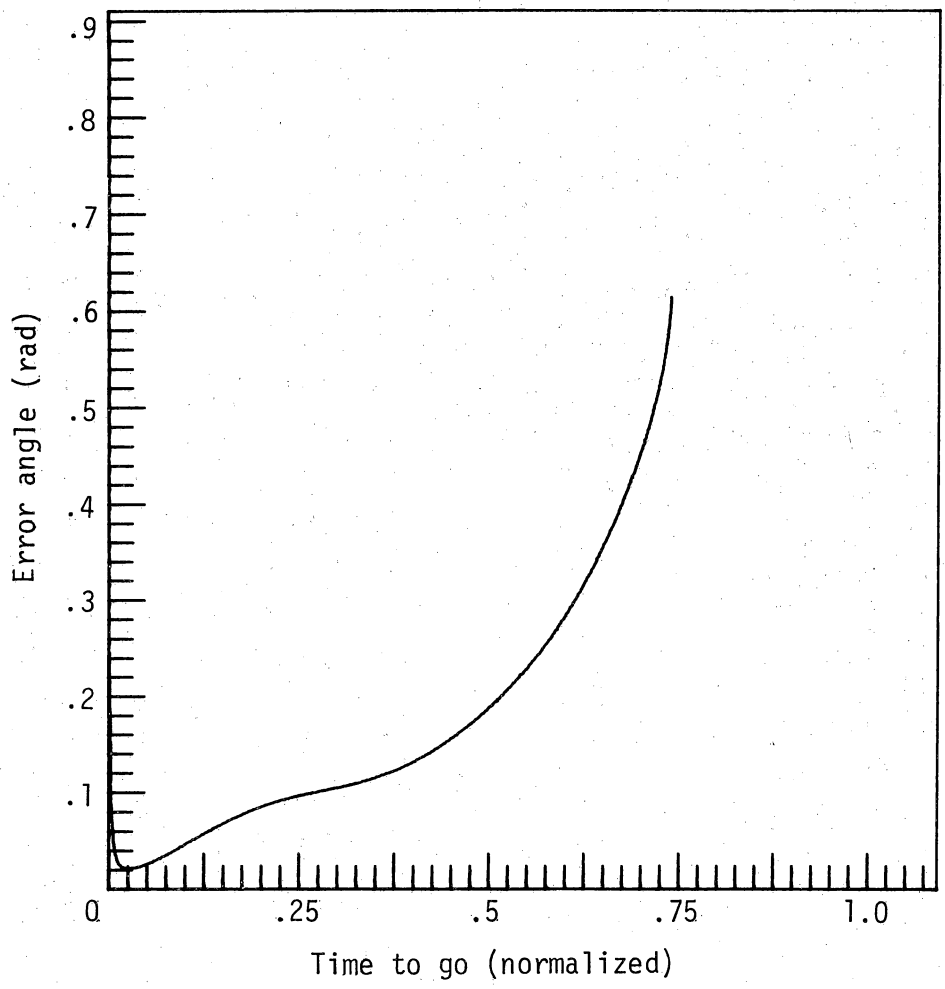

Parameters and initial conditions		
$k = 2.0$	$\phi_o = 0.0^o$	$\alpha_T = 10.0$ units
$\tau_\phi = .3$ sec	$\gamma_o = 0.0^o$	$p_L = 2.0$

Figure 6.4.- Error angle time histories for variations in guidance gain and initial error angle.

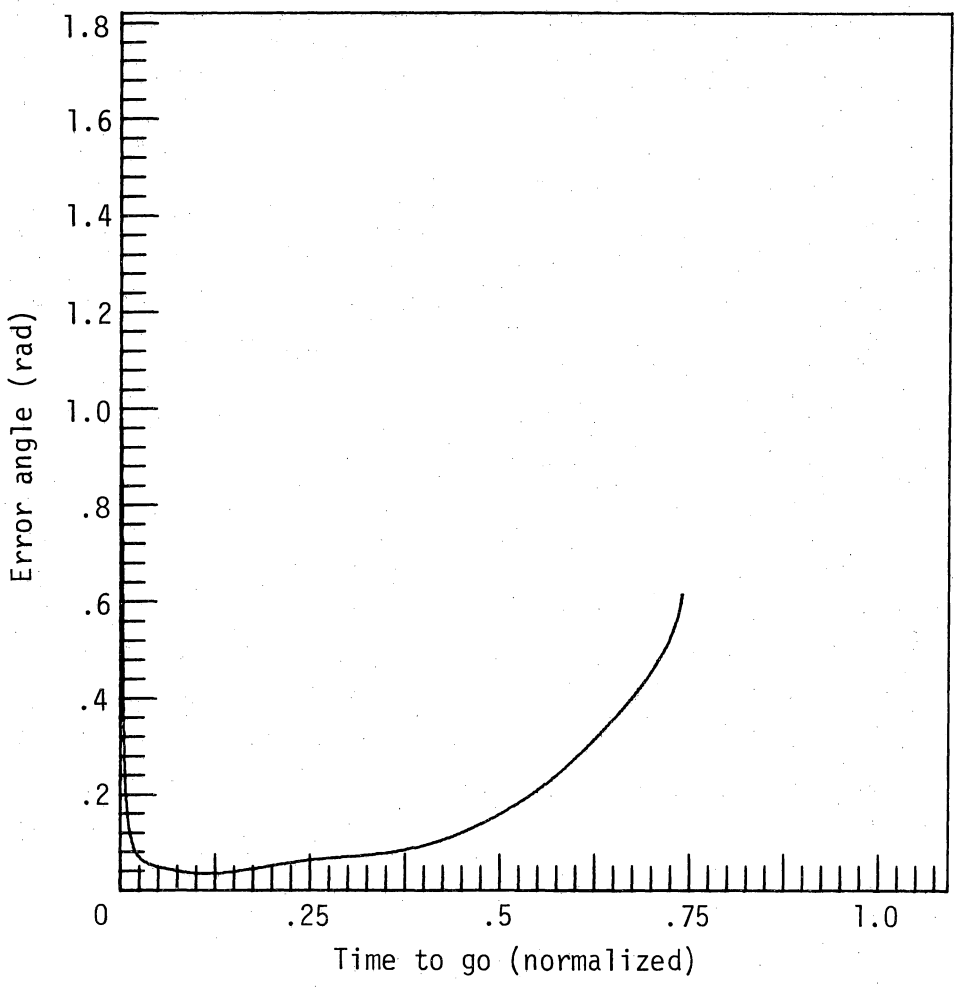

Parameters and initial conditions		
$k = 2.5$	$\phi_o = 0.0^o$	$\alpha_T = 10.0$ units
$\tau_\phi = .3$ sec	$\gamma_o = 0.0^o$	$p_L = 2.0$

Figure 6.5.- Error angle time-histories for variations in guidance gain and initial error angle.

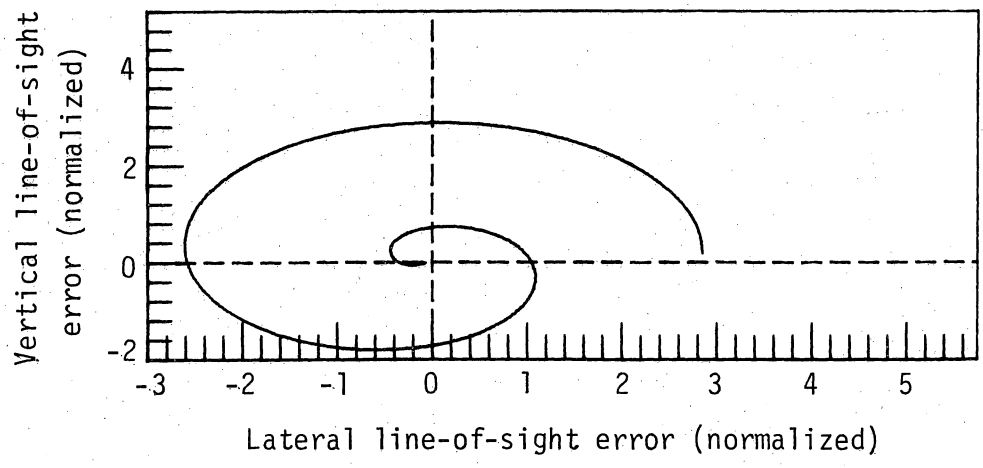

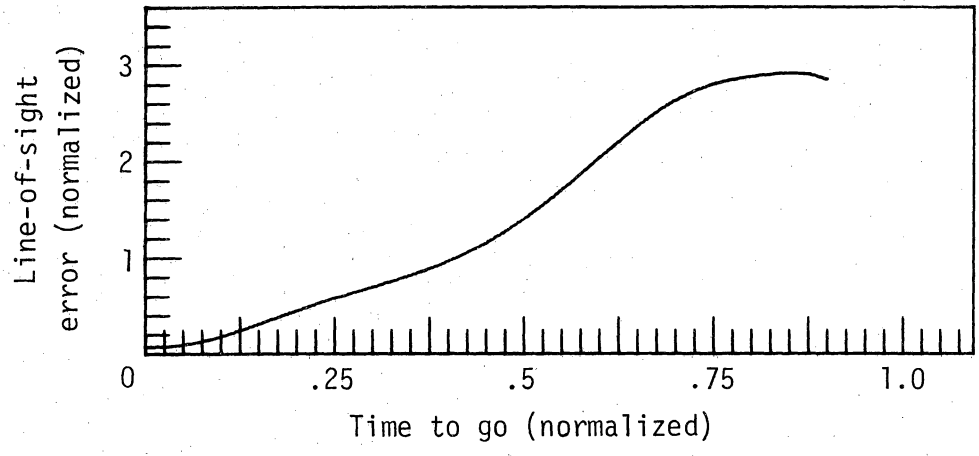

Parameters and initial conditions		
$k = 1.3$	$\phi_0 = 0.0^o$	$\alpha_T = 10.0$ units
$\tau_\phi = .3$ sec	$\gamma_0 = -35.0^o$	$p_L = 2.0$

Figure 7.1.- Line-of-sight error histories for variations in guidance gain and initial error angle.

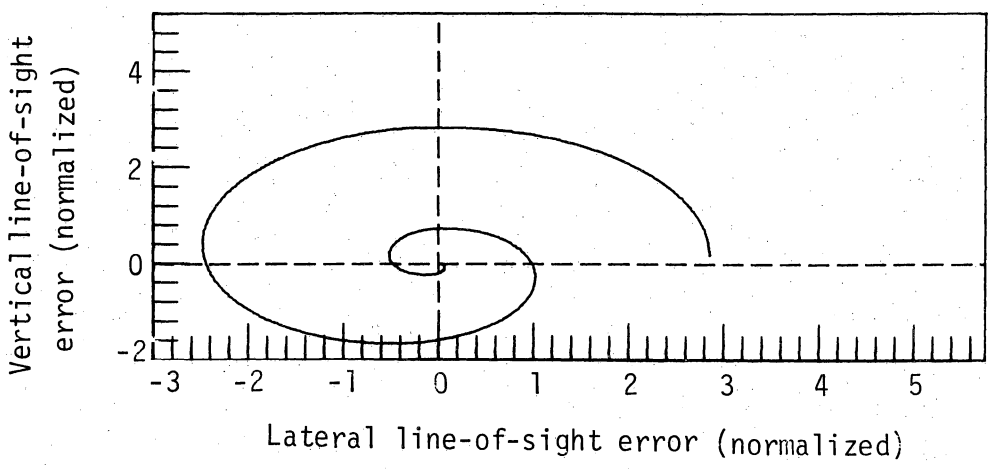

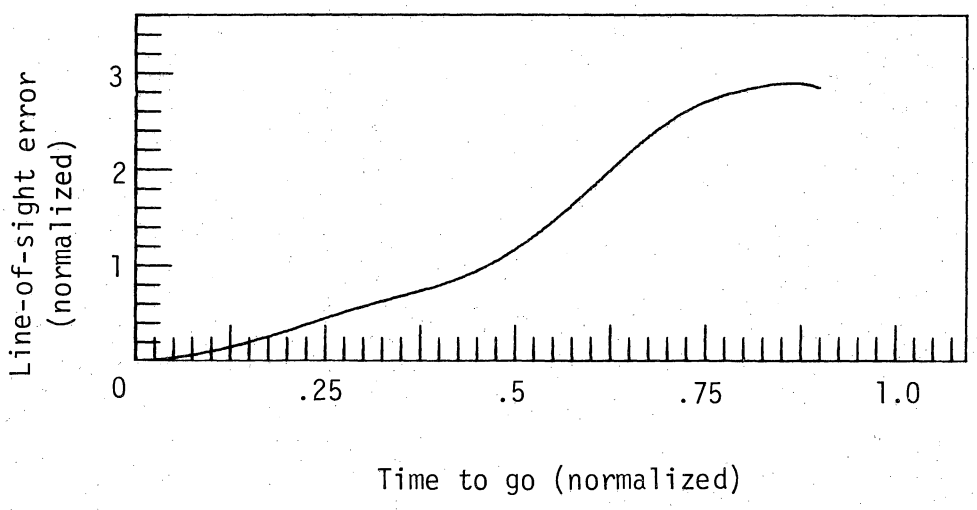

Parameters and initial conditions		
$k = 1.5$	$\phi_o = 0.0^o$	$\alpha_T = 10.0$ units
$\tau_\phi = .3$ sec	$\gamma_o = -35.0^o$	$p_L = 2.0$

Figure 7.2.- Line-of-sight error histories for variations in guidance gain and initial error angle.

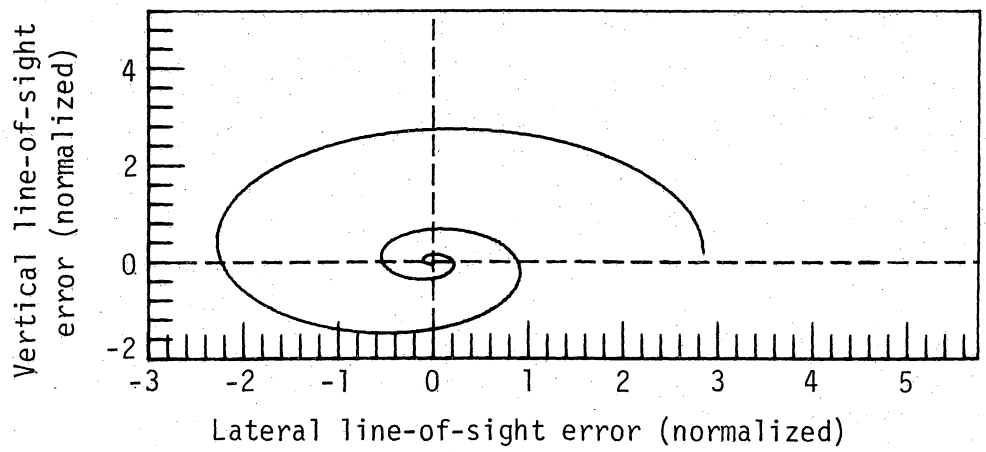

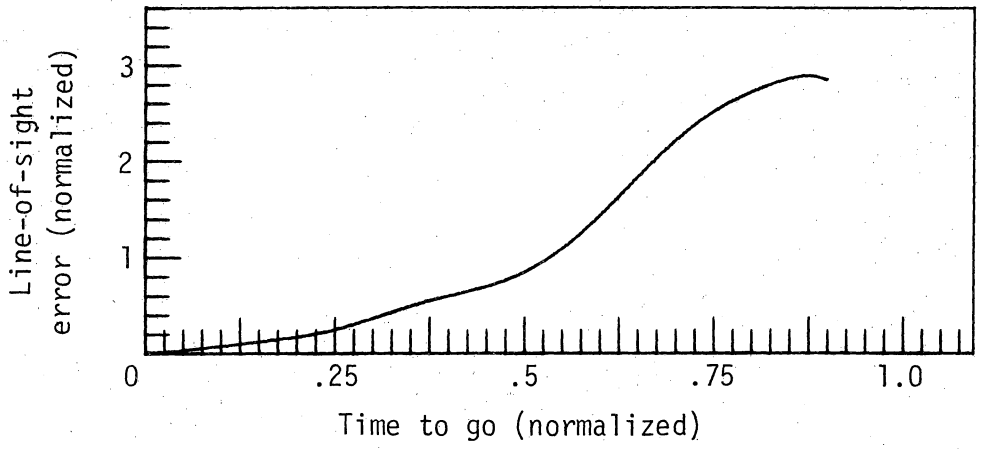

Parameters and initial conditions		
$k = 2.0$	$\phi_o = 0.0^o$	$\alpha_T = 10.0$ units
$\tau_\phi = .3$ sec	$\gamma_o = -35.0^o$	$p_L = 2.0$

Figure 7.3.- Line-of-sight error histories for variations in guidance gain and initial error angle.

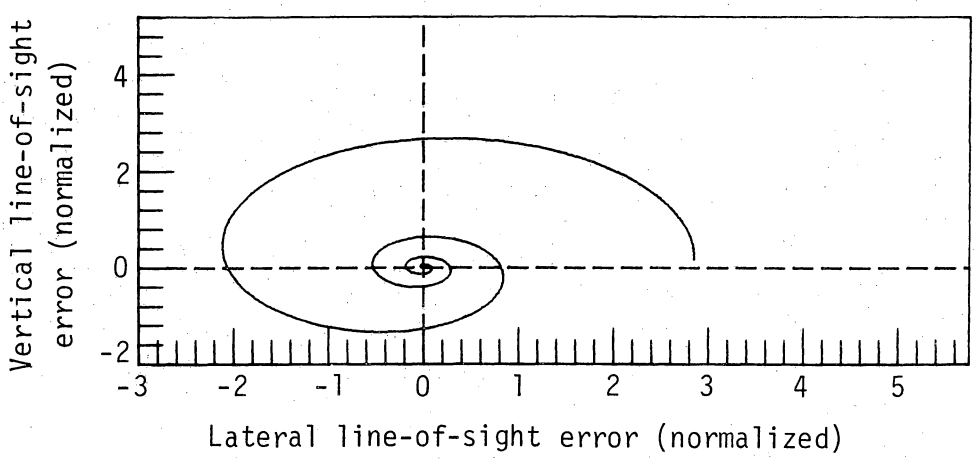

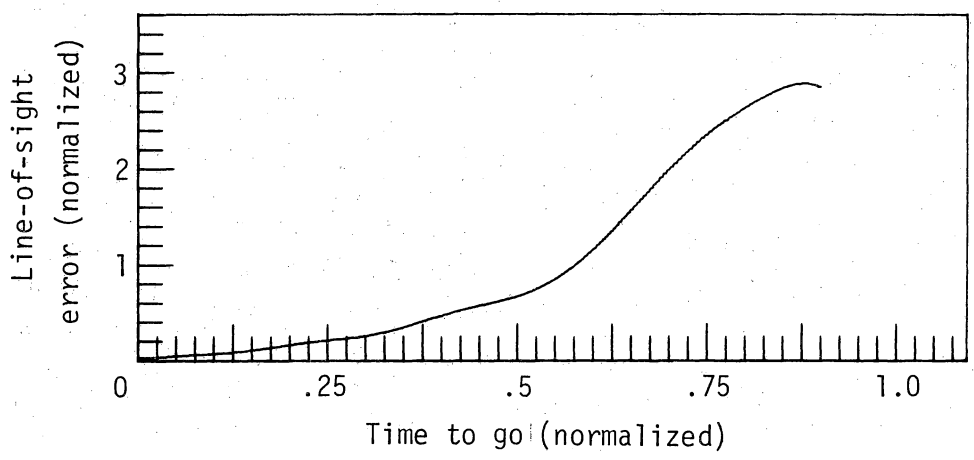

Parameters and initial conditions		
$k = 2.5$	$\phi_o = 0.0^o$	$\alpha_T = 10.0$ units
$\tau_\phi = .3$ sec	$\gamma_o = -35.0^o$	$p_L = 2.0$

Figure 7.4.- Line-of-sight error histories for variations in guidance gain and initial error angle.

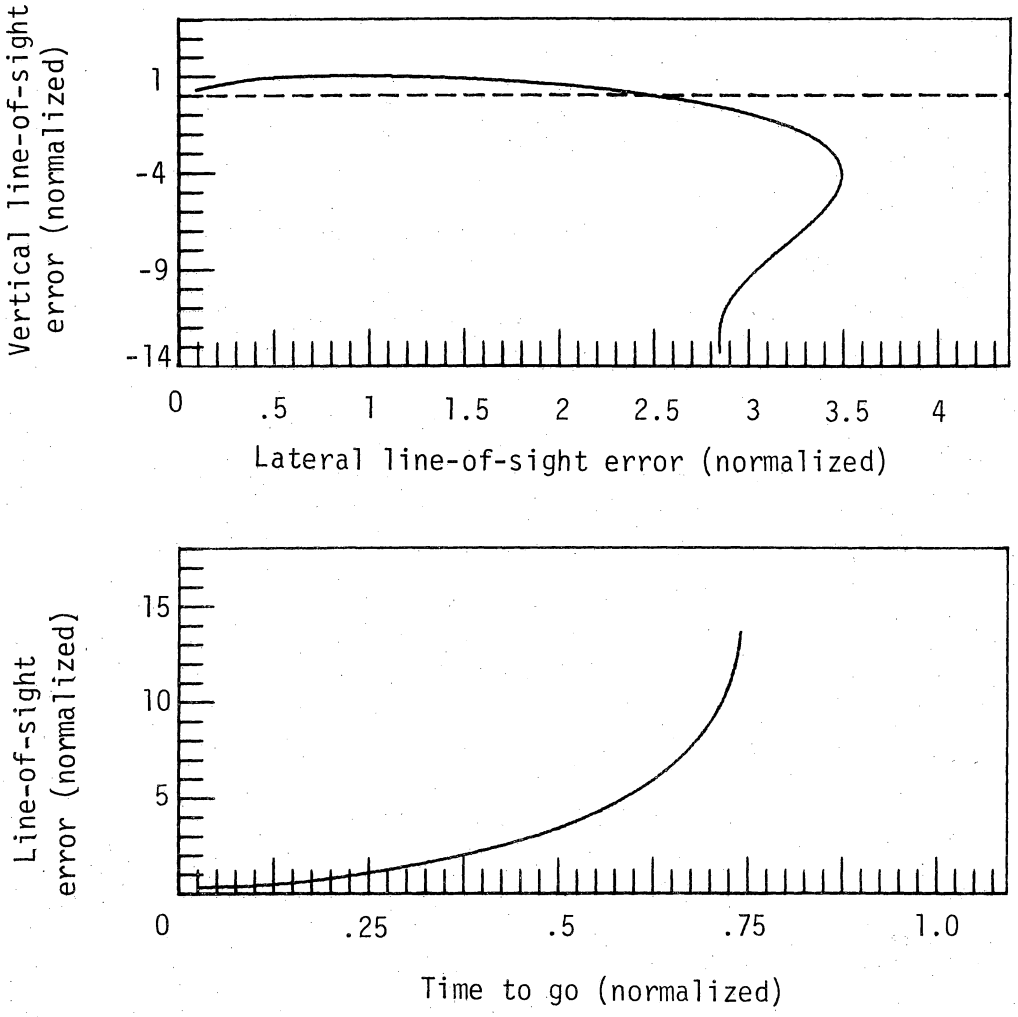

Parameters and initial conditions		
$k = 1.3$	$\phi_o = 0.0^o$	$\alpha_T = 10.0$ units
$\tau_\phi = .3$ sec	$\gamma_o = 0.0^o$	$p_L = 2.0$

Figure 8.1.- Line-of-sight error histories for variations in guidance gain and initial error angle.

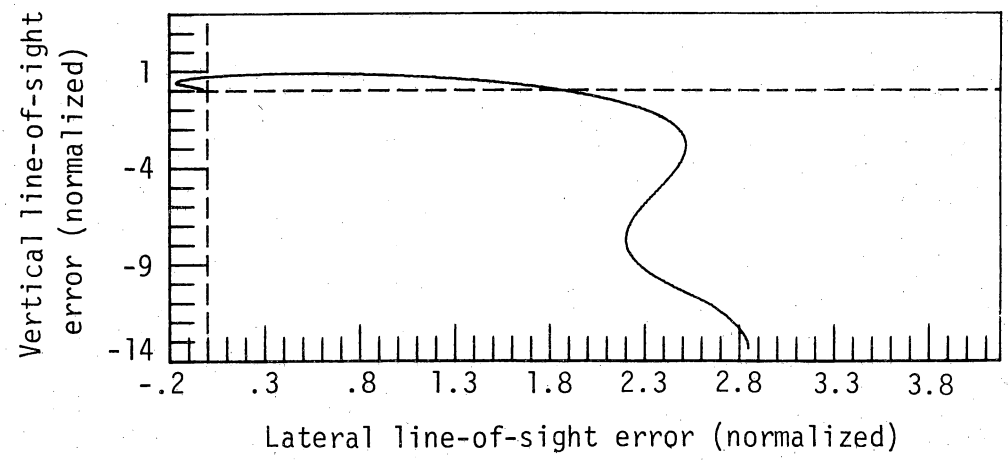

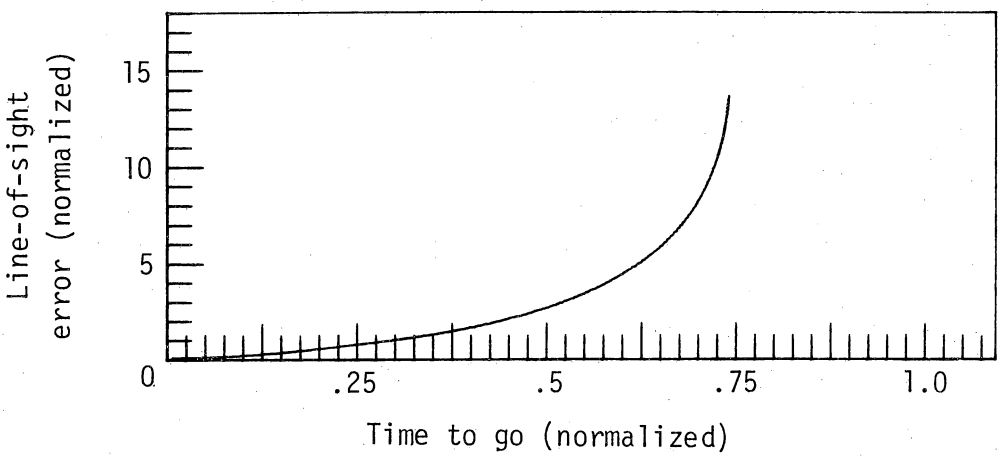

Parameters and initial conditions

$k = 1.5$ $\phi_o = 0.0^o$ $\alpha_T = 10.0$ units

$\tau_\phi = .3$ sec $\gamma_o = 0.0^o$ $P_L = 2.0$

Figure 8.2.- Line-of-sight error histories for variations in guidance gain and initial error angle.

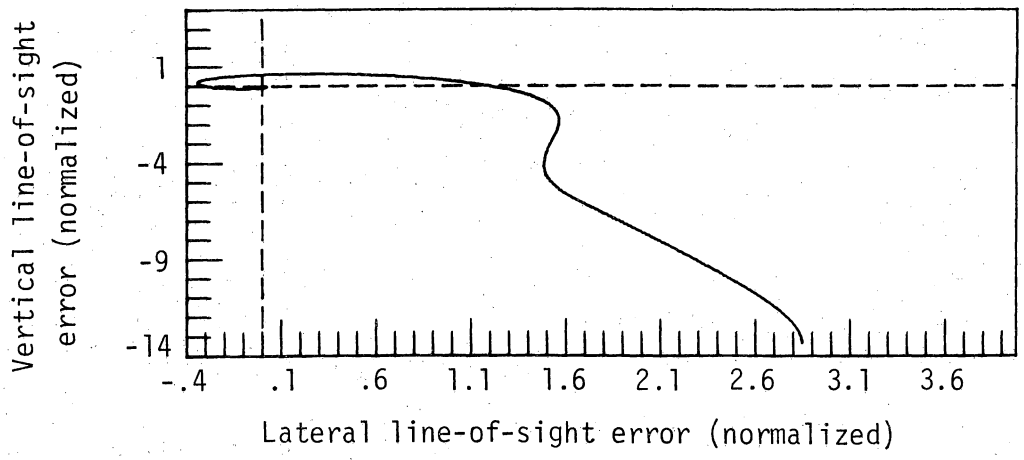

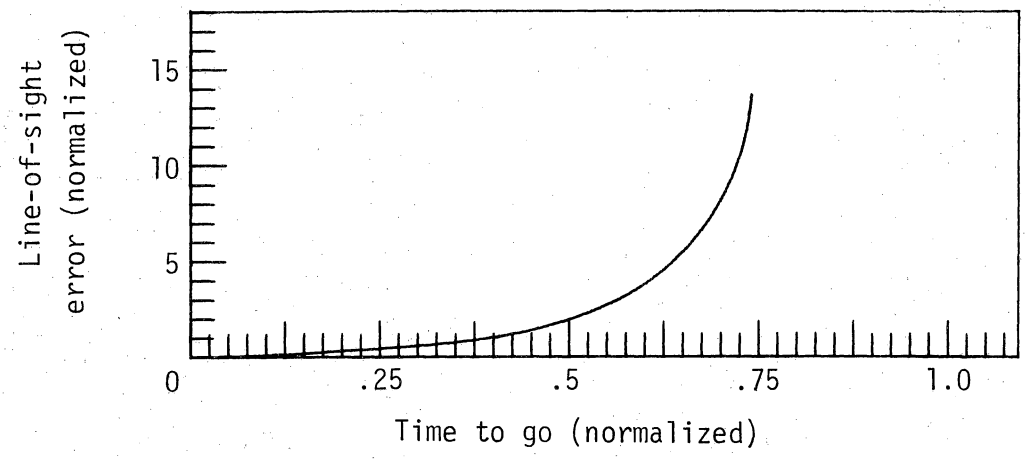

Parameters and initial conditions

$k = 2.0$ $\phi_o = 0.0^o$ $\alpha_T = 10.0$ units

$\tau_\phi = .3$ sec $\gamma_o = 0.0^o$ $P_L = 2.0$

Figure 8.3.- Line-of-sight error histories for variations in guidance gain and initial error angle.

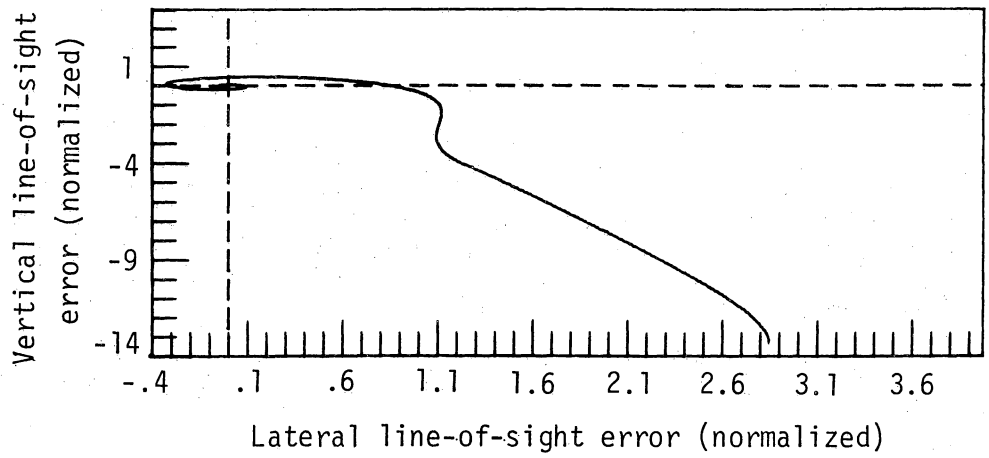

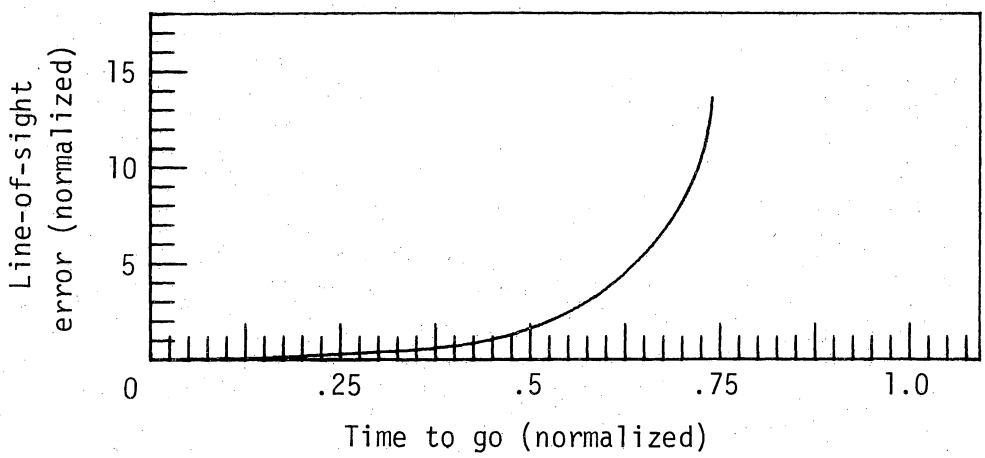

Parameters and initial conditions

$k = 2.5 \quad \phi_0 = 0.0^0 \quad \alpha_T = 10.0$ units

$\tau_\phi = .3$ sec $\quad \gamma_0 = 0.0^0 \quad P_L = 2.0$

Figure 8.4.- Line-of-sight error histories for variations in guidance gain and initial error angle.

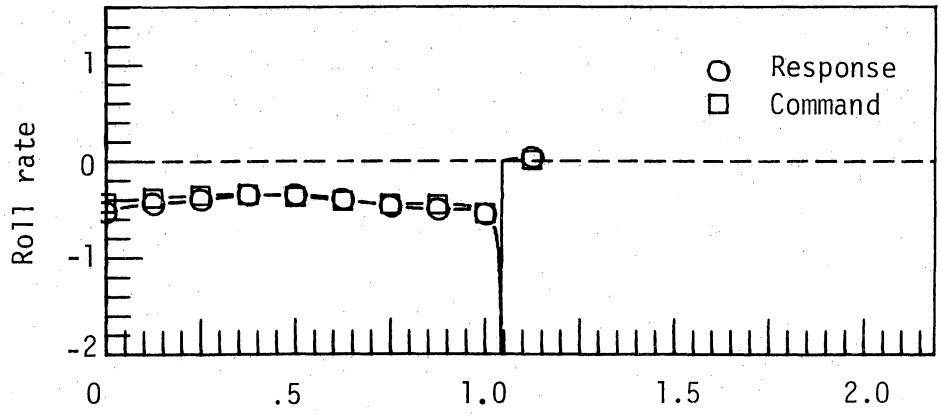

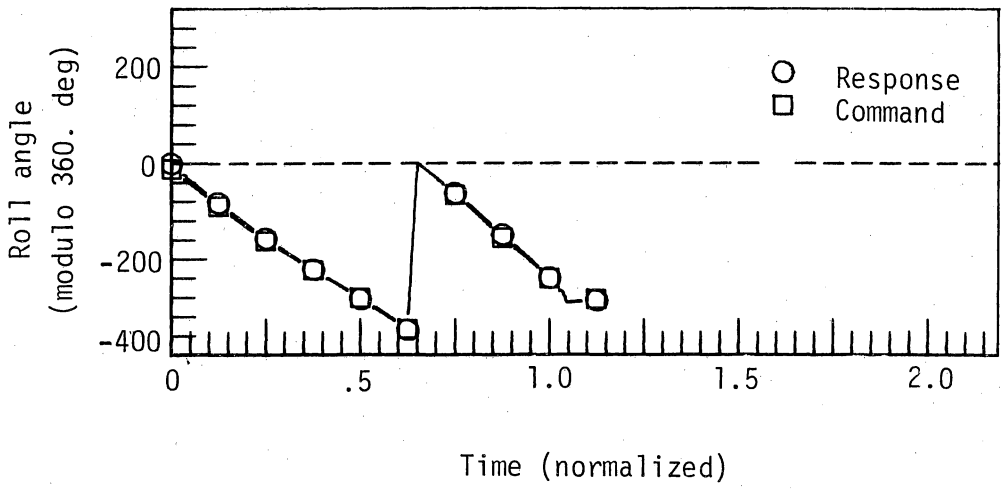

Parameters and initial conditions		
$k = 1.3$	$\phi_o = 0.0^o$	$\alpha_T = 10.0$ units
$\tau_\phi = .3$ sec	$\gamma_o = -35.0^o$	$p_L = 2.0$

Figure 9.1.- Roll time-histories for variations in guidance gain and initial error angle.

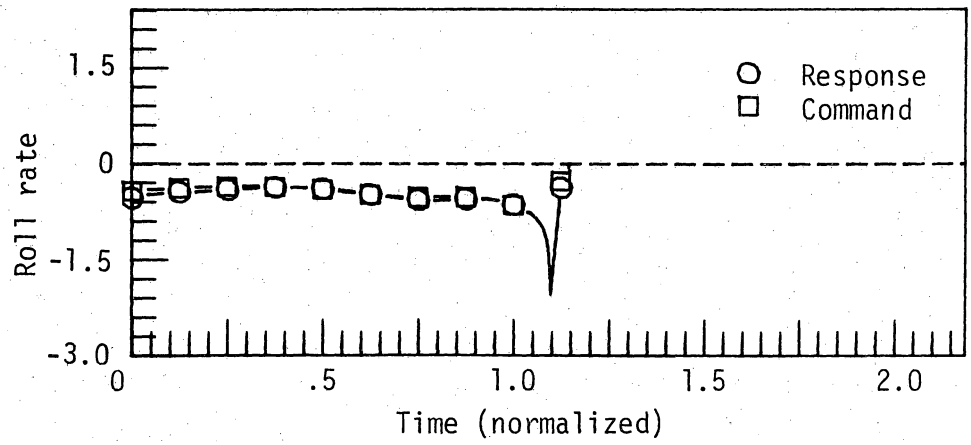

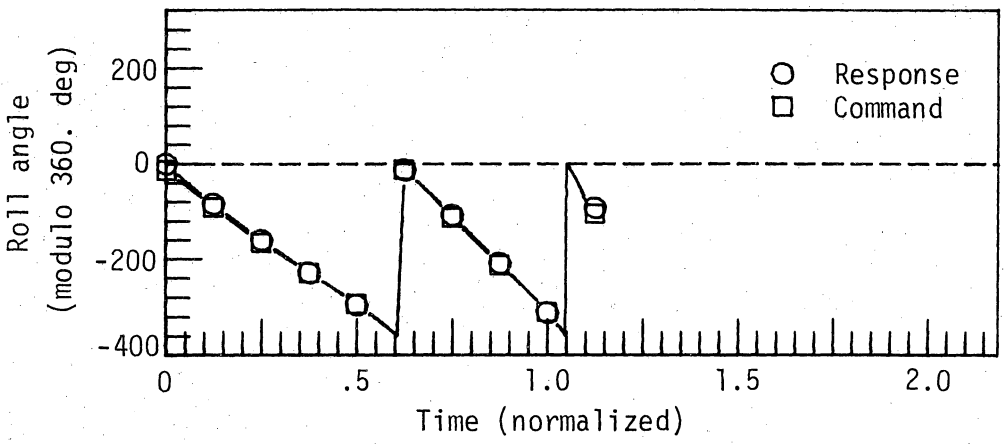

Parameters and initial conditions		
$k = 1.5$	$\phi_o = 0.0^o$	$\alpha_T = 10.0$ units
$\tau_\phi = .3$ sec	$\gamma_o = -35.0^o$	$p_L = 2.0$

Figure 9.2.- Roll time-histories for variations in guidance gain and initial error angle.

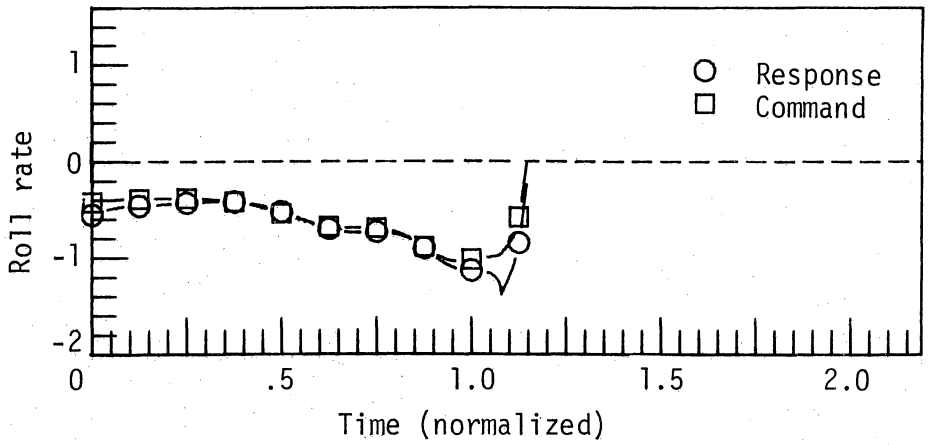

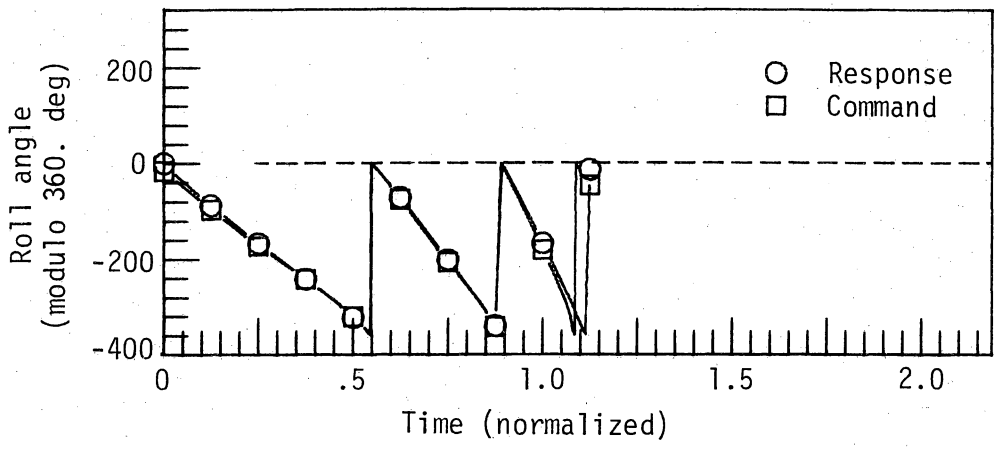

Parameters and initial conditions		
$k = 2.0$	$\phi_o = 0.0^o$	$\alpha_T = 10.0$ units
$\tau_\phi = .3$ sec	$\gamma_o = -35.0^o$	$p_L = 2.0$

Figure 9.3.- Roll time-histories for variations in guidance gain and initial error angle.

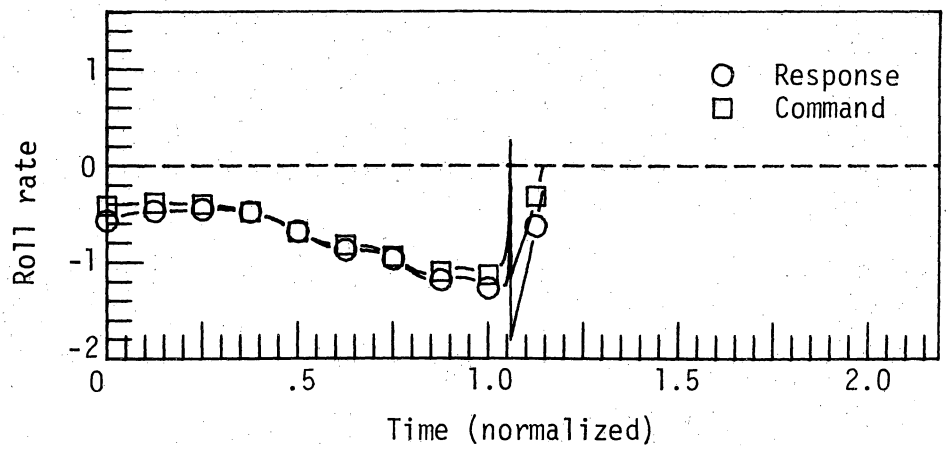

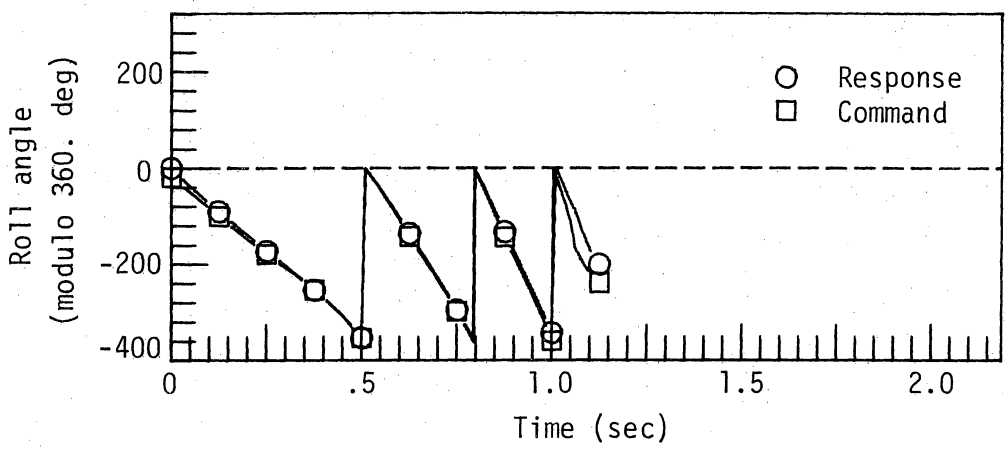

Parameters and initial conditions		
$k = 2.5$	$\phi_o = 0.0^o$	$\alpha_T = 10.0$ units
$\tau_\phi = .3$ sec	$\gamma_o = -35.0^o$	$p_L = 2.0$

Figure 9.4.- Roll time-histories for variations in guidance gain and initial error angle.

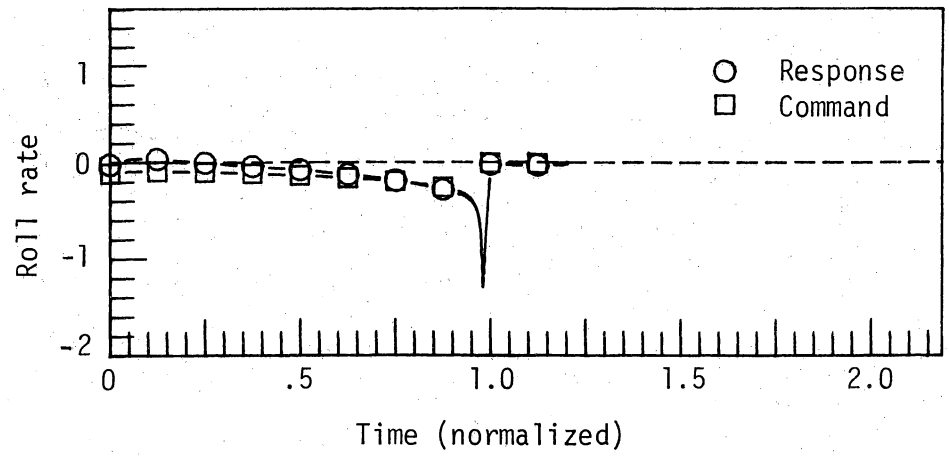

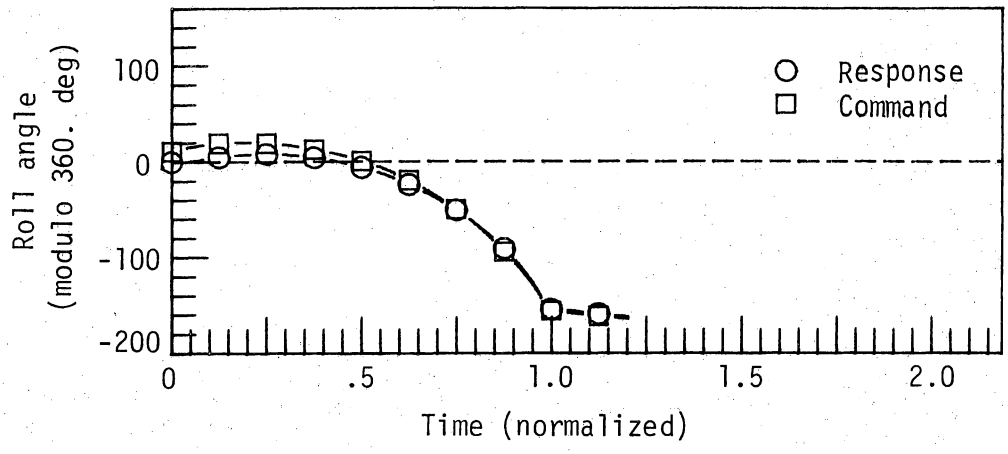

Parameters and initial conditions

$k = 1.3$ $\phi_0 = 0.0^o$ $\alpha_T = 10.0$ units

$\tau_\phi = .3$ sec $\gamma_0 = 0.0^o$ $P_L = 2.0$

Figure 10.1.- Roll time-histories for variations in guidance gain and initial error angle.

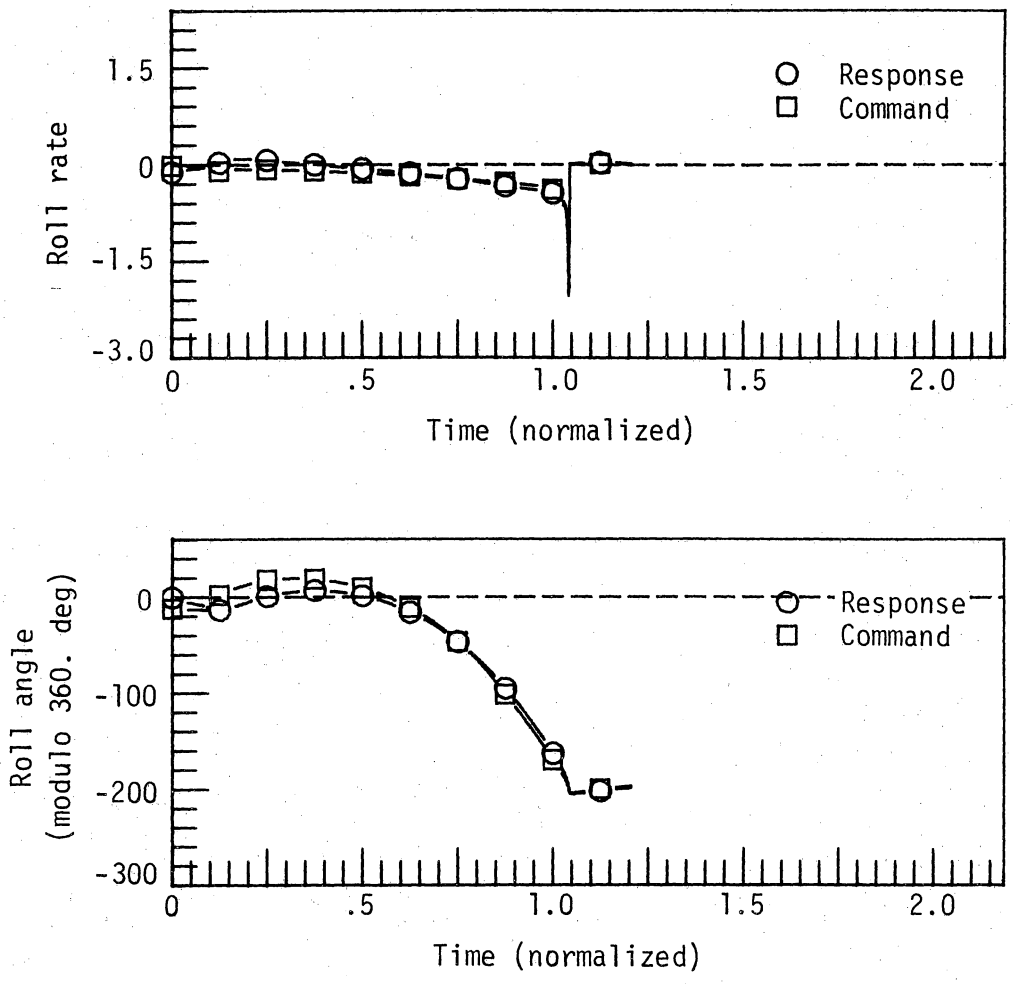

Parameters and initial conditions		
$k = 1.5$	$\phi_o = 0.0^o$	$\alpha_T = 10.0$ units
$\tau_\phi = .3$ sec	$\gamma_o = 0.0^o$	$p_L = 2.0$

Figure 10.2.- Roll time-histories for variations in guidance gain and initial error angle.

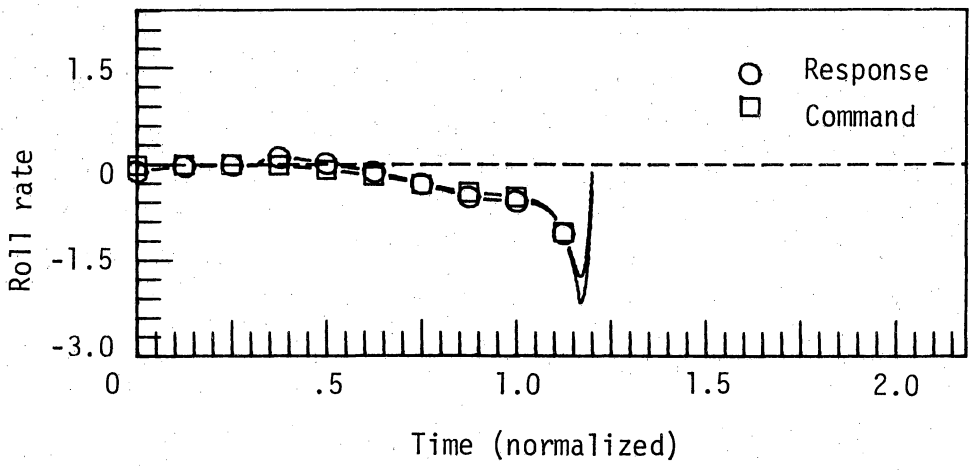

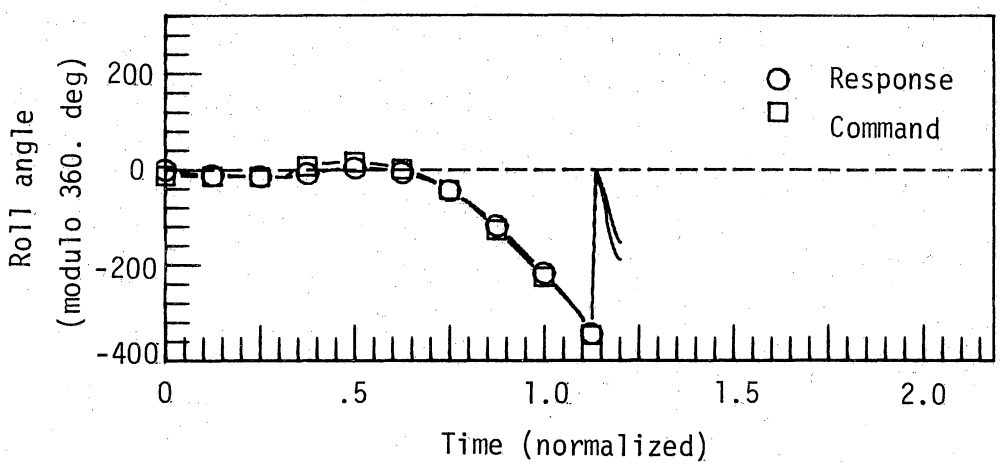

Parameters and initial conditions		
$k = 2.0$	$\phi_o = 0.0^o$	$\alpha_T = 10.0$ units
$\tau_\phi = .3$ sec	$\gamma_o = 0.0^o$	$p_L = 2.0$

Figure 10.3.- Roll time-histories for variations in guidance gain and initial error angle.

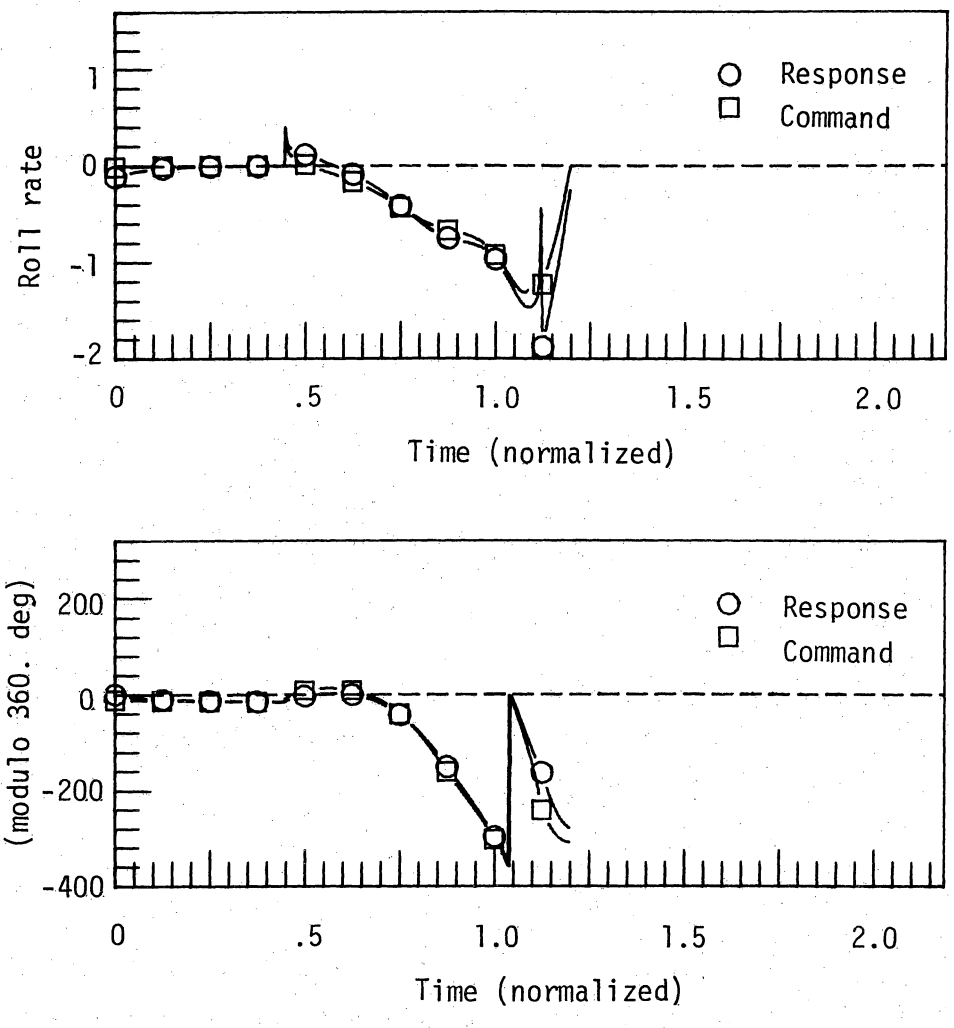

Parameters and initial conditions

$k = 2.5$ $\phi_o = 0.0^o$ $\alpha_T = 10.0$ units

$\tau_\phi = .3$ sec $\gamma_o = 0.0^o$ $P_L = 2.0$

Figure 10.4.- Roll time-histories for variations in guidance gain and initial error angle.

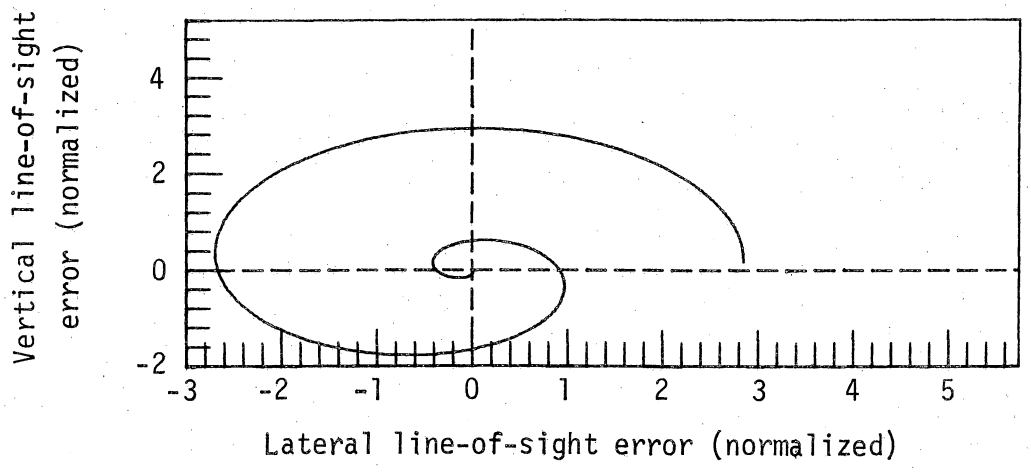

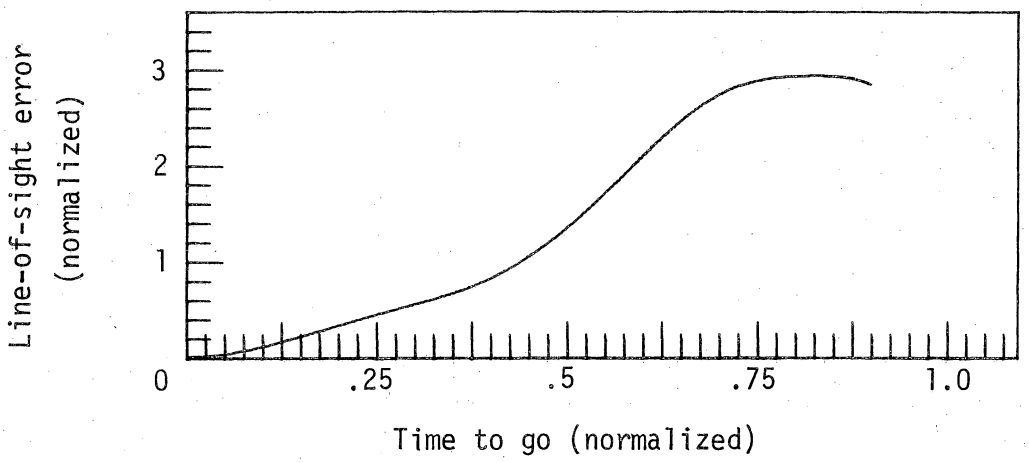

Parameters and initial conditions		
$k = 1.5$	$\phi_0 = 0.0^o$	$\alpha_T = 10.0$ units
$\tau_\phi = .5$ sec	$\gamma_0 = 35.0^o$	$P_L = 2.0$

Figure 11.1.- Line-of-sight error and roll time-histories for variations in roll time-constant and initial error angle.

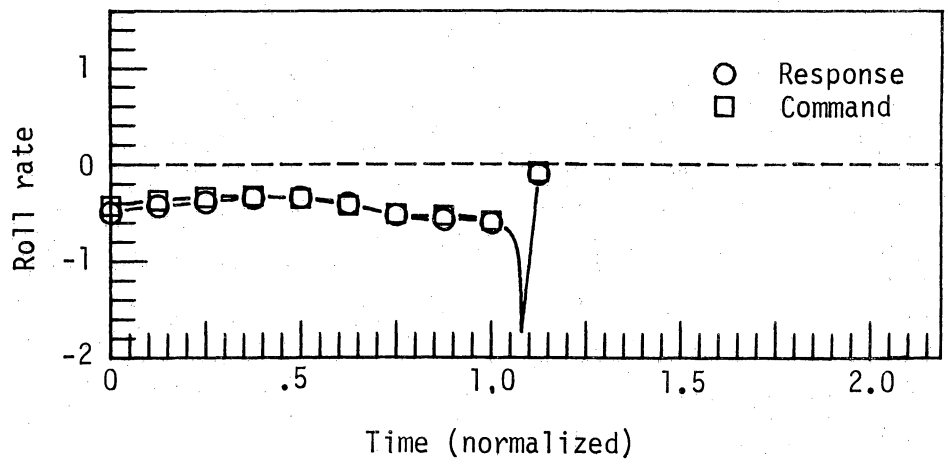

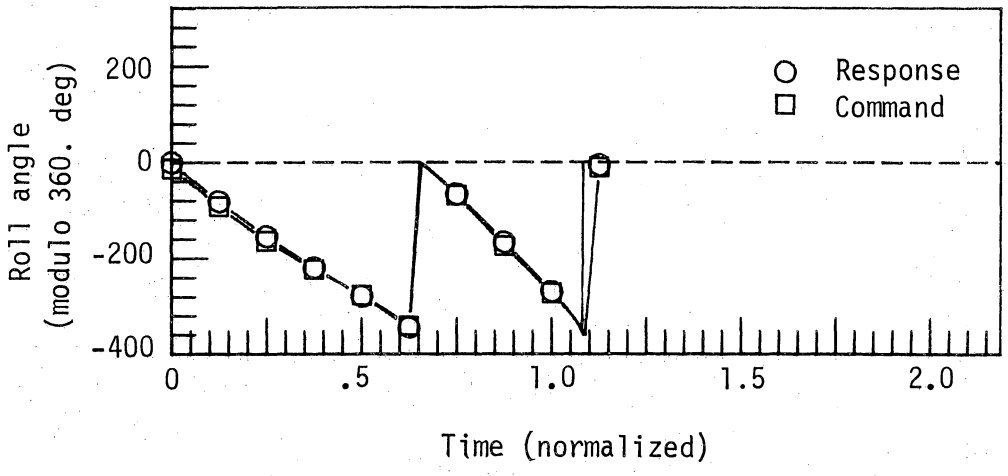

Parameters and initial conditions

$k = 1.5$ $\quad \phi_o = 0.0^o$ $\quad \alpha_T = 10.0$ units

$\tau_\phi = .5$ sec $\quad \gamma_o = 35.0^o$ $\quad P_L = 2.0$

Figure 11.2.- Line-of-sight error and roll time-histories for variations in roll time constant and initial error angle.

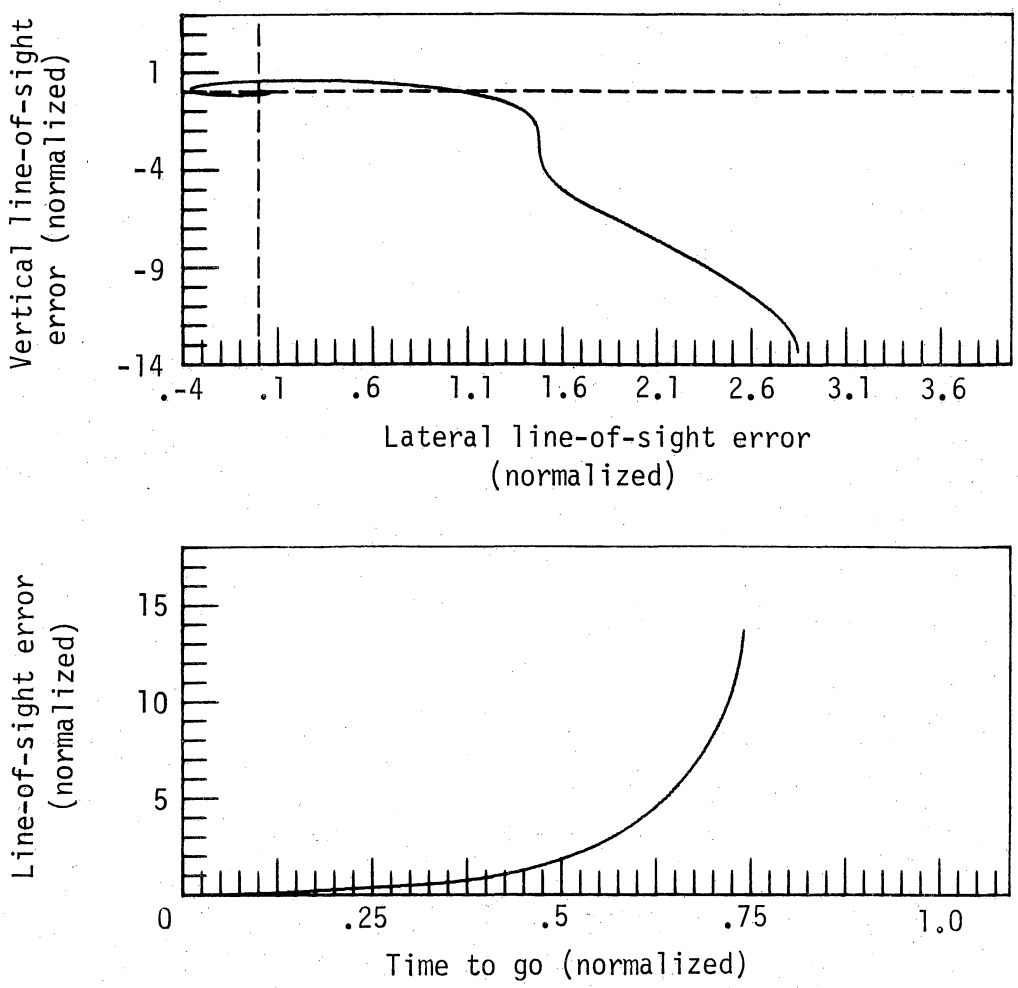

Parameters and initial conditions

$k = 2.0$ $\phi_o = 0.0^o$ $\alpha_T = 10.0$ units

$\tau_\phi = .5$ sec $\gamma_o = 0.0^o$ $P_L = 2.0$

Figure 11.3.- Line-of-sight error and roll time-histories for variations in roll time-constant and initial error angle.

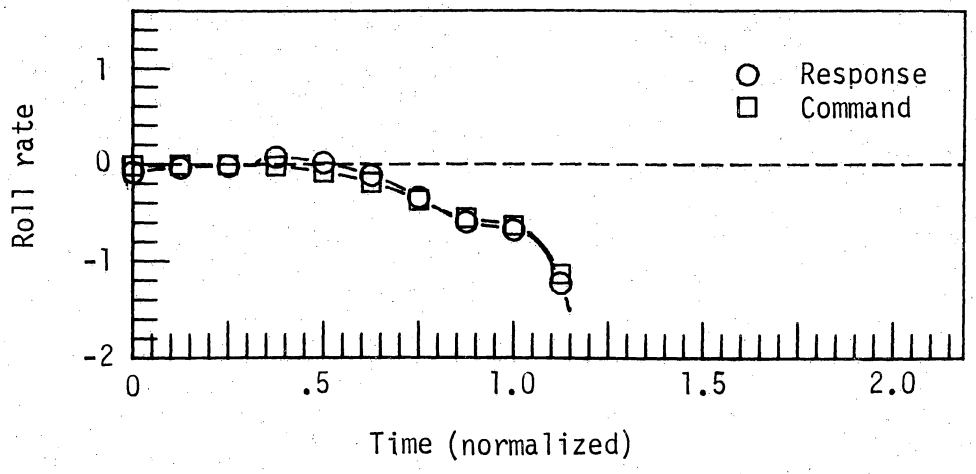

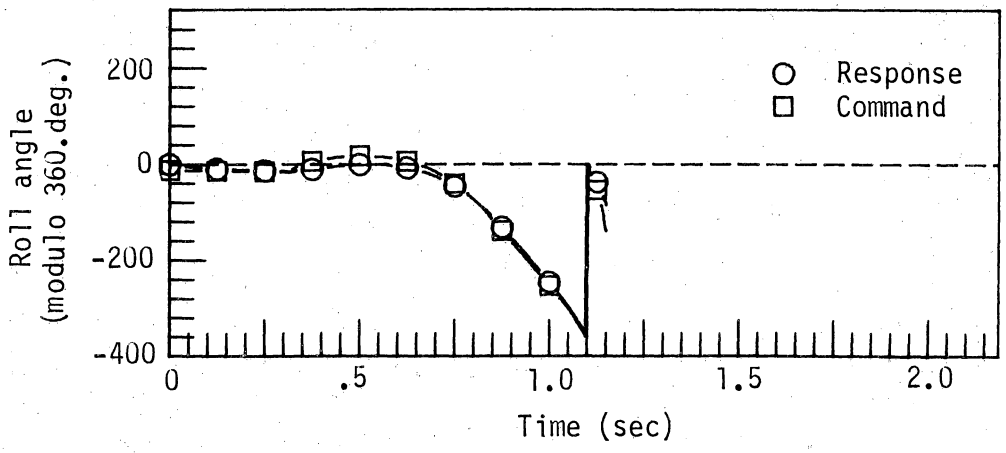

Parameters and initial conditions		
$k = 2.0$	$\phi_o = 0.0^o$	α_T 10.0 units
$\tau_\phi = .5$ sec	$\gamma_o = 0.0^o$	$P_L = 2.0$

Figure 11.4.- Line-of-sight error and roll time-histories for variations in roll time-constant and initial error angle.

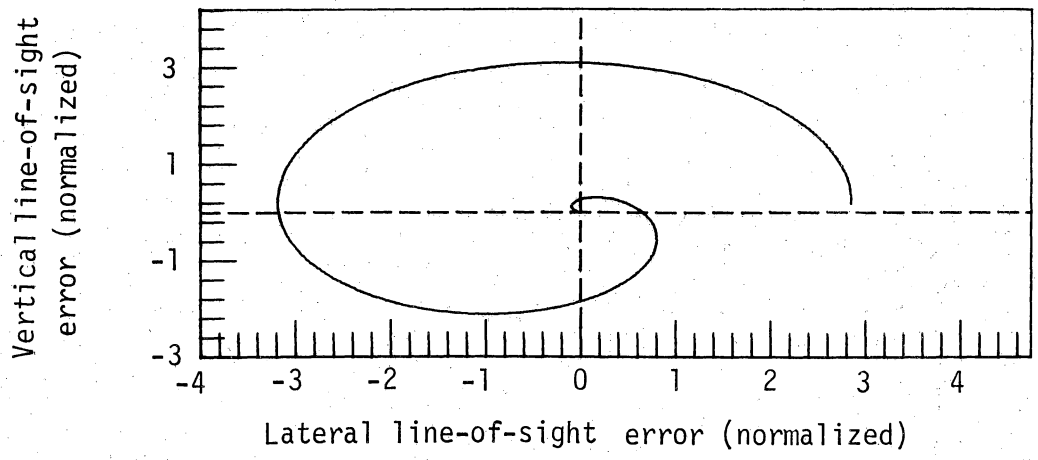

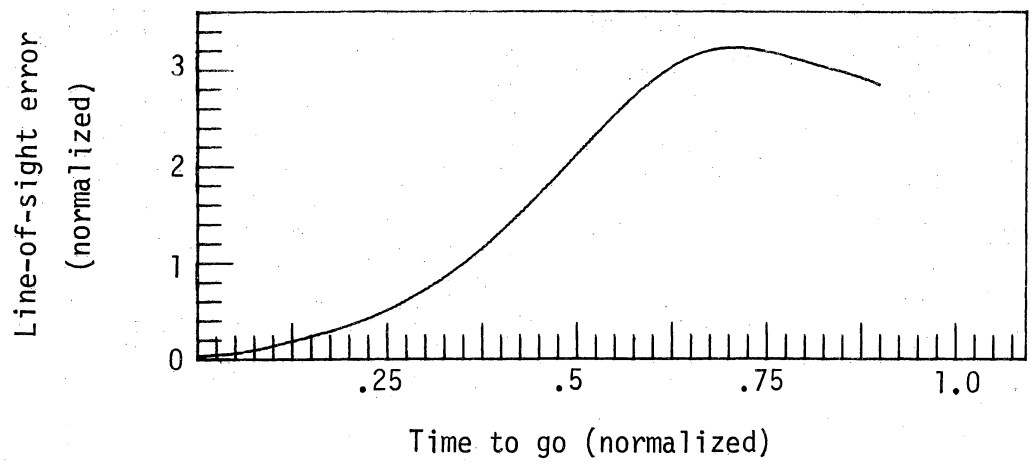

Parameters and initial conditions

$k = 1.5$ $\phi_0 = 0.0^0$ $\alpha_T = 10.0$ units

$\tau_\phi = 1.0$ sec $\gamma_0 = 35.0^0$ $P_L = 2.0$

Figure 12.1.- Line-of-sight error and roll time-histories for variations in roll time-constant and initial error angle.

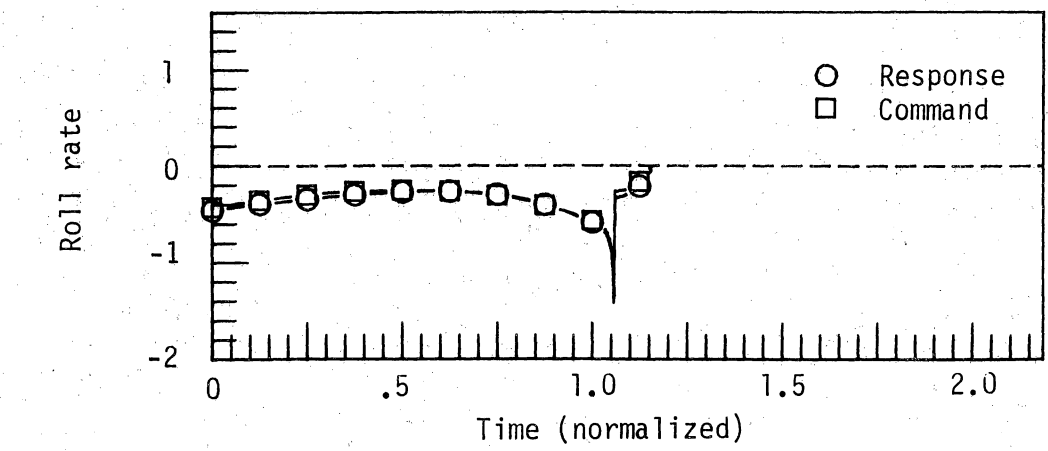

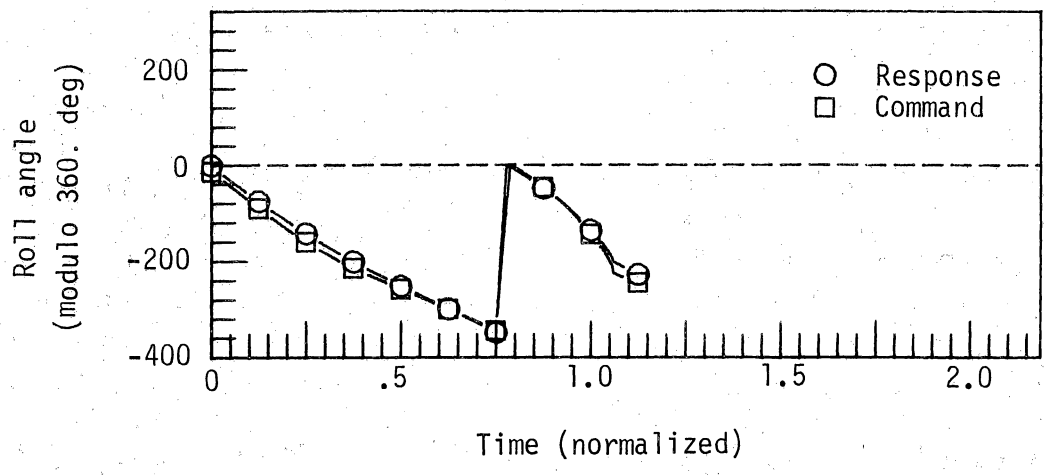

Parameters and initial conditions		
$k = 1.5$	$\phi_o = 0.0^o$	$\alpha_T = 10.0$ units
$\tau_\phi = 1.0$ sec	$\gamma_o = 35.0^o$	$P_L = 2.0$

Figure 12.2.- Line-of-sight error and roll time-histories for variations in roll time-constant and initial error angle.

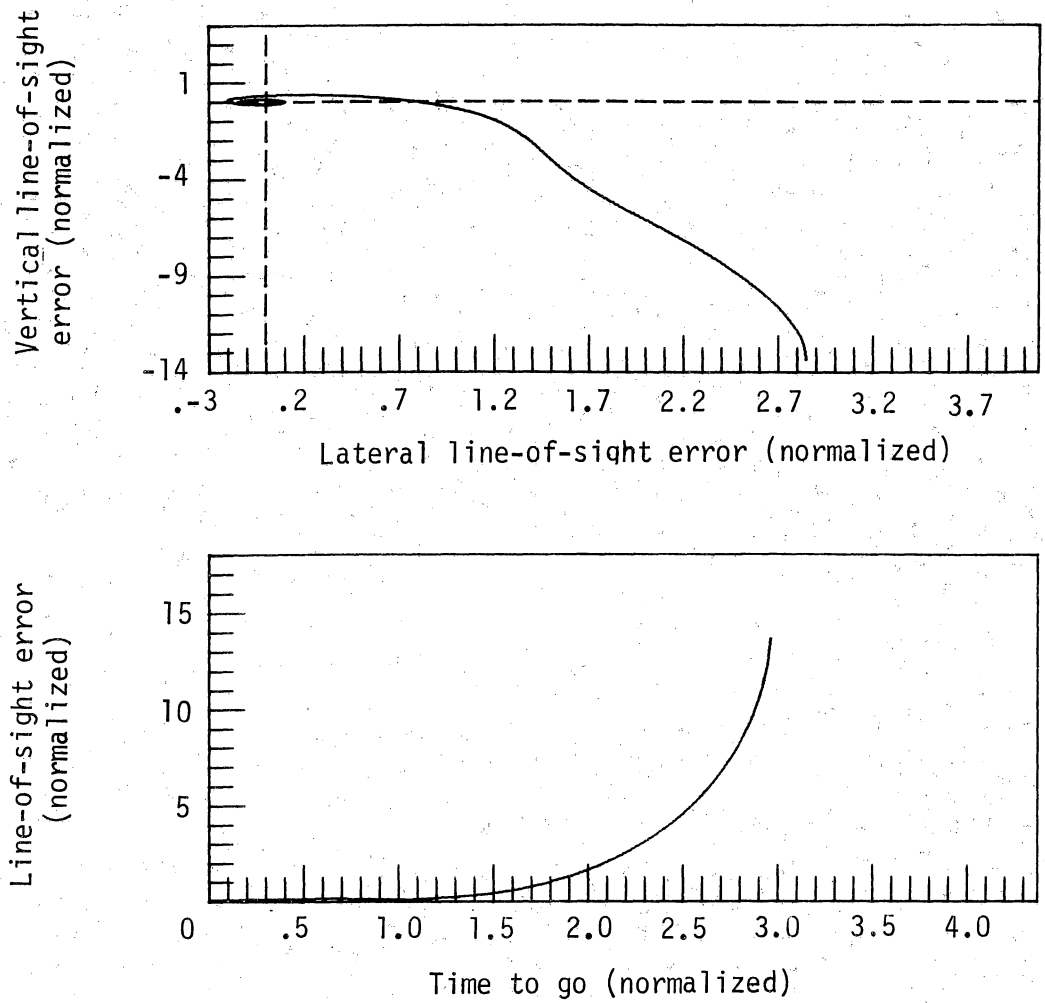

Parameters and initial conditions

$k = 2.0$ $\phi_0 = 0.0^0$ $\alpha_T = 10.0$ units

$\tau_\phi = 1.0$ sec $\gamma_0 = 0.0^0$ $P_L = 2.0$

Figure 12.3.- Line-of-sight error and roll time-histories for variations in roll time-constant and initial error angle.

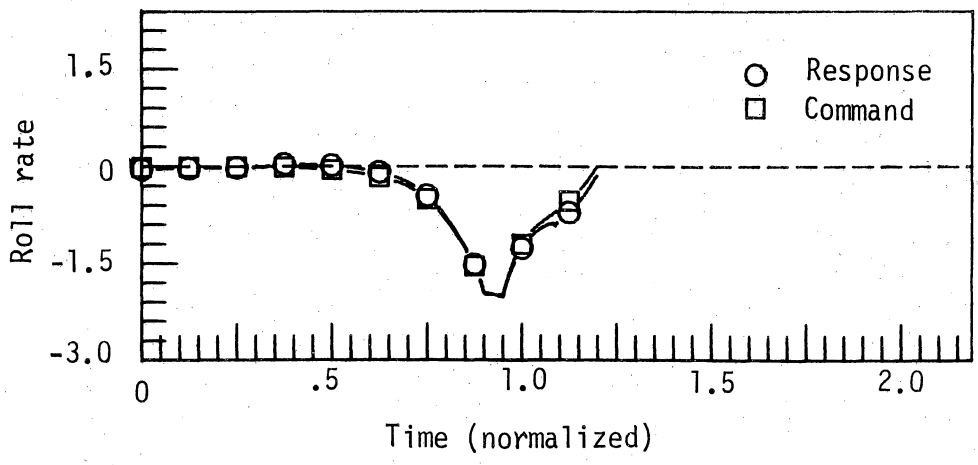

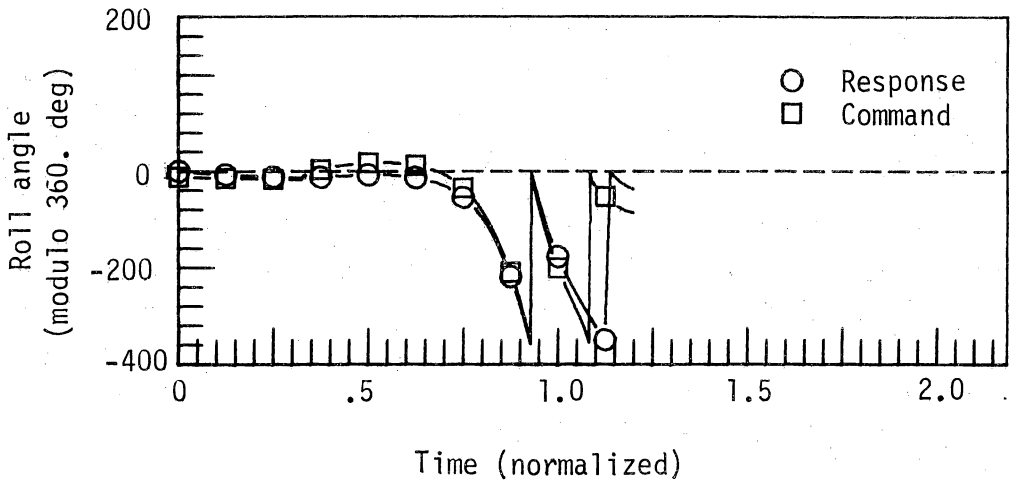

Parameters and initial conditions		
$k = 2.0$	$\phi_o = 0.0^o$	$\alpha_T = 10.0$ units
$\tau_\phi = 1.0$ sec	$\gamma_o = 0.0^o$	$p_L = 2.0$

Figure 12.4.- Line-of-sight error and roll time-histories for variations in roll time-constant and initial error angle.

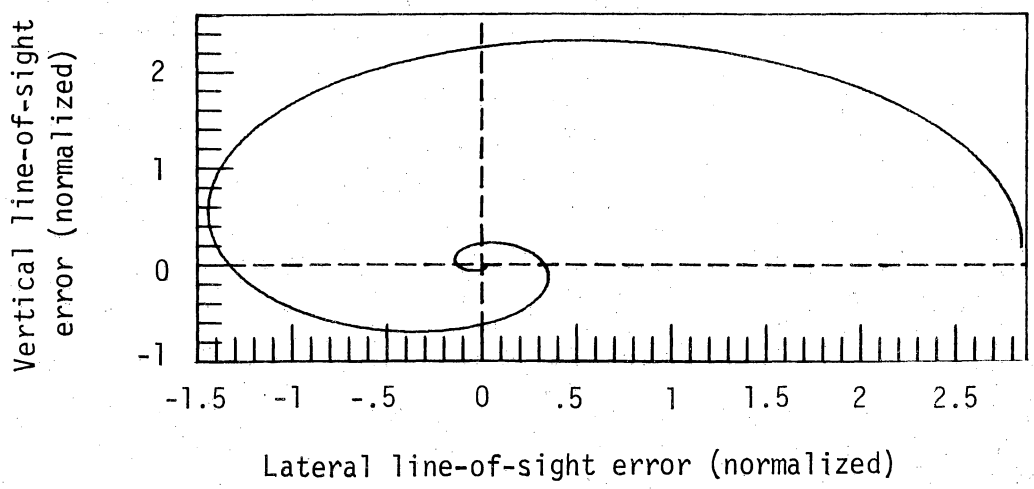

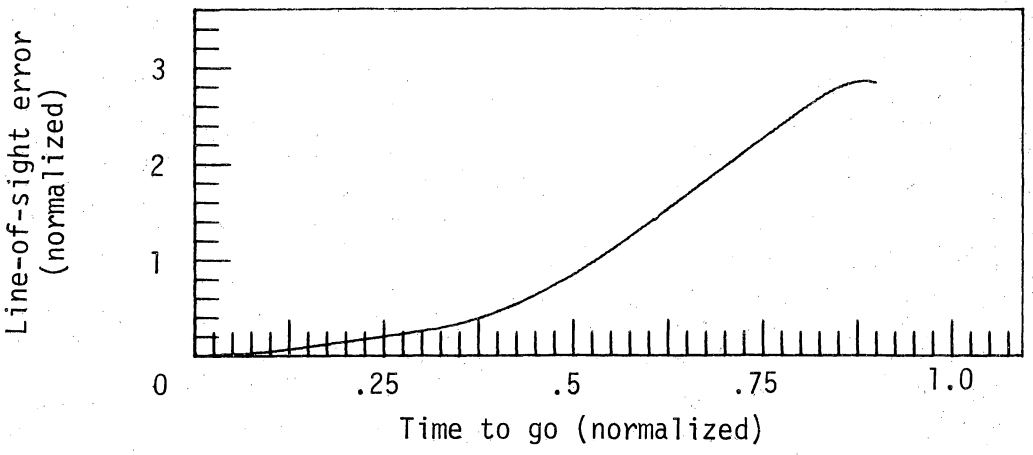

Parameters and initial conditions		
$k = 1.9$	$\phi_o = 0.0^o$	$\alpha_T = 6.0$ units
$\tau_\phi = .3$ sec	$\gamma_o = 35.0^o$	$p_L = 2.0$

Figure 13.1.- Line-of-sight error and roll time-histories for variations in trim angle of attack and initial error angle.

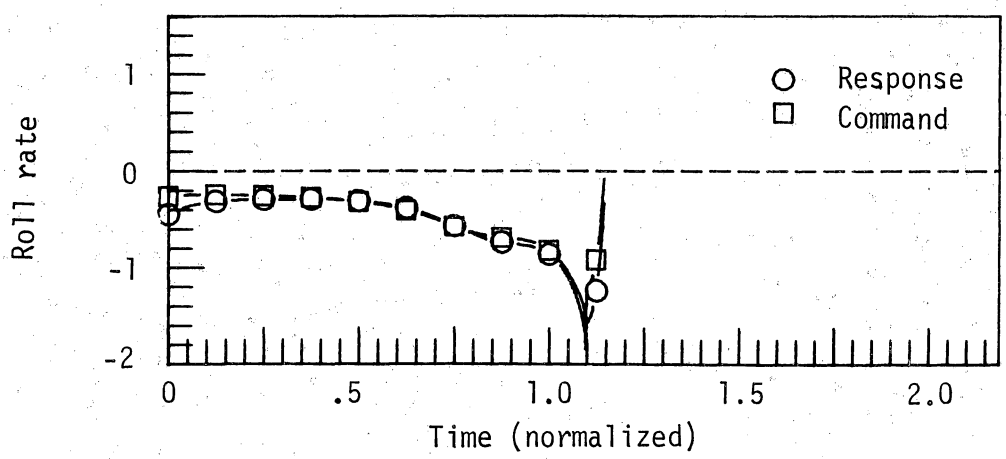

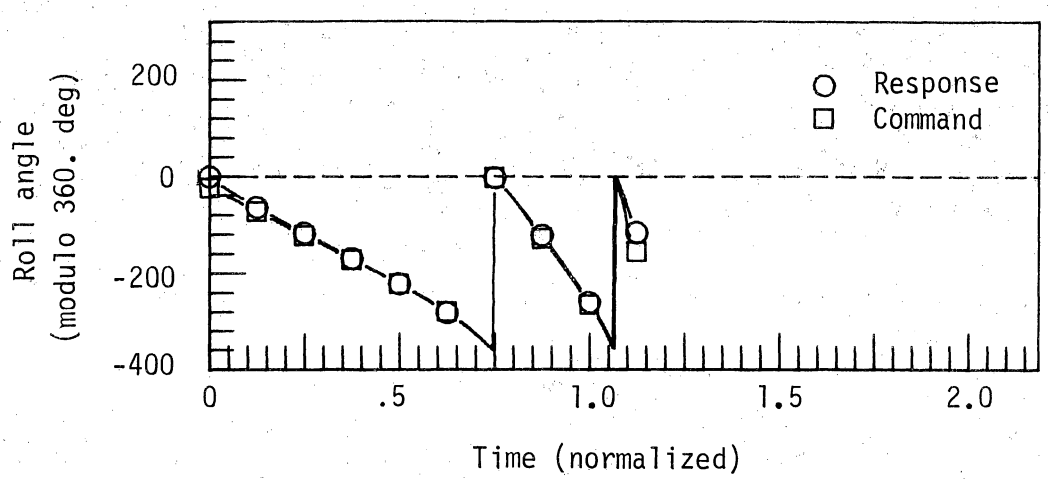

Parameters and initial conditions		
$k = 1.9$	$\phi_o = 0.0^o$	$\alpha_T = 6.0$ units
$\tau_\phi = .3$ sec	$\gamma_o = -35.0^o$	$p_L = 2.0$

Figure 13.2.- Line-of-sight error and roll time-histories for variations in trim angle of attack and initial error angle.

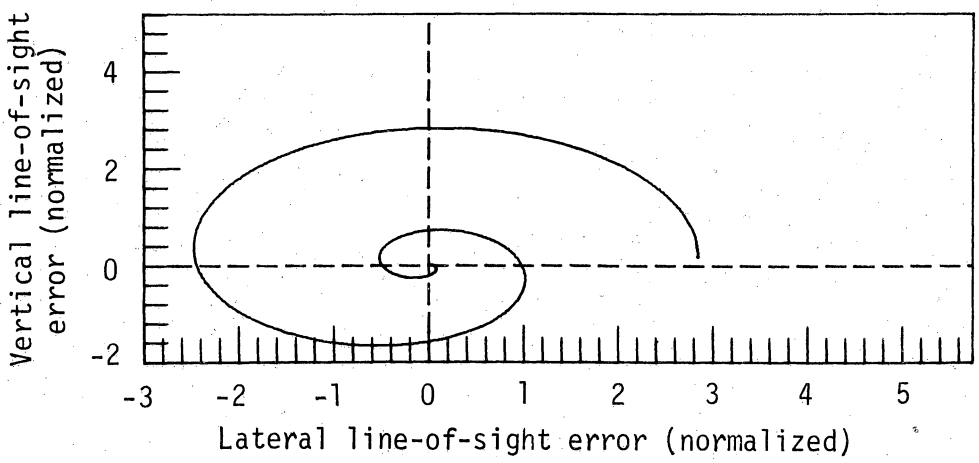

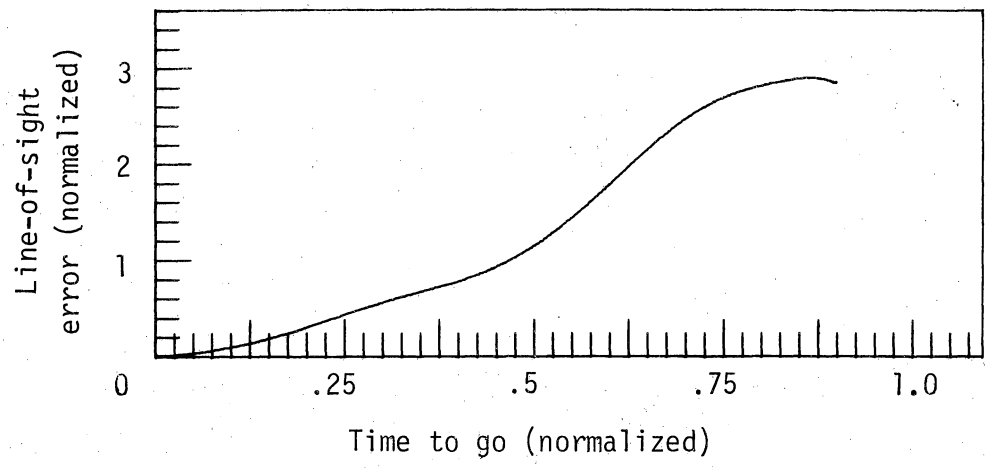

Parameters and initial conditions		
$k = 1.5$	$\phi_o = 0.0^o$	$\alpha_T = 10.0$ units
$\tau_\phi = .3$ sec	$\gamma_o = -35.0^o$	$p_L = 1.0$

Figure 14.1.- Line-of-sight error and roll time-histories for variations in roll-rate limit and initial error angle.

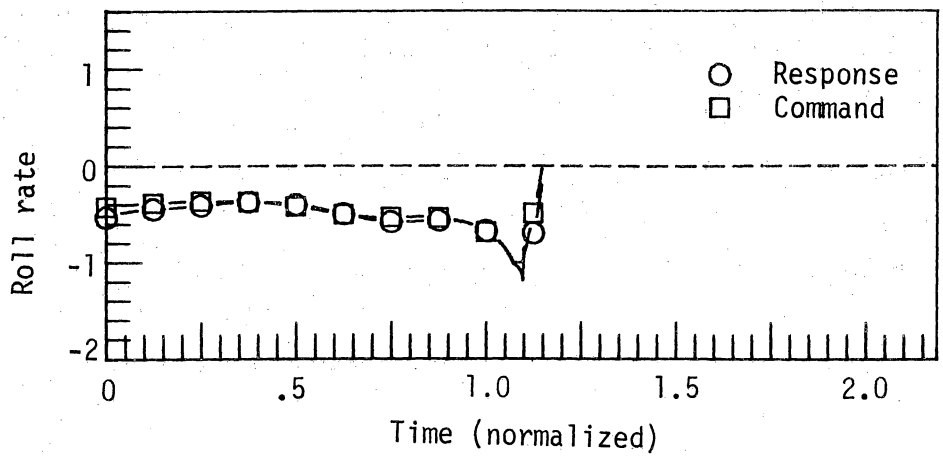

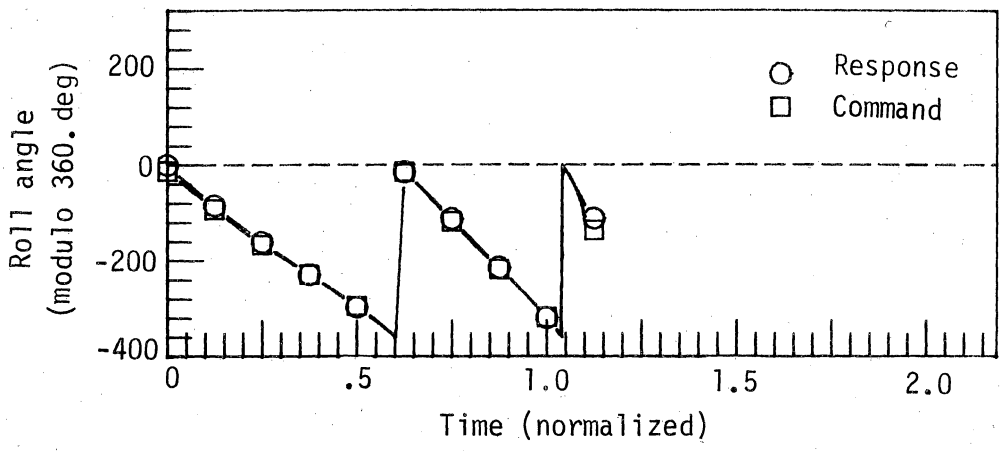

Parameters and initial conditions		
$k = 1.5$	$\phi_o = 0.0^o$	$\alpha_T = 10.0$ units
$\tau_\phi = .3$ sec	$\gamma_o = -35.0^o$	$P_L = 1.0$

Figure 14.2.- Line-of-sight error and roll time-histories for variations in roll rate limit and initial error angle.

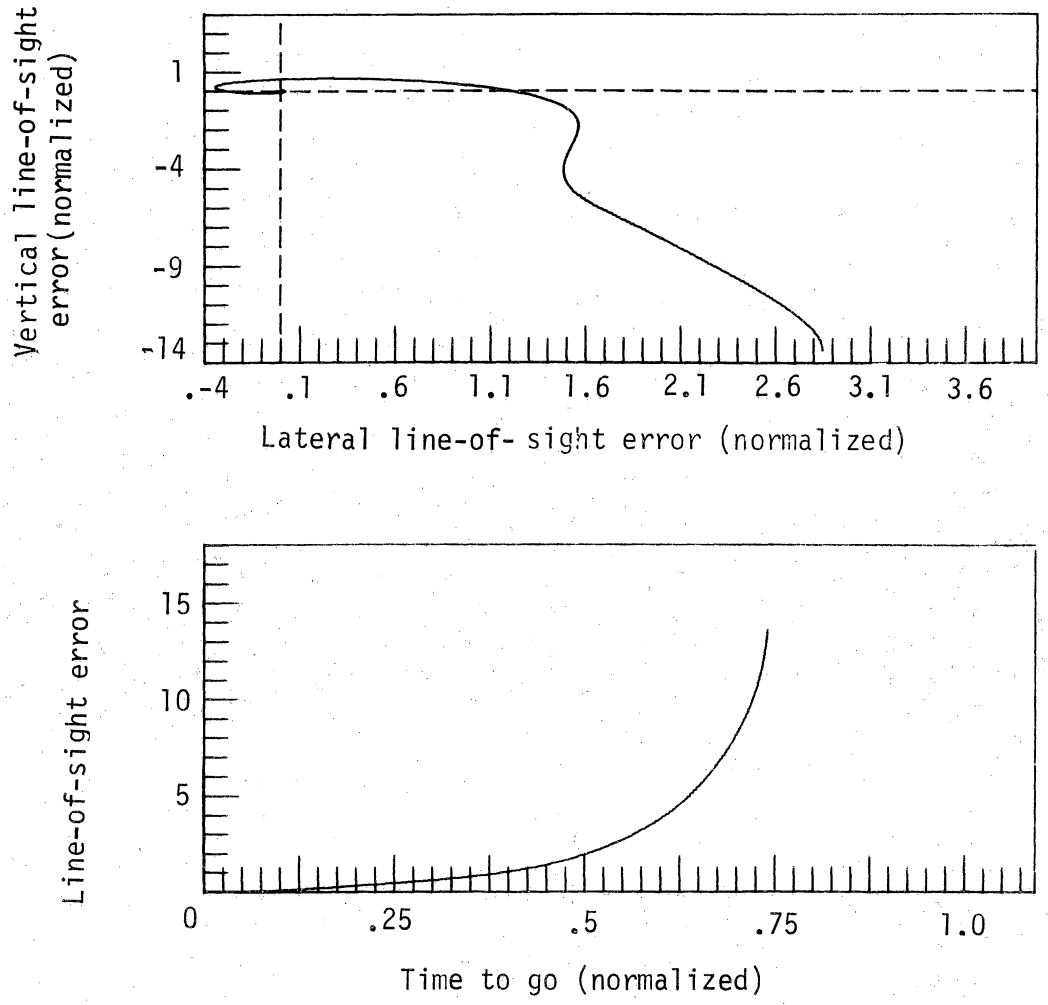

Parameters and initial conditions

$k = 2.0$ $\phi_o = 0.0^o$ $\alpha_T = 10.0$ units

$\tau_\phi = .3$ sec $\gamma_o = 0.0^o$ $P_L = 1.0$

Figure 14.3.- Line-of-sight error and roll time-histories for variations in roll-rate limit and initial error angle.

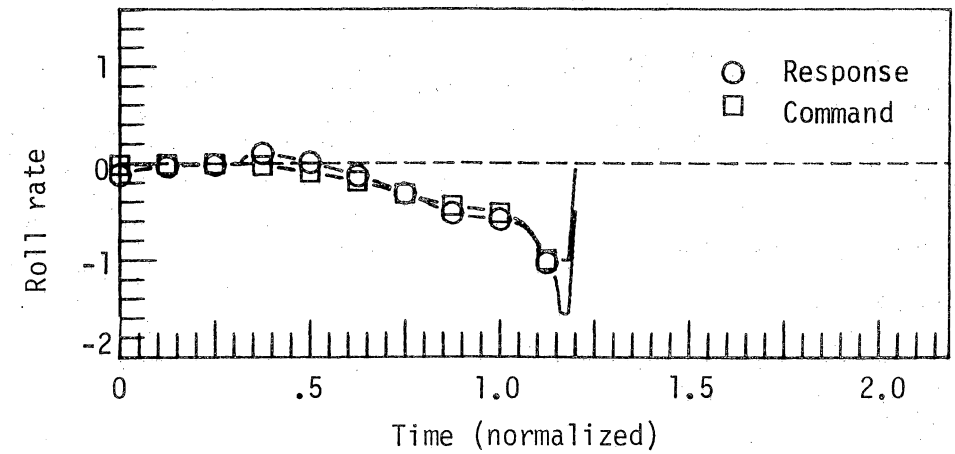

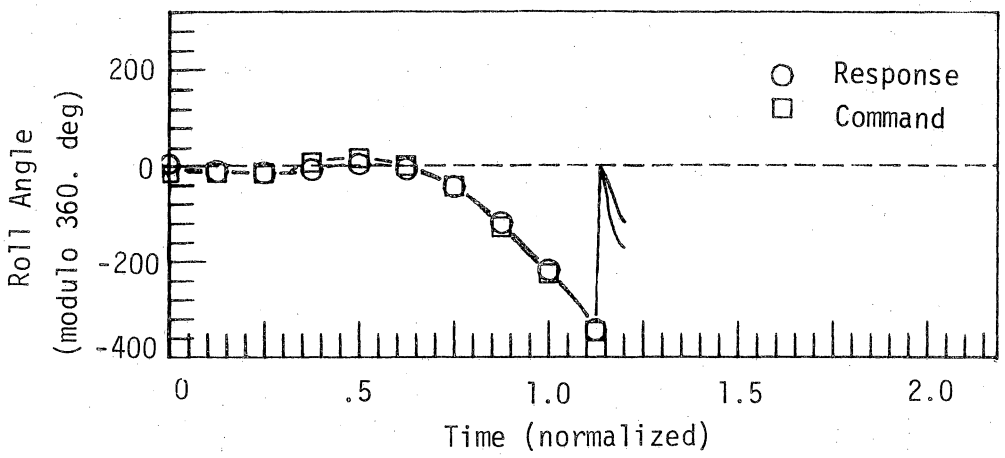

Parameters and initial conditions

$k = 2.0$ $\phi_o = 0.0^o$ $\alpha_T = 10.0$ units

$\tau_\phi = .3$ sec $\gamma_o = 0.0^o$ $P_L = 1.0$

Figure 14.4.- Line of-sight error and roll time-histories for variations in roll-rate limit and initial error angle.

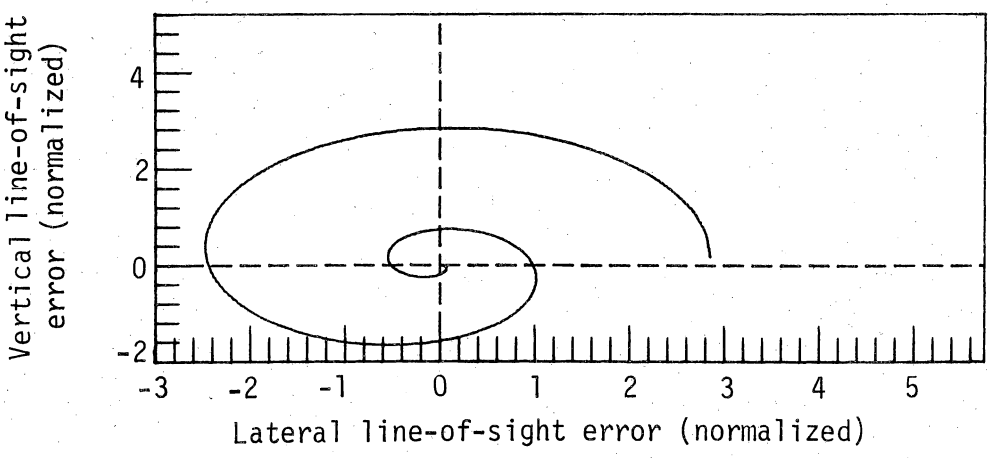

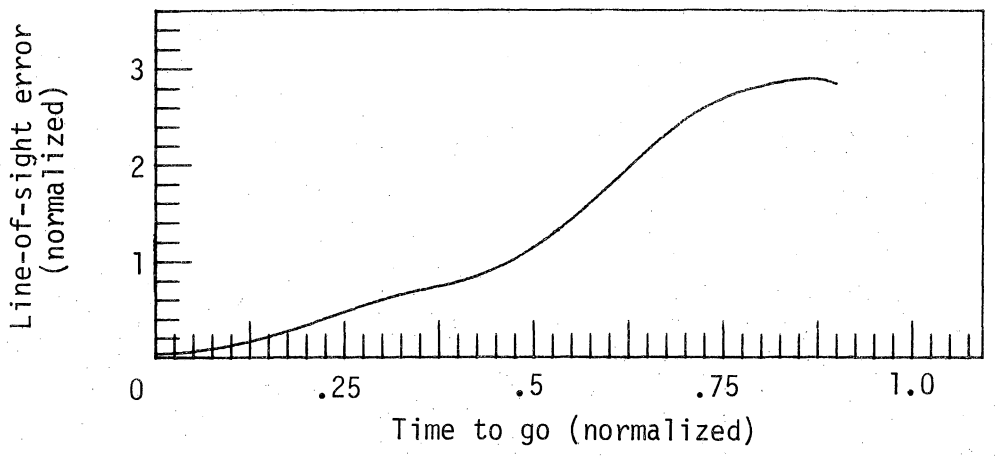

Parameters and initial conditions		
$k = 1.5$	$\phi_o = 0.0^o$	$\alpha_T = 10.0$ units
$\tau_\phi = .3$ sec	$\gamma_o = -35.0^o$	$p_L = .5$

Figure 15.1.- Line-of-sight error and roll time-histories for variations in roll-rate limit and initial error angle.

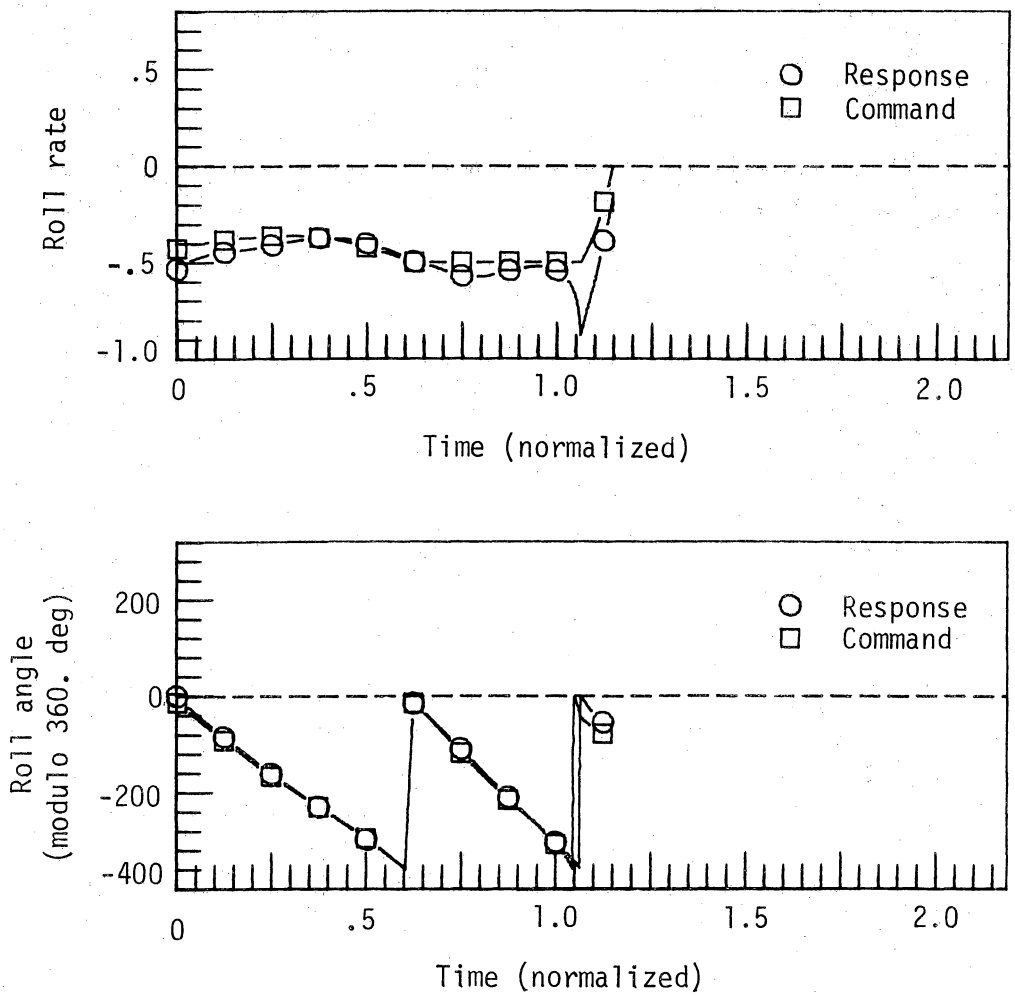

Parameters and initial conditions		
$k = 1.5$	$\phi_o = 0.0^o$	$\alpha_T = 10.0$ units
$\tau_\phi = .3$ sec	$\gamma_o = -35.0^o$	$p_L = .5$

Figure 15.2.- Line-of-sight error and roll time-histories for variations in roll-rate limit and initial error angle.

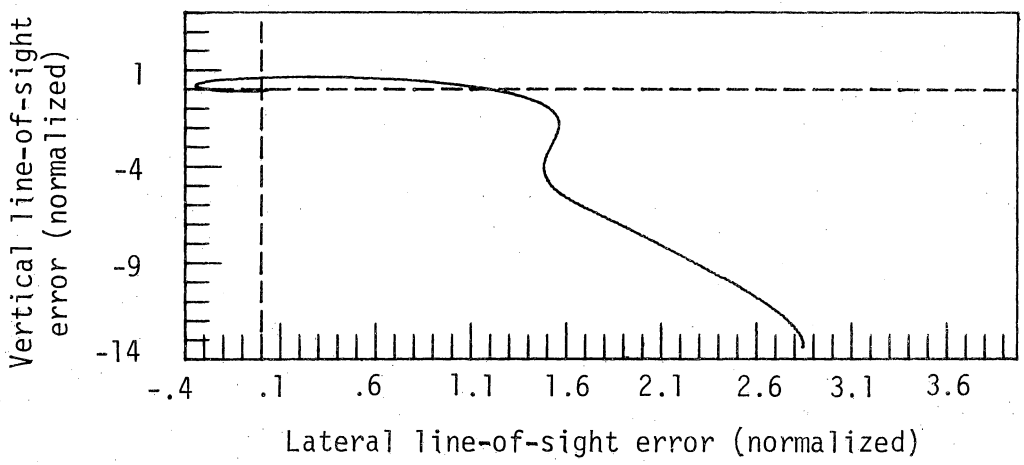

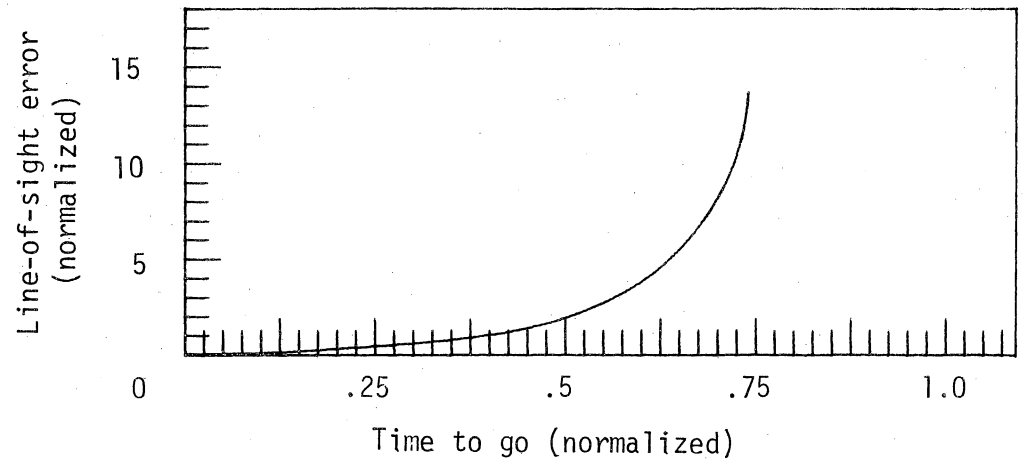

Parameters and initial conditions		
$k = 2.0$	$\phi_o = 0.0^o$	$\alpha_T = 10.0$ units
$\tau_\phi = .3$ sec	$\gamma_o = 0.0^o$	$p_L = .5$

Figure 15.3.- Line-of-sight error and roll time-histories for variations in roll-rate limit and initial error angle.

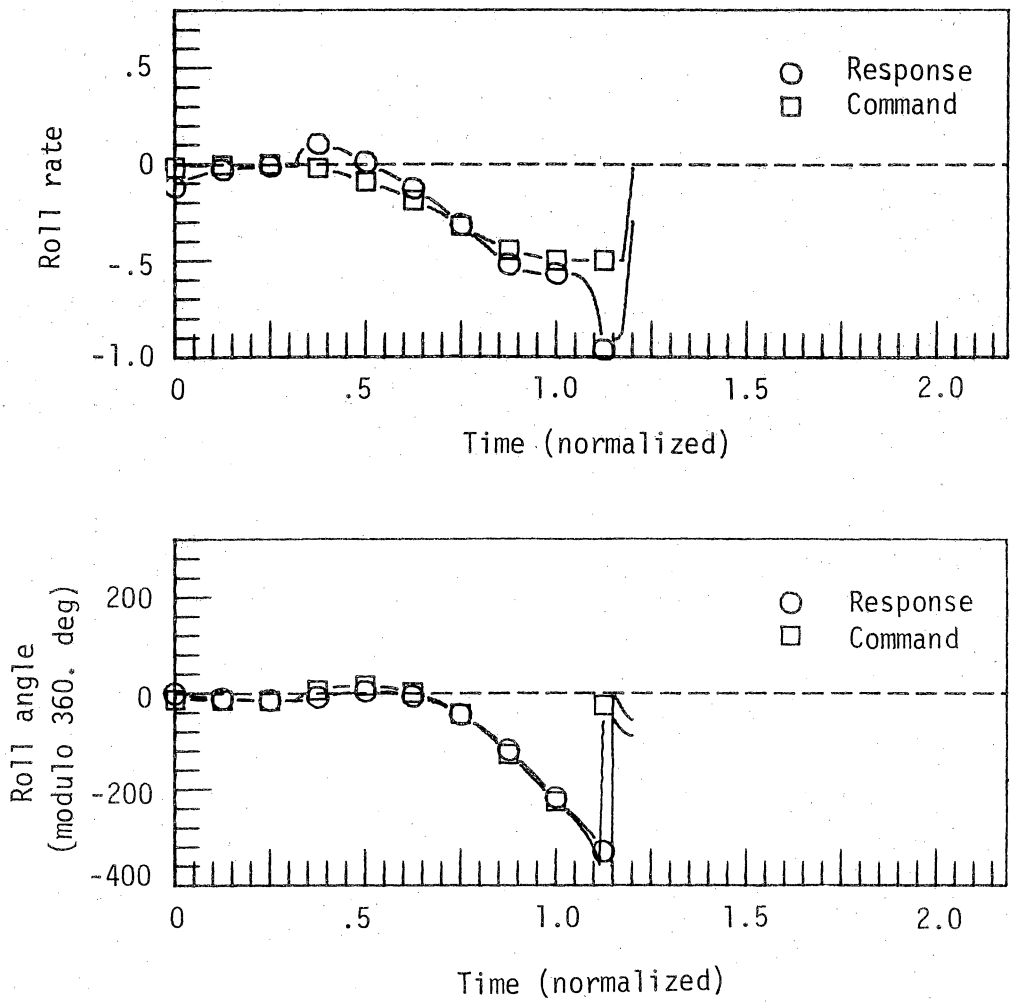

Parameters and initial conditions		
$k = 2.0$	$\phi_o = 0.0^o$	$\alpha_T = 10.0$ units
$\tau_\phi = .3$ sec	$\gamma_o = 0.0^o$	$p_L = .5$

Figure 15.4.- Line-of-sight error and roll time-histories for variations in roll-rate limit and initial error angle.

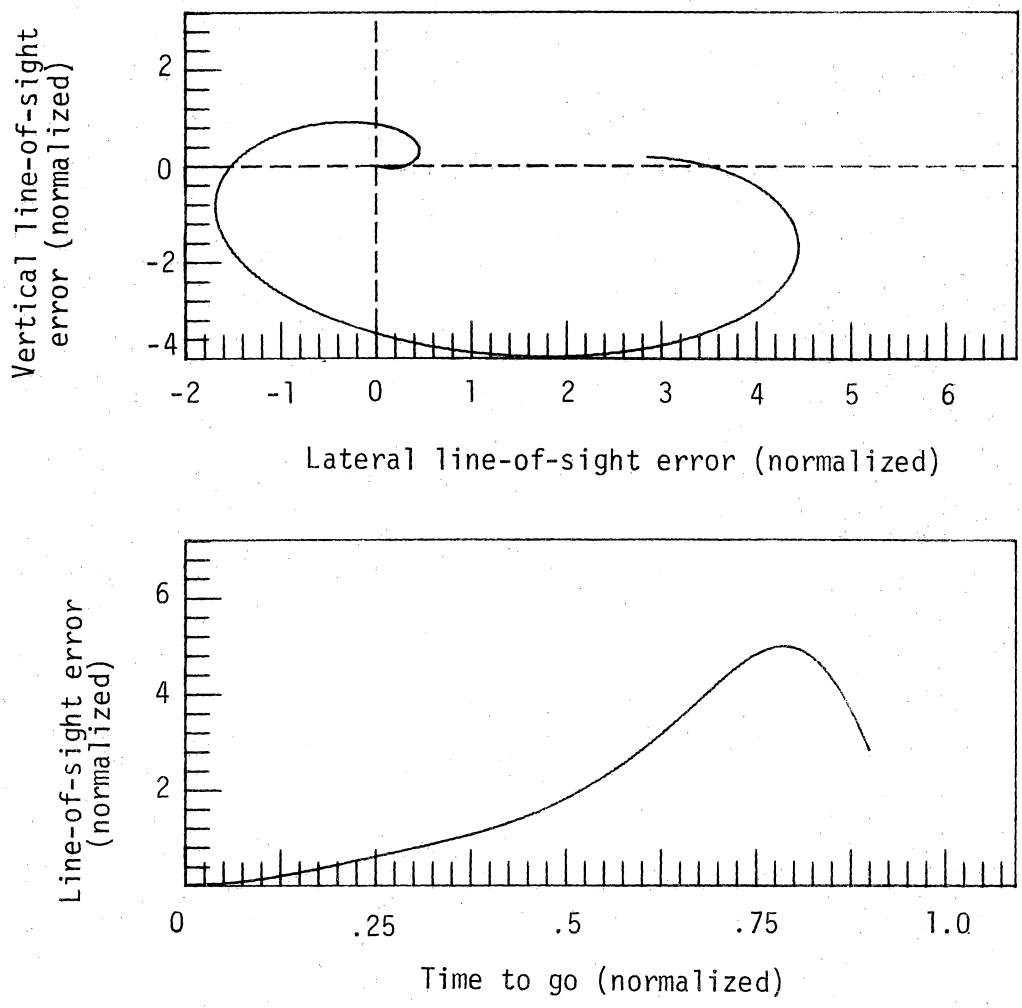

Parameters and initial conditions		
$k = 1.5$	$\phi_o = 90.0^o$	$\alpha_T = 10.0$ units
$\tau_\phi = .3$ sec	$\gamma_o = -35.0^o$	$p_L = 2.0$

Figure 16.1.- Line-of-sight error and roll time-histories for variations in initial roll angle.

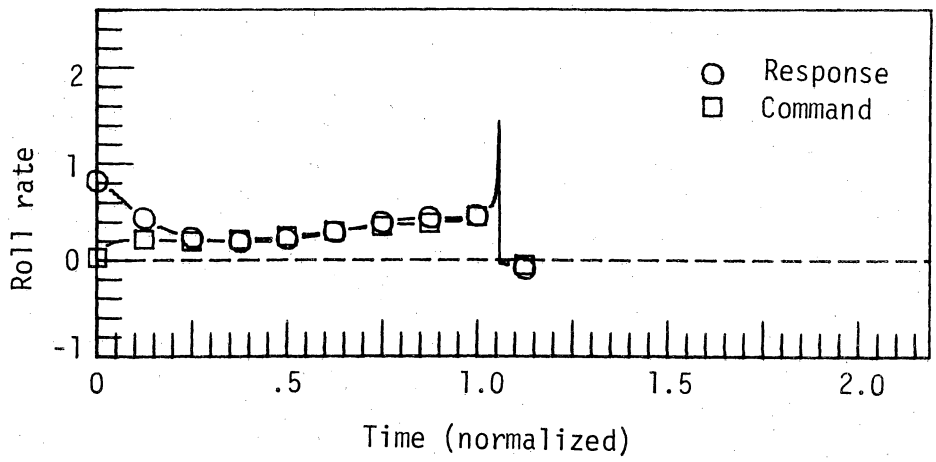

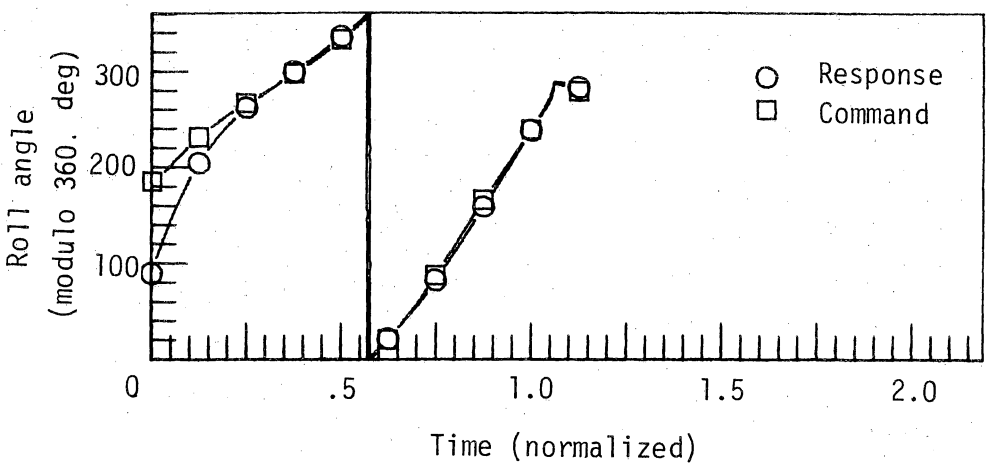

Parameters and initial conditions		
$k = -.5$	$\phi_o = 90.0^o$	$\alpha_T = 10.0$ units
$\tau_\phi = .3$ sec	$\gamma_o = -35.0^o$	$p_L = 2.0$

Figure 16.2.- Line-of-sight error and roll time-histories for variations in initial roll angle.

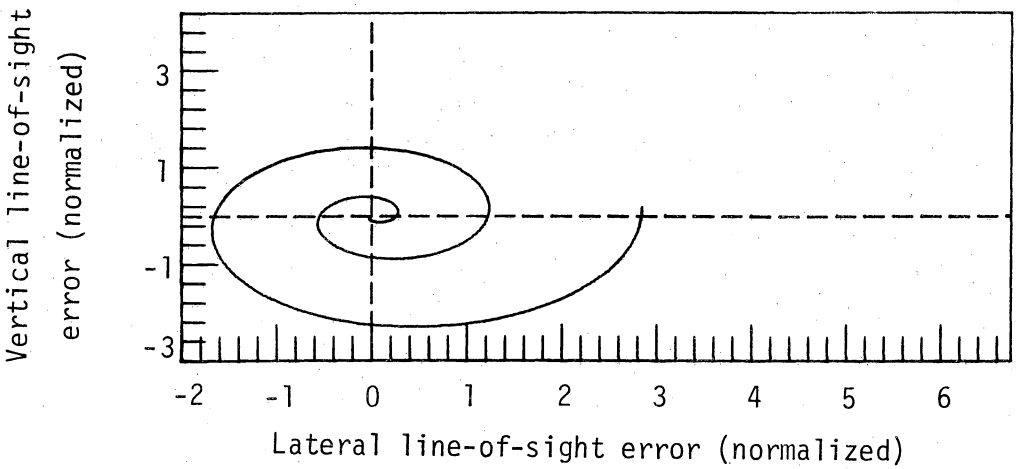

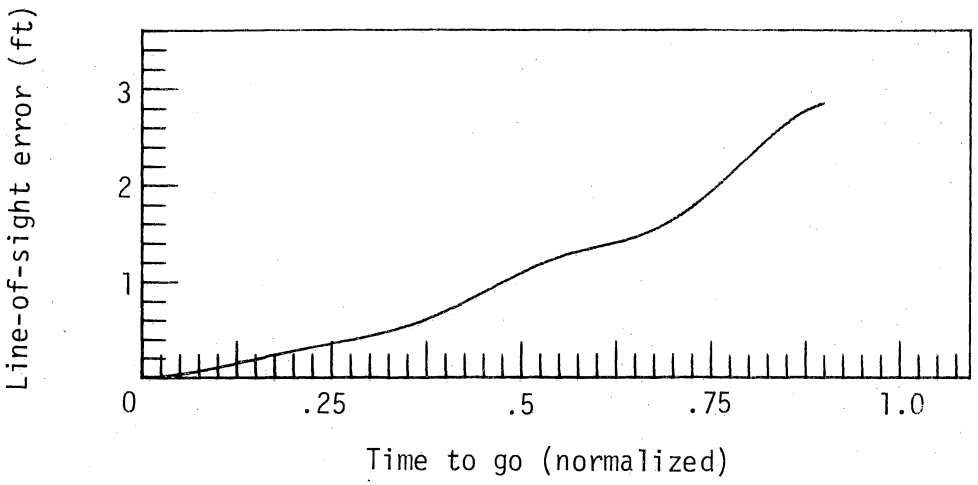

Parameters and initial conditions		
$k = 1.5$	$\phi_o = 180.0^o$	$\alpha_T = 10.0$ units
$\tau_\phi = .3$ sec	$\gamma_o = -35.0^o$	$p_L = 2.0$

Figure 16.3.- Line-of-sight error and roll time-histories for variations in initial roll angle.

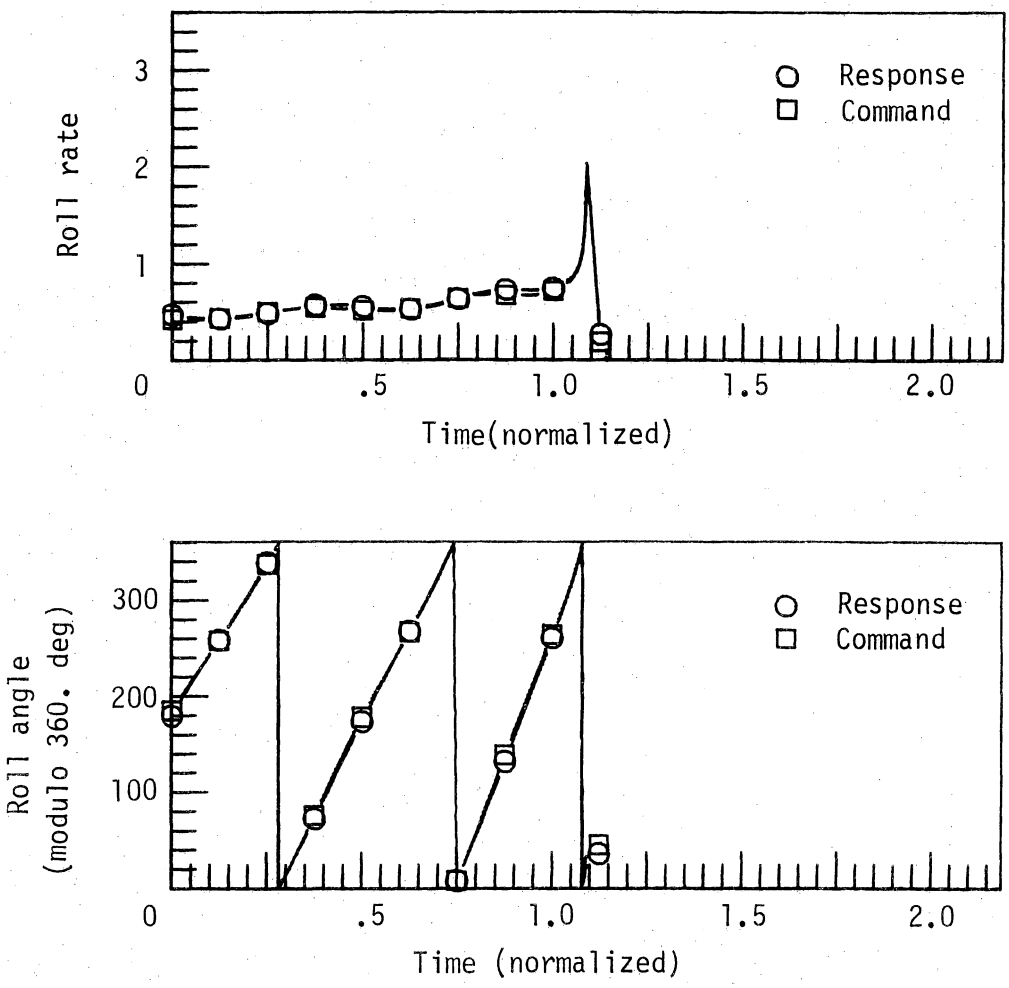

Parameters and initial conditions		
$k = 1.5$	$\phi_0 = 180.0^0$	$\alpha_T = 10.0$ units
$\tau_\phi = .3$ sec	$\gamma_0 = -35.0^0$	$P_L = 2.0$

Figure 16.4.- Line-of-sight error and roll time-histories for variations in initial roll angle.

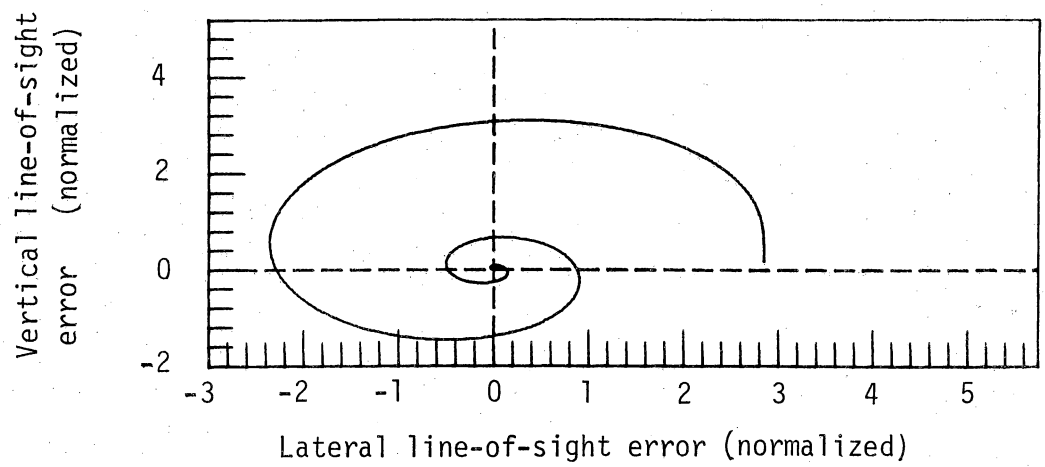

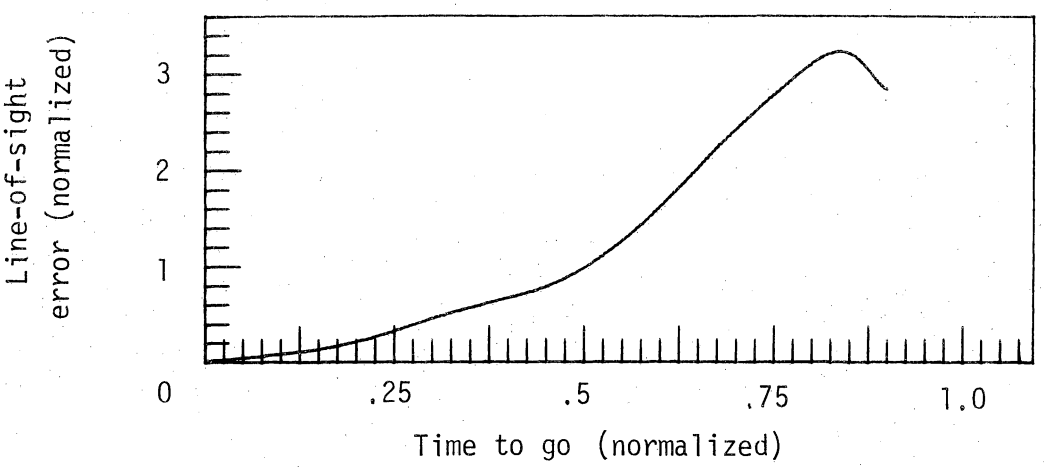

Parameters and initial conditions

$k = 1.5$ $\phi_0 = 0.0^0$ $\alpha_T = 10.0$ units

$\tau_\phi = .3$ sec $\gamma_0 = -35.0^0$ $P_L = 1.0$

Figure 17.1.- Line-of-sight error and roll time-histories for a fifth order roll system.

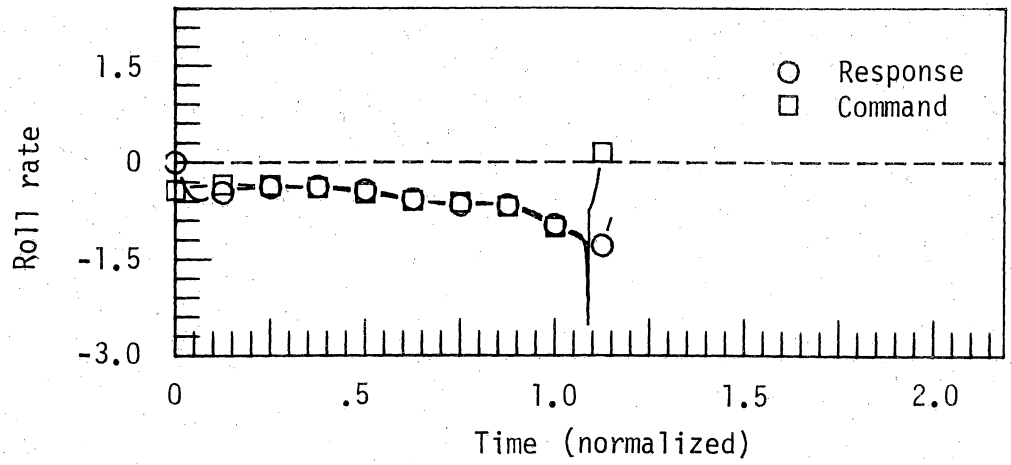

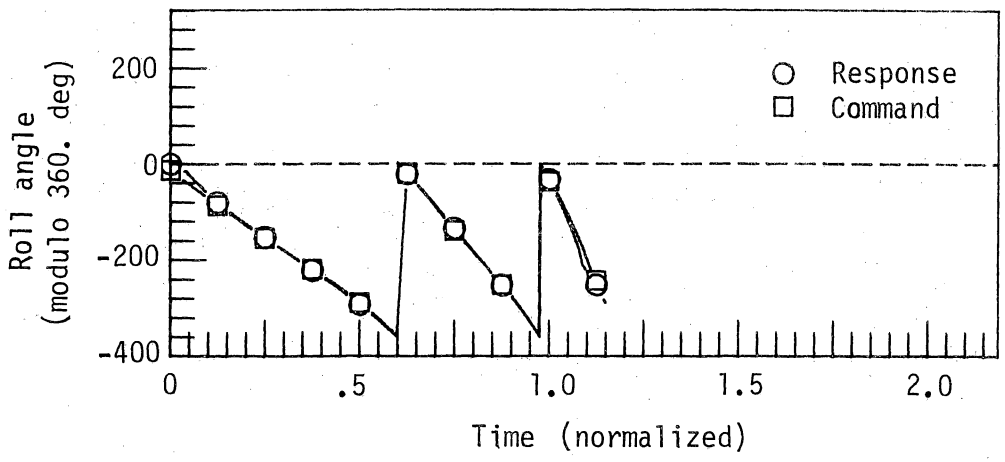

Parameters and initial conditions

$k = 1.5$ $\quad \phi_0 = 0.0^o$ $\quad \alpha_T = 10.0$ units

τ_ϕ = NA $\quad \gamma_0 = -35.0^o$ $\quad P_L$ = NA

Figure 17.2.- Line-of-sight error and roll time-histories for a fifth order roll system.

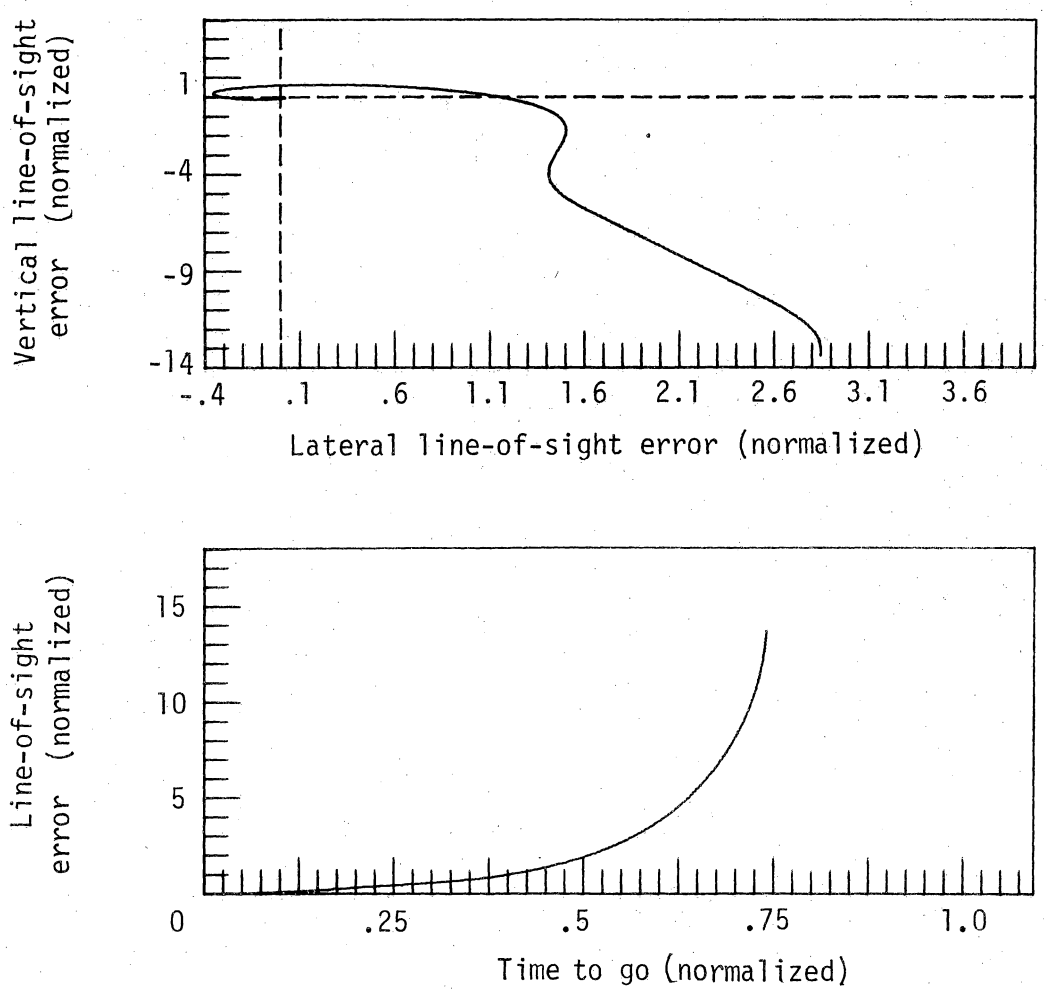

Parameters and initial conditions		
$k = 2.0$	$\phi_o = 0.0^o$	$\alpha_T = 10.0$ units
τ_ϕ = NA	$\gamma_o = 0.0^o$	P_L = NA

Figure 17.3.- Line-of sight error and roll time-histories for a fifth order roll system.

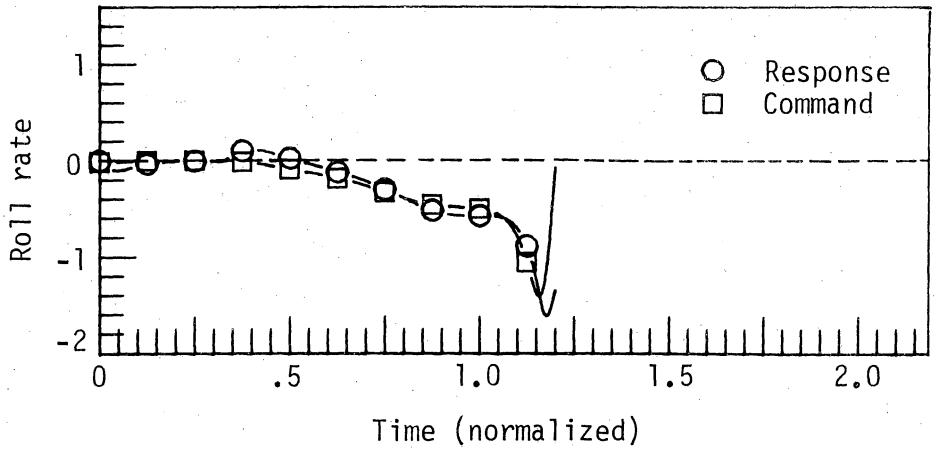

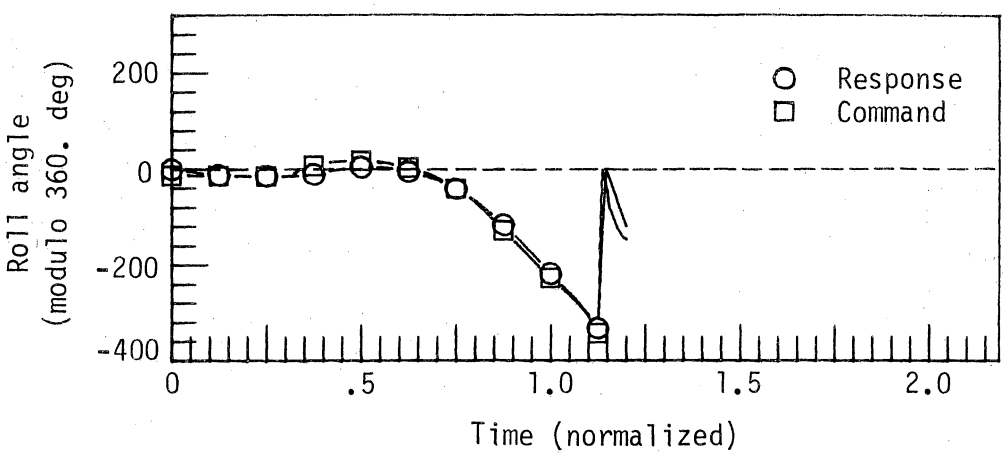

Parameters and initial conditions		
k = 2.0	ϕ_o = 0.0°	α_T = 10.0 units
τ_ϕ = NA	γ_o = 0.0°	P_L = NA

Figure 17.4.- Line-of-sight error and roll time-histories for a fifth order roll system.

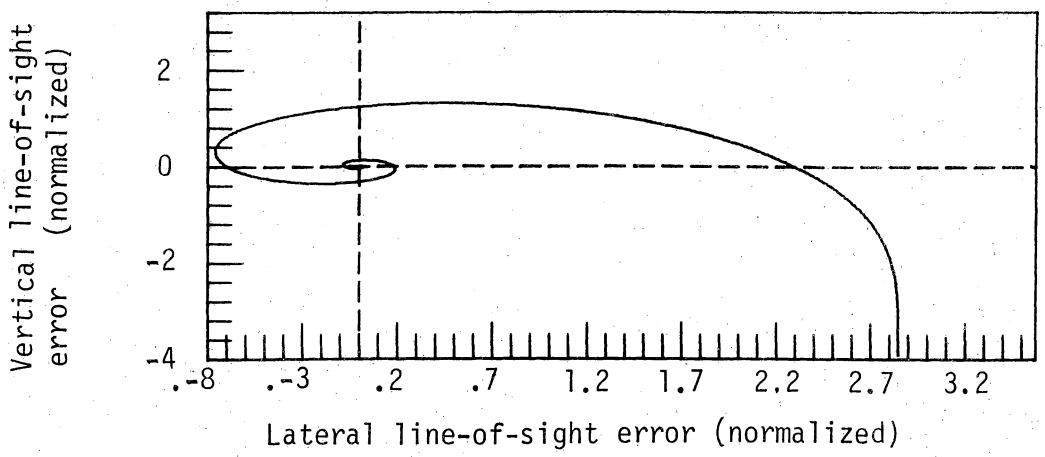

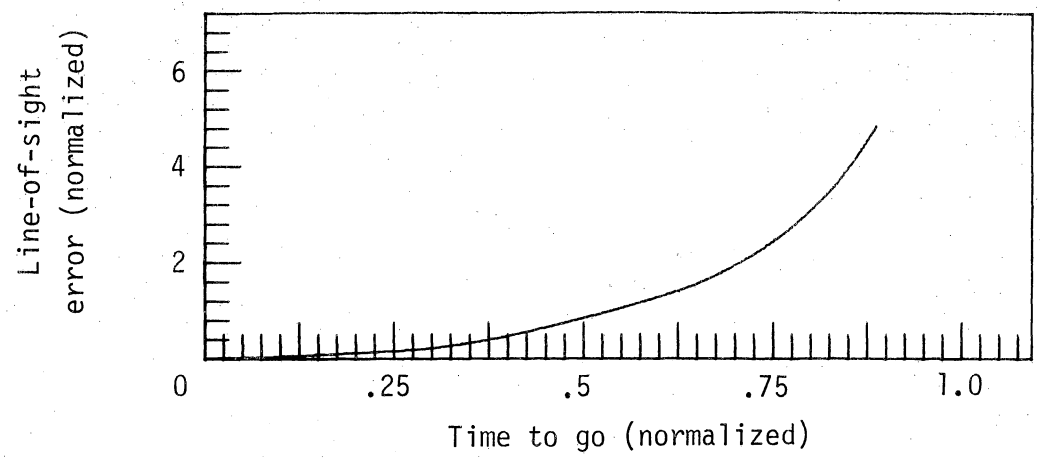

Parameters and initial conditions

$k = 2.0$ $\quad \phi_0 = 0.0^0$ $\quad \alpha_T = 6.0$ units

τ_ϕ = NA $\quad \gamma_0 = -25.0^0$ $\quad P_L$ = NA

Figure 18.1.- Line-of-sight error and roll time-histories for a fifth order roll system.

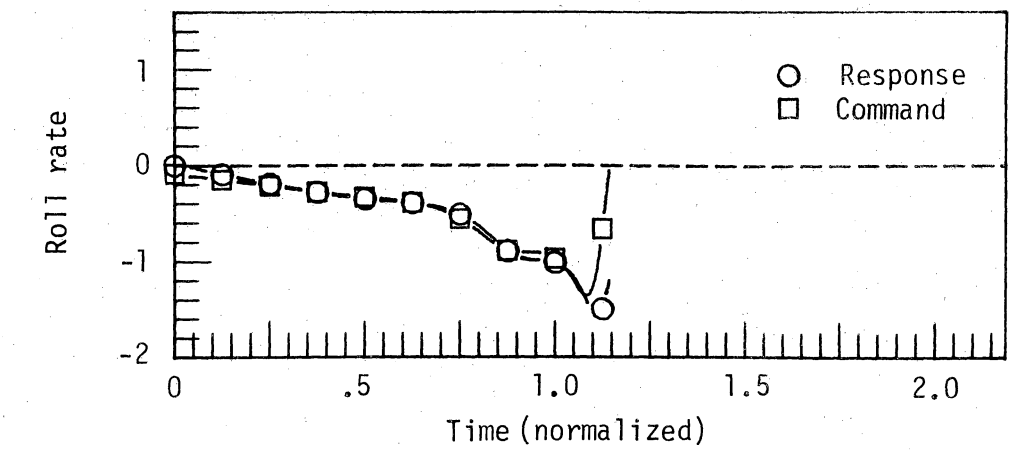

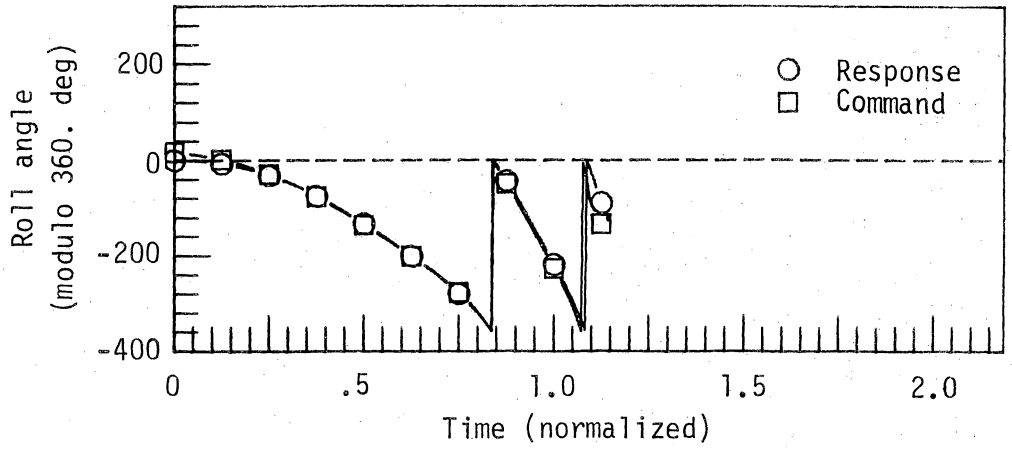

Parameters and initial conditions

$k = 2.0$ $\quad \phi_o = 0.0^o$ $\quad \alpha_T = 6.0$ units

τ_ϕ = NA $\quad \gamma_o = -25.0^o$ $\quad P_L$ = NA

Figure 18.2.- Line-of-sight error and roll time-histories for a fifth order roll system.

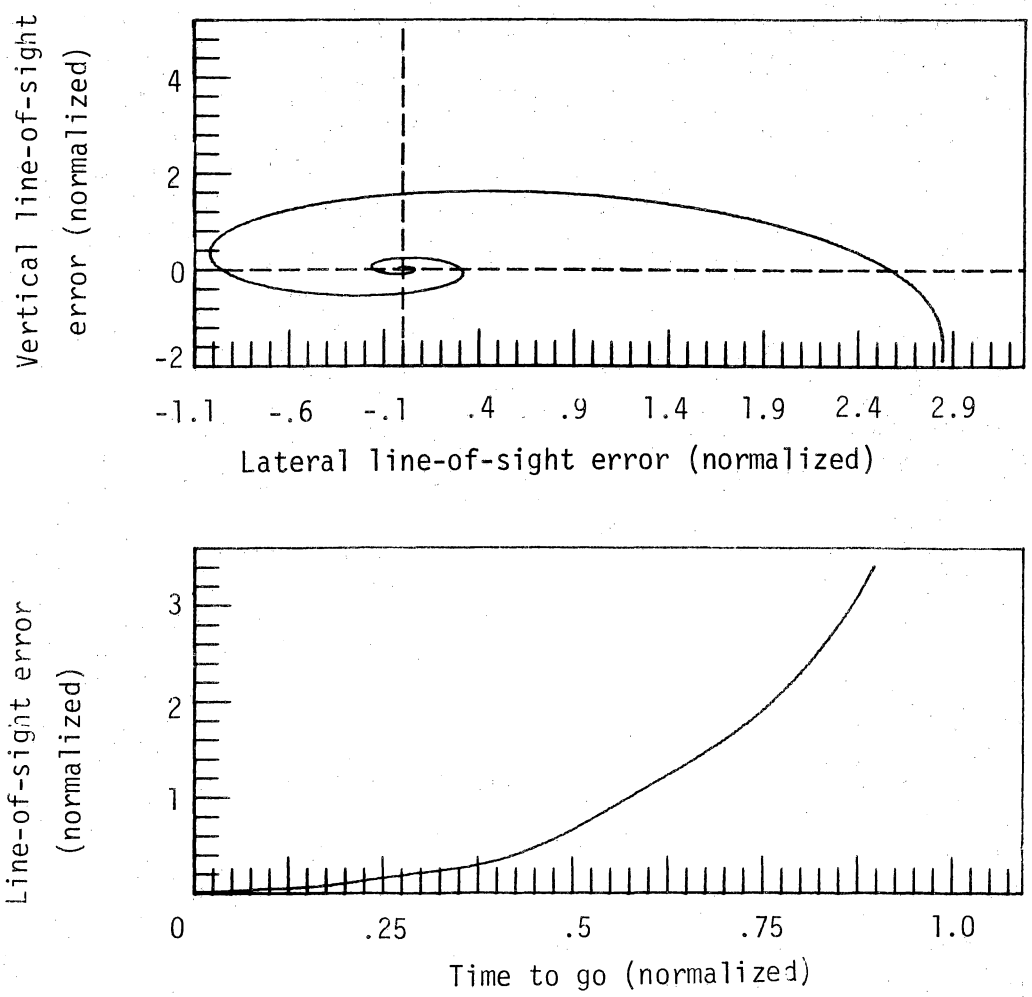

Parameters and initial conditions		
$k = 2.0$	$\phi_o = 0.0^o$	$\alpha_T = 6.0$ units
τ_ϕ = NA	$\gamma_o = -30.0^o$	P_L = NA

Figure 18.3.- Line-of-sight error and roll time-histories for a fifth order roll system.

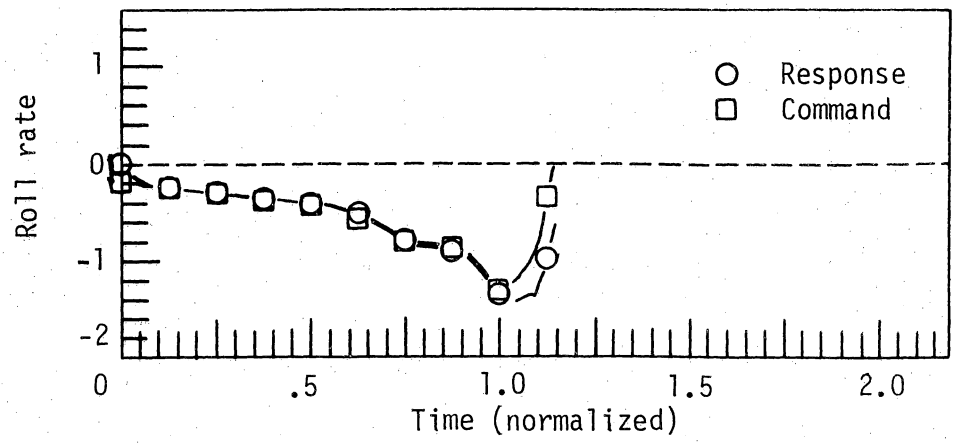

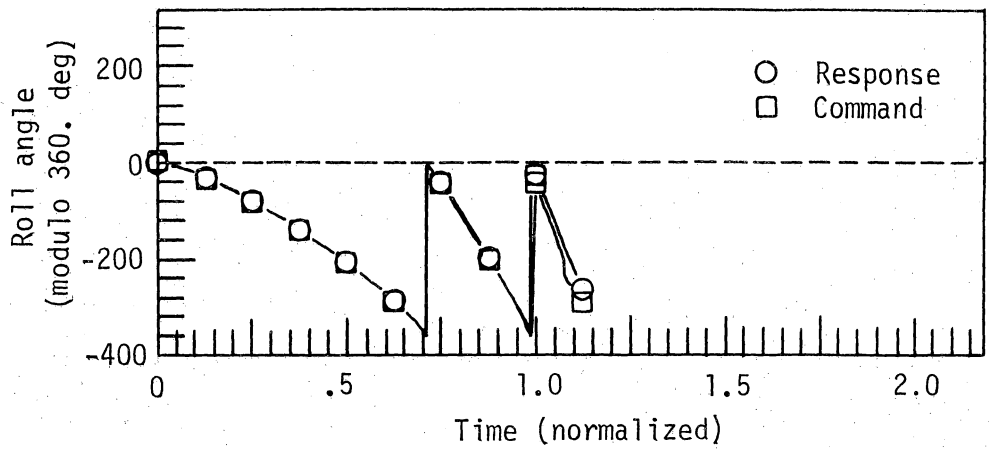

Parameters and initial conditions		
$k = 2.0$	$\phi_o = 0.0^o$	$\alpha_T = 6.0$ units
τ_ϕ = NA	$\gamma_o = -30.0^o$	P_L = NA

Figure 18.4.- Line-of-sight error and roll time-histories for a fifth order roll system.

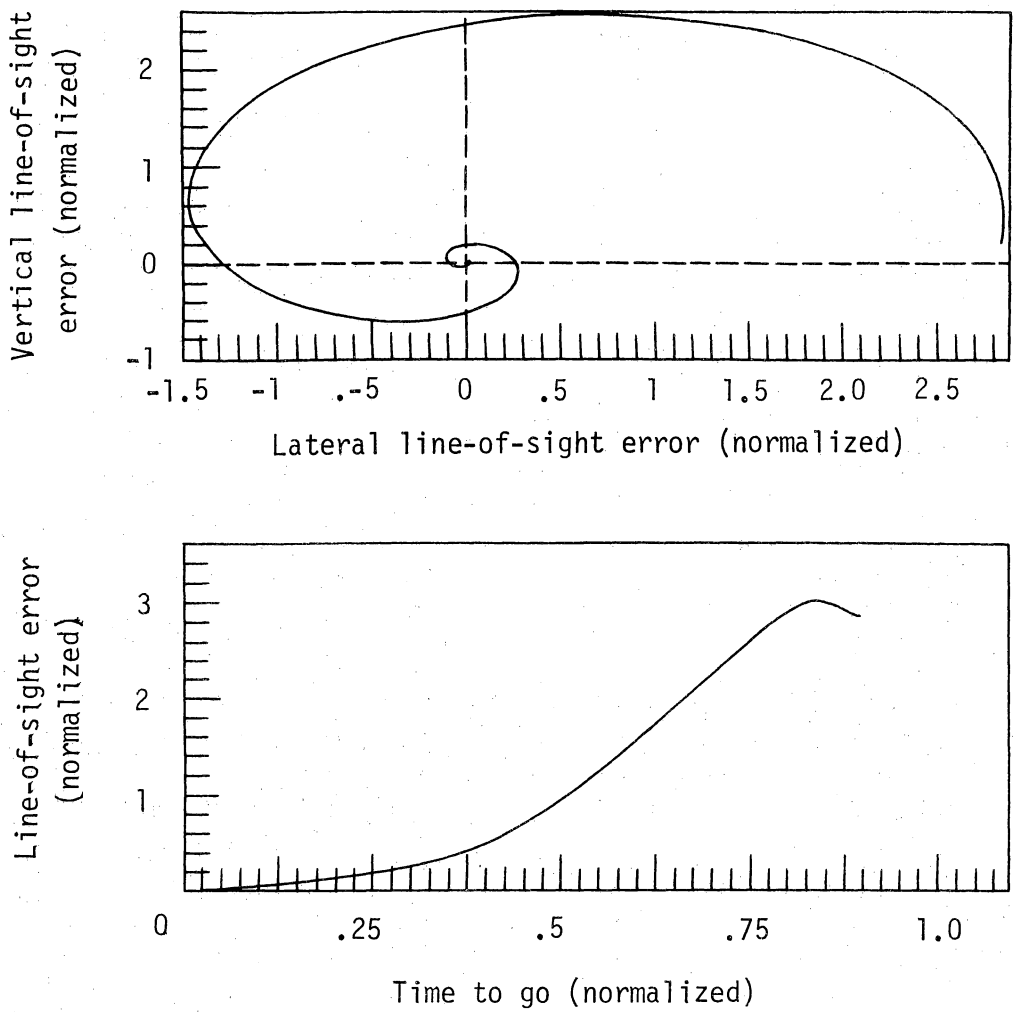

Figure 19.1.- Line-of-sight error and roll time-histories for a fifth order roll system.

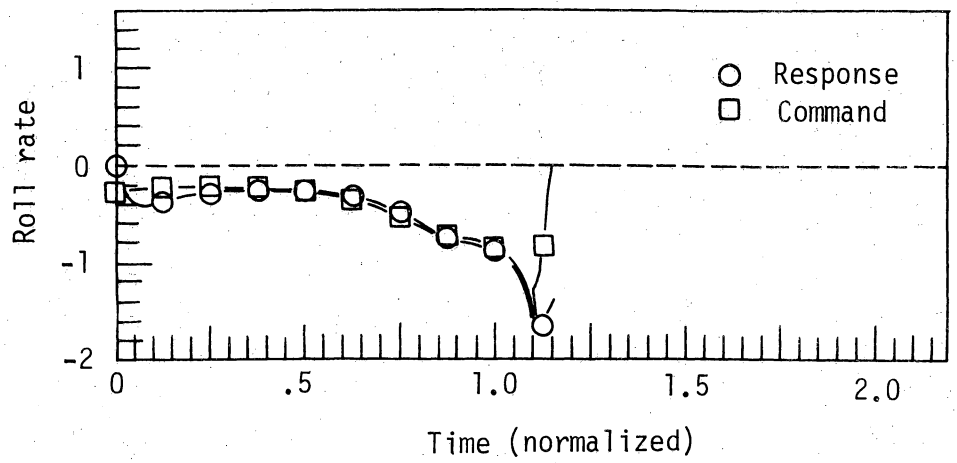

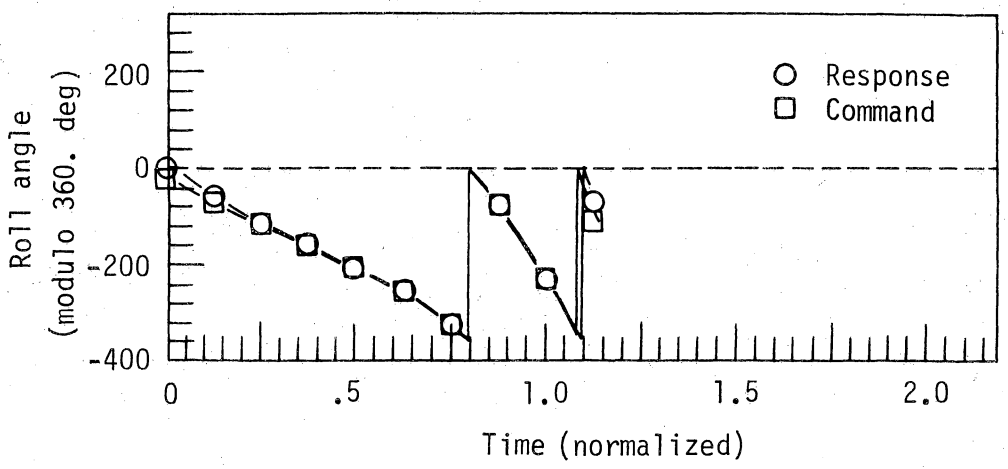

Parameters and initial conditions		
$k = 2.0$	$\phi_o = 0.0^o$	$\alpha_T = 6.0$ units
τ_ϕ = NA	$\gamma_o = -35.0^o$	P_L = NA

Figure 19.2.- Line-of-sight error and roll time-histories for a fifth order roll system.

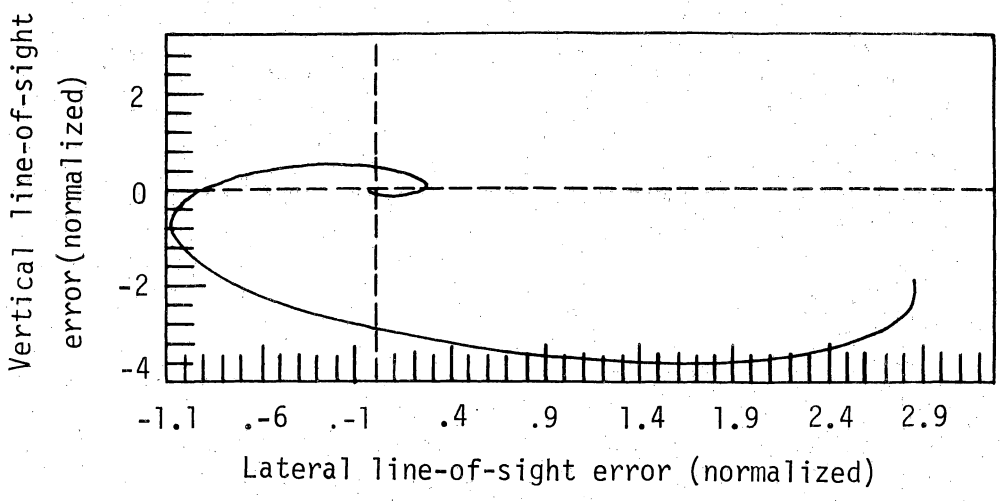

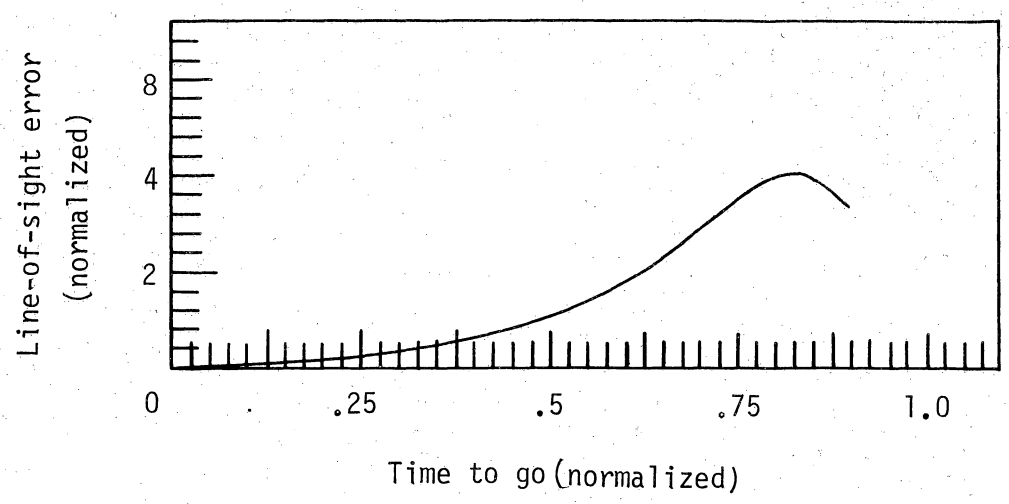

Parameters and initial conditions		
$k = 2.0$	$\phi_o = 0.0^o$	α_T =10.0 units
τ_ϕ = NA	$\gamma_o = 0.0^o$	P_L = NA

Figure 19.3.- Line-of-sight error and roll time-histories for a fifth order roll system

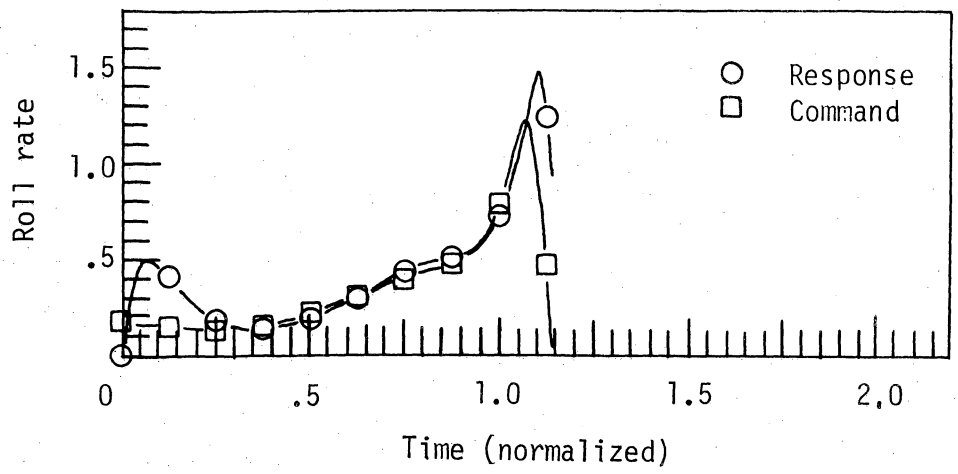

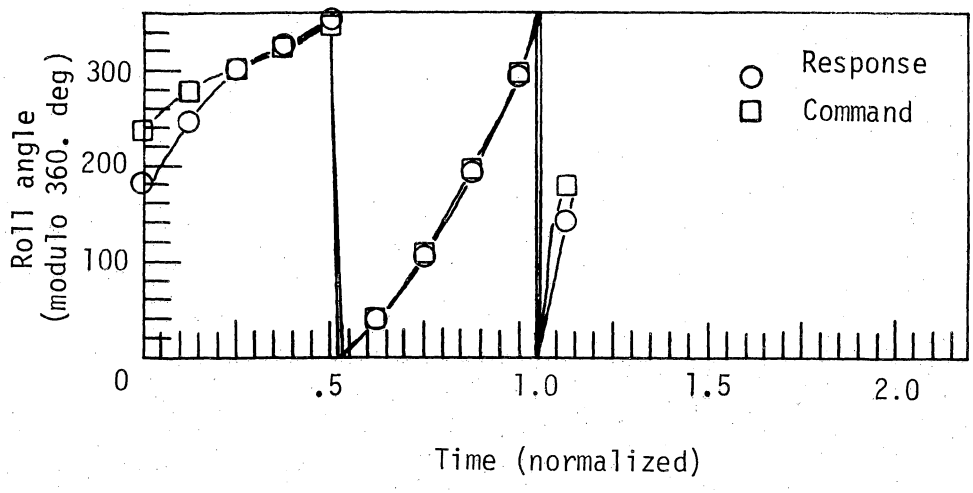

Parameters and initial conditions

$k = 2.0$ $\quad \phi_o = 180.0^o$ $\quad \alpha_T = 6.0$ units

τ_ϕ = NA $\quad \gamma_o = -30.0^o$ $\quad P_L$ = NA

Figure 19.4.- Line-of-sight error and roll time-histories for a fifth order roll system.

Table 2

Normalized Steering Errors at the Aimpoint Due to Initial Flight Path Angle Variation, $\alpha_T = 10.$

Initial Flight Path Angle, γ_o, (deg.)	Guidance Mode		
	EQ. (9) $k_1 - k_2 = 1.$	EQ. (16) $k_\phi = 2/3$	Present Anal. $k = 1. + 5.\mu_o$
0.	92.	132.	1.
-20.	57.	88.	2.
-25.	21.	123.	2.
-30.	58.	100.	2.
-35.	63.	149.	3.
-40.	32.	185.	1.
-45.	56.	18.	3.
-50.	79.	129.	3.

Table 3

Normalized Steering Errors at the Aimpoint Due to Initial Flight Path Angle Variation

$\alpha_T = 6.$

Initial Flight Path Angle, γ_o, (deg.)	Guidance Mode		
	EQ. (9) $k_1 = k_2 = 1.$	EQ. (16) $k_\phi = 2/3$	Present Anal. $k = 1. + 5.\mu_o$
0.	537.	541.	537.
-20.	29.	59.	1.
-25.	22.	91.	1.
-30.	20.	7.	1.
-35.	17.	25.	1.
-40.	84.	129.	2.
-45.	38.	211.	1.
-50.	455.	456.	336.

IX. CONCLUSIONS AND RECOMMENDATIONS

Based upon the results of Chapter VIII the following conclusions are reached:

The approximate, reduced-order description of the motion of a fixed-trim re-entry vehicle, obtained in Chapter V, was found to be sufficiently accurate to deduce a feedback control law and feedforward compensation technique which did, when implemented in the numerical model described in Chapters II and VII.B, accurately steer the vehicle to the aimpoint.

The feedforward compensation technique is essential in successfully steering the vehicle by reducing the lag in roll-angle response. The compensation technique was shown to be applicable to both first and fifth-order, non-linear roll-system models.

The non-dimensional parameter, μ_0, defined in Chapter VIII, can be used to calculate guidance gains that will accurately steer the vehicle while maintaining moderate roll-rates. This parameter can also be used in design studies to establish maneuver levels and in targeting studies to define nominal aimpoints.

The current algorithm exhibits an order-of-magnitude improvement in steering accuracy in numerical comparisons with existing guidance laws.

Based upon these conclusions, the following recommendation is made:

The present steering algorithm is a serious challenger to existing, fixed-trim steering laws and should be further examined in computer simulations that incorporate a rigid body model for the vehicle and navigation and control system errors.

X. SUMMARY

A fixed-trim, maneuvering re-entry system has been described and a computational model given for studying the terminal guidance problem. An initial steering law was derived by applying the time-optimal regulator solution to the present study. Since the time-optimal steering law required refinement during the roll-modulation portion of the flight and because the model used to describe the guidance problem obscured a refinement technique, a transformation of the original state system was made to illuminate this aspect of the problem.

The transformation of variables and subsequent linearization of the motion made possible a reduction in the order of the system states describing the terminal steering problem. Even though the final, reduced-order approximation was both non-linear and time-varying, it did illuminate the entire steering problem. A synthesis of a feedback control law was made possible by inspection of the reduced-order system. Large roll-angle-response lags, characteristic of a bank-to-turn steering mode, were substantially reduced using a feedforward compensation technique.

Specific formulas for implementing the feedback control scheme and feedforward compensation technique were provided for use in analyzing the steering algorithm in the numerical model of the re-entry system. A realistic, roll model that accounted for missile motion, actuator dynamics, and autopilot was described for purposes of illustrating the feedforward implementation procedure and as a final "test bed" for evaluating the proposed steering algorithm.

Preliminary, numerical studies, conducted using a first-order, roll-system model, provided the necessary insight to establish a formula for computing guidance gains that would produce accurate steering at moderate roll-rates. Further studies with the first-order roll model indicated an insensitivity of the present steering algorithm to initial condition and parameter variations.

Encouraged by the results obtained using a first-order roll model, the proposed steering law was implemented in the fifth-order, non-linear roll model, which incorporated realistic limits on roll-commands. The results of these numerical studies indicated that the feedback control scheme in conjunction with the feedforward compensation technique were able to accurately steer the vehicle by maintaining small lags in roll-angle response. The robustness of the proposed steering algorithm, a characteristic of explicit guidance laws, was demonstrated by numerous trajectory simulations.

A comparison of the proposed steering law with several, existing, fixed-trim laws indicated that an order-of-magnitude improvement in steering accuracy was achieved. Based on these results, it was recommended that the proposed guidance algorithm be investigated further in higher fidelity simulations of the re-entry system.

APPENDIX I

EQUATIONS OF MOTION FOR A FIXED-TRIM, RE-ENTRY BODY IN A ROLLING, VELOCITY FRAME

The governing equation for the translational motion of a re-entry body may be written in a rolling, velocity frame as

$$m(\dot{\underline{V}} + \underline{\omega}_{V_R} \times \underline{V}) = \Sigma F, \tag{90}$$

where, the angular velocity of the rotating frame is given by

$$\underline{\omega}_{V_R} = \begin{bmatrix} \dot{\delta} \\ 0 \\ 0 \end{bmatrix} + \begin{bmatrix} 1 & 0 & 0 \\ 0 & \cos & \sin\delta \\ 0 & -\sin & \cos\delta \end{bmatrix} \left\{ \begin{bmatrix} 0 \\ \dot{\gamma} \\ 0 \end{bmatrix} + \begin{bmatrix} \cos\gamma & 0 & -\sin\gamma \\ 0 & 1 & 0 \\ \sin\gamma & 0 & \cos\gamma \end{bmatrix} \begin{bmatrix} 0 \\ 0 \\ \dot{\chi} \end{bmatrix} \right\} \tag{91}$$

or

$$\underline{\omega}_{V_R} = \begin{bmatrix} \dot{\delta} - \dot{\chi}\sin\gamma \\ \dot{\gamma}\cos\delta + \dot{\chi}\sin\delta\cos\gamma \\ -\dot{\gamma}\sin\delta + \dot{\chi}\cos\delta\cos\gamma \end{bmatrix} \tag{92}$$

Equation (90) may be expanded into components to yield

$$\dot{V} = -D/m \tag{93.1}$$

$$-\dot{\gamma}\sin\delta + \dot{\chi}\cos\delta\cos\gamma = -(L/mV)\sin(\phi_V - \delta) \tag{93.2}$$

$$-\dot{\gamma}\cos\delta - \dot{\chi}\sin\delta\cos\gamma = (L/mV)\cos(\phi_V - \delta) \tag{93.3}$$

Equations (93.2) and (93.3) may be solved simultaneously for $\dot{\gamma}$ and $\dot{\chi}$ to yield

$$\dot{\gamma} = -(L/mV)\cos \phi_V \tag{94}$$

$$\dot{\chi} = -(L/mV \cos \gamma) \sin \phi_V. \tag{95}$$

Thus, as expected, the scalar relations, (93.1), (94), and (95), governing the translational dynamics of the vehicle in the rolling, velocity frame are identical to those obtained using a non-rolling, velocity (or "wind" axes) frame.

The kinematic relations, necessary to complete a description of the translational motion of the vehicle, are derived by noting that the time-rate-of-change of a vector with respect to an inertial set of axes (d/dt_I) equals the time-rate-of-change of the vector with respect to a rotating frame (d/dt_R) plus the cross-product of the angular velocity of the rotating frame with the vector. Therefore, the vector differential equation governing the motion of the line-of-sight vecotr, $\underline{\rho}$, may be written as

$$d/dt_I(\underline{\rho}) = d/dt_R(\underline{\rho}) + \underline{\omega}_{V_R} \times \underline{\rho}. \tag{96}$$

Since, $\dot{\underline{r}} = \underline{V}$ and $\underline{\rho} = -\underline{r}$, equation (96) may be rewritten as

$$d/dt_R(\underline{\rho}) + \underline{\omega}_{V_R} \times \underline{\rho} = -\underline{V}, \tag{97}$$

where,

$$\underline{\rho} = (\rho \cos \varepsilon,\ 0,\ \rho \sin \varepsilon)^T$$

$$\varepsilon = \tan^{-1}(\rho_{v_p}/\rho_{v_x})$$

$$\rho_{v_p} = \sqrt{\rho_{v_y}^2 + \rho_{v_z}^2}$$

$$\delta = \tan^{-1}(-\rho_{v_y}/\rho_{v_z}),$$

and $(\rho_{v_x},\rho_{v_y},\rho_{v_z})^T$ is the projection of the line-of-sight vector onto the non-rolling, velocity frame. Expanding (97) into its scalar components yields

$$\dot{\rho} \cos \varepsilon - \rho\dot{\varepsilon} \sin \varepsilon + \rho \sin \varepsilon(\dot{\gamma} \cos \delta + \dot{\chi} \sin \delta \cos \gamma) = -V \tag{98}$$

$$\rho \cos \varepsilon(-\dot{\gamma} \sin \delta + \dot{\chi} \cos \delta \cos \gamma) - \rho \sin \varepsilon(\dot{\delta} - \chi \sin \gamma) = 0 \tag{99}$$

$$\dot{\rho} \sin \varepsilon + \rho\dot{\varepsilon} \cos \varepsilon - \rho \cos \varepsilon(\dot{\gamma} \cos \delta + \dot{\chi} \sin \delta \cos \gamma) = 0. \tag{100}$$

The velocity vector angular rates may be eliminated from (98) through (100) by using the dynamic relationships, (94) and (95), to obtain

$$\ddot{\rho} \cos \varepsilon - \rho\dot{\varepsilon} \sin \varepsilon - (L/mV)\ \rho \sin \varepsilon \cos(\phi_V - \delta) = -V \tag{101}$$

$$-(L/mV)\ \rho\ \cos\ \delta\ \sin(\phi_V-\delta)\ -\rho\ \sin\ \varepsilon[\dot{\delta}\ +\ (L/mV)\ \sin\ \phi_V\ \tan\ \gamma]\ =\ 0 \tag{102}$$

$$\dot{\rho}\ \sin\ \varepsilon\ +\ \rho\dot{\varepsilon}\ \cos\ \varepsilon\ +\ (L/mV)\ \rho\ \cos\ \varepsilon\ \cos(\phi_V-\delta)\ =\ 0. \tag{103}$$

Thus, the transformation to a rolling, velocity frame has effectively introduced the lift force into the kinematic relationships. Solving (101) through (103) for $\dot{\rho}$, $\dot{\varepsilon}$, and $\dot{\delta}$ yields

$$\dot{\rho}\ =\ -V\ \cos\ \varepsilon \tag{104}$$

$$\dot{\varepsilon}\ =\ (V/\rho)\ \sin\ \varepsilon\ -\ (L/mV)\ \cos(\phi_V-\delta) \tag{105}$$

$$\dot{\delta}\ =\ -(L/mV)[\cos\ \varepsilon\ \sin(\phi_V-\delta)\ +\ \tan\ \gamma\ \sin\ \phi_V]. \tag{106}$$

In summary, then, the transformation from a non-rolling to a rolling velocity frame produces no change in the relations describing the dynamics of the vehicle's motion, but it does serve both to simplify and make possible an order reduction in the state system by changing the kinematic description of the motion. The transformed system is thus described by the following sixth-order system:

$$\dot{V}\ =\ -D/m \tag{107.1}$$

$$\dot{\gamma}\ =\ -(L/mV)\ \cos\ \phi_V \tag{107.2}$$

$$\dot{\chi}\ =\ -(L/mV\ \cos\ \gamma)\ \sin\ \phi_V \tag{107.3}$$

$$\dot{\rho}\ =\ -V\ \cos\ \varepsilon \tag{107.4}$$

$$\dot{\varepsilon} = (V/\rho) \sin \varepsilon - (L/mV) \cos(\phi_V - \delta) \tag{107.5}$$

$$\dot{\delta} = -(L/mV)[\cos \varepsilon \sin(\phi_V - \delta) + \tan \gamma \sin \phi_V]. \tag{107.6}$$

APPENDIX II

DERIVATION OF THE ROLL-RATE COMMAND

The roll-angle command, given by equation (62), may be rewritten as

$$\cos(\phi_c-\delta) = \cos \zeta_c = \begin{cases} \hat{k}\varepsilon; & \varepsilon < 1/\hat{k} \\ h(t); & \varepsilon \geq 1/\hat{k} \end{cases} \tag{108}$$

Differentiating both sides of (108), one obtains

$$-\sin \zeta_c(\dot{\phi}_c-\dot{\delta}) = \begin{cases} \hat{k}\dot{\varepsilon} + \dot{\hat{k}}\varepsilon; & \varepsilon < 1/\hat{k} \\ \dot{h}(t); & \varepsilon \geq 1/\hat{k} \end{cases} \tag{109}$$

From equations (49) and (53),

$$\hat{k}\dot{\varepsilon} + \dot{\hat{k}}\varepsilon = \hat{k}(1-k)\varepsilon/(t_f-t) + \hat{k}\varepsilon/(t_f-t) \tag{110}$$

$$\hat{k}\dot{\varepsilon} + \dot{\hat{k}}\varepsilon = \hat{k}(2-k)\varepsilon/(t_f-t). \tag{111}$$

Substituting (111) into (109) and noting that the derivative of the step function is the impulse function, one obtains

$$\dot{\phi}_c = \begin{cases} \dot{\delta} - \hat{k}\varepsilon(2-k)/(t_f-t) \sin \zeta_c; & \varepsilon < 1/\hat{k} \\ \dot{\delta} + \delta_i(t); & \varepsilon \geq 1/\hat{k}. \end{cases} \tag{112}$$

REFERENCES

1. Balbirnie, E. C., L. P. Sheporaitis, and C. W. Merriam, "Merging Conventional and Optimal Control Techniques for Practical Missile Terminal Guidance," AIAA Paper No. 75-1127, AIAA Guidance and Control Conference, Boston, Massachusetts, August 20-22, 1975.

2. Battin, R. H., Astronautical Guidance, McGraw-Hill, New York, 1964.

3. Bryson, A. E., and Y.-C. Ho, Applied Optimal Control, John Wiley and Sons, 1975.

4. Cameron, J. D. M., "Explicit Guidance Equations for Maneuvering Re-entry Vehicles," Proceedings of the 1977 IEEE Conference on Decision and Control, Vol. 1, pp. 670-678, New Orleans, Louisiana, December 7-9, 1977.

5. D'Azzo, J. J., and C. H. Houpis, Feedback Control System Analysis and Synthesis, McGraw-Hill, 1966.

6. Graham, R. E., "Linear Servo Theory," Bell System Technical Journal, Vol. 25, pp. 616-651, 1946.

7. Kelley, J. H., E. M. Cliff, C. Gracey, and S. C. Houlihan, "Fixed-Trim Re-entry Guidance," Department of Aerospace and Ocean Engineering TN, Virginia Polytechnic Institute and State University, Blacksburg, Virginia, April 1979.

8. Kelley, H. J., J. Skinar, and D. Bar-Moshe, "Variable-Sweep Optimization," Automatica, Vol. 15, pp. 403-409, 1979.

9. Leitmann, G., An Introduction to Optimal Control, McGraw-Hill, 1966.

10. Moore, H. R., "Combination Open-Cycle Closed-Cycle Systems," Proceedings of the Institute of Radio Engineers, Vol. 29, pp. 1421-1432, 1951.

11. Page, J. A., and R. O. Rogers, "Guidance and Control of Maneuvering Re-entry Vehicles," Proceedings of the 1977 IEEE Conference on Decision and Control, Vol. 1, pp. 659, 663, New Orleans, Louisiana, December 7-9, 1977.

The vita has been removed from the scanned document

FIXED-TRIM RE-ENTRY GUIDANCE ANALYSIS

by

Christopher Gracey

(ABSTRACT)

The terminal guidance problem for a fixed-trim re-entry body is formulated with the objective of synthesizing a closed-loop steering law. A transformation of variables is made that reduces the order of the state system for the guidance problem, and a subsequent linearization with motion along the sight line to the target as a reference produces a further order reduction. The final, reduced-order system, although nonlinear and time-varying, is simple enough to lend itself to synthesis of a class of guidance laws. A generalization of the feed-forward device of classical control theory is successfully employed for compensation of roll-autopilot lags. A comparison with existing fixed-trim guidance laws is carried out computationally with a simulation model idealizing the navigation and control systems as error-free. The proposed guidance law exhibits superior miss-distance performance in the comparison.